THE DEVELOPMENT OF A RAPID TEST FOR VASCULAR ENDOTHELIAL GROWTH FACTOR (VEGF) DETECTION AND THE EFFECTS OF VEGF AND ANTI-VEGF ON PERMEABILITY OF ENDOTHELIAL CELLS

LIM SHENG JYE

DOCTOR OF PHILOSOPHY
(MEDICAL SCIENCE)

FACULTY OF MEDICINE AND HEALTH SCIENCES

UNIVERSITI TUNKU ABDUL RAHMAN

MAY 2022

THE DEVELOPMENT OF A RAPID TEST FOR VASCULAR ENDOTHELIAL GROWTH FACTOR (VEGF) DETECTION AND THE EFFECTS OF VEGF AND ANTI-VEGF ON PERMEABILITY OF ENDOTHELIAL CELLS

By

LIM SHENG JYE

A thesis submitted to the Department of Pre-clinical Sciences,

Faculty of Medicine and Health Sciences,

Universiti Tunku Abdul Rahman,

in partial fulfilment of the requirements for the degree of

Doctor of Philosophy (Medical Science)

May 2022

This thesis is submitted in partial fulfilment of the requirements for the degree of Doctor of Philosophy (Medical Science) at Universiti Tunku Abdul Rahman (UTAR). This thesis represents the work of the author, except where due acknowledgment has been made in the text. No part of this thesis may be reproduced, stored, or transmitted in any form or by any means, whether electronic, mechanical, photocopying, recording, or otherwise, without the prior written permission of the author or UTAR, in accordance with UTAR's Intellectual Property Policy.

ABSTRACT

THE DEVELOPMENT OF A RAPID TEST FOR VASCULAR ENDOTHELIAL GROWTH FACTOR (VEGF) DETECTION AND THE EFFECTS OF VEGF AND ANTI-VEGF ON PERMEABILITY OF ENDOTHELIAL CELLS

Lim Sheng Jye

Vascular endothelial growth factor (VEGF) is one of the proteins involved in the immunopathogenesis of dengue. It is highly expressed in severe dengue, where it contributes to vascular permeability and plasma leakage. Since a rapid test for predicting severe dengue is not available and the currently available methods are expensive, the development of VEGF rapid tests using lateral flow immunoassay and 3D dielectrophoresis (DEP) microfluidic chip may provide potential benefits in the management of severe dengue. In addition, it is still unclear how much VEGF and anti-VEGF therapy contribute to the effects of plasma leakage in severe dengue cases. Thus, the objectives of this study were the development of a VEGF rapid test kit and the study of the effects of VEGF and VEGF/anti-VEGF treatment on endothelial cells using a vascular permeability assay and microarray gene expression profiling. Lateral flow immunoassay was able to

detect VEGF levels of 10 ng/ml and above, while for 3D DEP microfluidic assay, it was more sensitive, detecting as low as 5 pg/ml of VEGF. In permeability assay, VEGF-treated endothelial cells showed higher permeability than VEGF/anti-VEGF treated and untreated cells. For microarray gene expression profiling, the genes upregulated in VEGF-treated cells were enriched for inflammatory response, regulation of endothelial barrier, regulation of nitric oxide synthesis, regulation of angiogenesis, and the NOD-like receptor signalling pathway. In conclusion, 3D DEP microfluidic chip has better sensitivity and can be designed to be more user-friendly for clinical use. VEGF treatment increased permeability across endothelial cells, while the addition of anti-VEGF reduced the degree of leakage caused by VEGF. The microarray profiling generated from treated endothelial cells showed dysregulated genes implicated in severe dengue. The prospect of using anti-VEGF antibodies to neutralise VEGF gives hope for future effective therapy to stop the progression of dengue into severe dengue.

Keywords: vascular endothelial growth factor; anti-vascular endothelial growth factor; endothelial cells; severe dengue; vascular permeability; gene expression profiling

Subject Area: QH301-705.5 Biology (General)

ACKNOWLEDGEMENT

First and foremost, I would like to express my deepest gratitude to my current supervisor, Professor Ngeow Yun Fong and co-supervisor, Dr. Ong Hooi Tin, for their guidance, motivation, and support during my PhD study. Besides, I would like to thank my first supervisor, from October 2016 until his retirement in November 2020, Dr. Gan Seng Chiew for his advice and support throughout my postgraduate studies. And special thanks to Dr. Gary Low Kim Kuan for sharing his experience and advice. Thank you to my labmates, especially Erica Choong Pei Fen, Norlaily and Boo Lily, for constantly helping me during my research. Furthermore, I would like to express my gratitude to UTAR for providing the facilities and internal funding, UTARSRF (Programme Number: IPSR/RMC/UTARSRF/PROGRAMME 2014-C1/002; PI: Dr. Gan Seng Chiew) and UTARRF (Project Number: IPSR/RMC/UTARRF/2018-C2/G01; PI: Dr. Gan Seng Chiew) for my project. Not forget, I would like to thank Professor Chang Hsien-Chang, who provided me with the materials that I needed to complete my project. Finally, I would like to express my deepest gratitude to my family, who constantly supported me emotionally and financially.

APPROVAL SHEET

This thesis entitled **"THE DEVELOPMENT OF A RAPID TEST FOR VASCULAR ENDOTHELIAL GROWTH FACTOR (VEGF) DETECTION AND THE EFFECTS OF VEGF AND ANTI-VEGF ON PERMEABILITY OF ENDOTHELIAL CELLS"** was prepared by LIM SHENG JYE and submitted as partial fulfilment of the requirements for the degree of Doctor of Philosophy in Medical Science at Universiti Tunku Abdul Rahman.

Approved by:

_____

(Prof. Dr. Ngeow Yun Fong) Date: _____

Senior Professor/Supervisor

Department of Pre-clinical Sciences

Faculty of Medicine & Health Sciences

Universiti Tunku Abdul Rahman

_____

(Dr. Ong Hooi Tin) Date: _____

Assistant Professor/Co-supervisor

Department of Pre-clinical Sciences

Faculty of Medicine & Health Sciences

Universiti Tunku Abdul Rahman

FACULTY OF MEDICINE & HEALTH SCIENCES

UNIVERSITI TUNKU ABDUL RAHMAN

Date: MAY 2022

SUBMISSION OF THESIS

It is hereby certified that **Lim Sheng Jye** (ID No: **16UMD07556**) has completed this thesis entitled "**THE DEVELOPMENT OF A RAPID TEST FOR VASCULAR ENDOTHELIAL GROWTH FACTOR (VEGF) DETECTION AND THE EFFECTS OF VEGF AND ANTI-VEGF ON PERMEABILITY OF ENDOTHELIAL CELLS**" under the supervision of Professor Ngeow Yun Fong (Supervisor) from the Department of Pre-clinical Sciences, Faculty of Medicine and Health Sciences, and Dr. Ong Hooi Tin (Co-Supervisor) from the Department of Pre-clinical Sciences, Faculty of Medicine and Health Sciences.

I understand that the University will upload softcopy of my thesis in pdf format into UTAR Institutional Repository, which may be made accessible to UTAR community and public.

Yours truly,

_____

(Lim Sheng Jye)

DECLARATION

I hereby declare that the thesis is based on my original work except for quotations and citations which have been duly acknowledged. I also declare that it has not been previously or concurrently submitted for any other degree at UTAR or other institutions.

_____

(LIM SHENG JYE)

Date: May 2022

TABLE OF CONTENT

LIST OF TABLES

LIST OF FIGURES

LIST OF ABBREVIATIONS

ADE	Antibody-dependent enhancement
AEC	3-Amino-9-ethylcarbazole
AST	Aspartate transaminase
ALT	Alanine transaminase
BSA	Bovine serum albumin
cDNA	Complementary deoxyribonucleic acid
CO_2	Carbon dioxide
DAB	3,3'-Diaminobenzidine tetrahydrochloride
DAPI	4',6-diamidino-2-phenylindole
DENV	Dengue virus
DHF	Dengue haemorrhagic fever
DEP	Dielectrophoresis
DF	Dengue fever
DNA	Deoxyribonucleic acid
DSS	Dengue shock syndrome
EDC	1-Ethyl-3-(3-dimethylaminopropyl)carbodiimide
EDTA	Ethylenediaminetetraacetic acid
ELISA	Enzyme-linked immunosorbent assay
FAM	6-Carboxyfluorescein
FITC-Dextran	Fluorescein isothiocyanate–dextran
GO	Gene Ontology
hMSC	Human mesenchymal stem cell
HIA	Haemagglutination inhibition assay
HPMEC	Human pulmonary microvascular endothelial cell
Hz	Hertz
IgG	Immunoglobulin G
IgM	Immunoglobulin M
nDEP	Negative dielectrophoresis
NHS	N-hydroxysuccinimide
NS1	Non-structural protein 1
PBS	Phosphate-buffered saline
pDEP	Positive dielectrophoresis
PDMS	Polydimethylsiloxane
PCR	Polymerase chain reaction
PFU	Plaque forming unit
POC	Point-of-care
PRNT	Plaque reduction neutralising test
qRT-PCR	Quantitative real time-polymerase chain reaction
RBC	Red blood cell
RNA	Ribonucleic acid
RT-PCR	Reverse transcription-polymerase chain reaction
TMB	3,3',5,5'-tetramethylbenzidine
VEGF	Vascular endothelial growth factor
VEGFR1	Vascular endothelial growth factor receptor 1
VEGFR2	Vascular endothelial growth factor receptor 2
V_{pp}	Voltage peak-to-peak

CHAPTER 1

INTRODUCTION

1.1 Background

Dengue fever may present as an asymptomatic infection or a febrile illness with rashes, muscle and joint pain, and other signs and symptoms (World Health Organization, 2012b). It could progress to severe and fatal forms of dengue known as dengue haemorrhagic fever (DHF) and dengue shock syndrome (DSS) (Katzelnick, Coloma and Harris, 2017). The infection is caused by four serotypes of the dengue virus (DENV 1, 2, 3, and 4), which are genetically and antigenically different, with a 30-35% difference in amino acid sequence (Sim and Hibberd, 2016).

Dengue virus is transmitted by mosquitoes, mainly the *Aedes aegypti* and *Aedes albopictus* (World Health Organization, 2012b; Harapan *et al.*, 2020). The two main factors that contributed to the rapid spread of dengue are urbanisation and globalisation. Rapid urbanisation is the result of increasing human migration to the big cities. The population pressure in the cities led to haphazard city development and poor sewage and waste management (Gubler, 2011). During globalisation, better modes of transportation such as aeroplanes and ships are necessary since there will be an increase in international travel routes for humans and products (Gubler, 2011; Harapan *et al.*, 2020). These situations created

perfect conditions for mosquito breeding and dengue virus transmission (Gubler, 2011).

Mosquitoes spread dengue to many parts of the world. Brady *et al.* (2012) had identified 128 countries affected by dengue fever, while the World Health Organization (WHO) had identified more than 100 countries where local transmission of dengue occurs regularly (World Health Organization, 2021). Many of these countries are located in tropical regions where the weather is warm throughout the year (Gubler, 2011). This endemic situation has created a heavy burden on the country's healthcare system, with an estimated 100 – 400 million cases reported worldwide every year and more than 4 billion people exposed to the risk of getting dengue (Bhatt *et al.*, 2013; Stanaway *et al.*, 2016; World Health Organization, 2020). The official number of dengue cases recorded in 2019 was 4.2 million (World Health Organization, 2020), and this amount may underscore the severity of dengue infection worldwide as there are many unreported dengue cases and misdiagnosed cases. The underreported cases theory is supported by the high number of estimated dengue cases reported in these two studies. In a study by Stanaway *et al*. (2016), the authors estimated that the dengue cases were around 58.4 million per year, while Bhatt *et al*. (2013) had predicted 96 million symptomatic dengue cases occurred yearly using mathematical modelling on existing databases.

Malaysia is one of the endemic countries for dengue infection. The number of cases recorded in 2020 was 90,304 and 145 deaths (Ravindran, 2021). The number of dengue cases peaked in 2019, with 130,101 cases were recorded. There were some studies conducted on the economic burden of dengue in Malaysia. The economic burden of dengue infection was estimated to be around US$56 million or RM196 million, according to a study done in 2012 (Shepard *et al.*, 2012). In another study done in Seremban, Malaysia, the burden of dengue infection was US$365.16 per case (Mia *et al.*, 2016). This burden was considered a large amount of expenditure for the country since this is the cost of treating only one disease without factoring in other costs. Some of the reasons that contributed to the increased costs are unnecessary hospital admission for dengue patients with low platelet counts and repeated clinical assessment and tests for patients during hospitalisation (Wong, Wong and AbuBakar, 2020).

The diagnostic tools commonly used to confirm dengue cases are the rapid immunochromatographic test, ELISA and haemagglutination inhibition assay for NS1, IgG and IgM detection or nucleic acid amplification test (Muller, Depelsenaire and Young, 2017). Doctors usually diagnose suspected dengue patients based on signs and symptoms before performing more tests. Diagnosis of dengue based on signs and symptoms can be challenging. Early detection of severe dengue before it happens is still not possible. The progression to severe dengue in patients usually occurs very quickly, and it will either resolve by itself or worsen within a short period. The patients are assessed based on signs and symptoms such as persistent vomiting, severe abdominal pain, mucosal

bleeding, signs of hypovolemic shock, increase in haematocrit, and rapid decline of platelet (World Health Organization, 2009). Thus, it is important to look at biomarkers that identify severe dengue patients that need hospitalisation from the self-limiting dengue fever (Wong, Wong and AbuBakar, 2020).

The biomarker is an indicator of the medical state measured outside of the patient (Strimbu and Tavel, 2010). An ideal biomarker should serve as an early indicator of severe dengue. Furthermore, multiple biomarkers detection at the same time could accurately diagnose more severe dengue cases (Wong, Wong and AbuBakar, 2020). Several factors are involved in tandem to control vascular leakages, such as endothelial cells receptors, adherens junctions, cytokines, permeability factors, clotting factors and platelets (Dalrymple and MacKow, 2012). Furthermore, there is no test available or diagnostic tool for biomarker detection in severe dengue diagnosis when many studies have identified predictive biomarkers for diagnosis for severe dengue (Wong, Wong and AbuBakar, 2020).

The pathogenesis of severe dengue is still not completely known. It is hypothesized that the antibodies and T cells generated during a primary infection not only provide incomplete immunity to a subsequent heterotypic infection but also elicit altered immune responses that lead to severe disease (St. John and Rathore, 2019). One of the proteins implicated in the immunopathogenesis of dengue is the vascular endothelial growth factor (VEGF) protein. This protein is

involved in normal physiological functions in the skeletal, neural, and hematopoietic systems (Ballmer-Hofer, 2018). VEGF, referred to VEGF-A in this study, is a signalling protein that plays an important role in vasculogenesis and promotes angiogenesis for homeostasis. However, it has also been implicated in diseases (Apte, Chen and Ferrara, 2019). VEGF has been reported to be highly expressed in severe dengue (Tseng *et al.*, 2005; Srikiatkhachorn *et al.*, 2006; Low, Gan and Ho, 2015; Thakur *et al.*, 2016; Low *et al.*, 2018), in which, severe plasma leakage is attributed to VEGF-induced increase in vascular permeability (Low *et al.*, 2018; Mutiara *et al.*, 2019).

There are many methods currently used for dengue diagnosis. The most used test for dengue diagnosis is lateral flow immunoassay because it is easy to use and produce a rapid result. Lateral flow immunoassay (also known as immunochromatographic strip test or rapid test) relies on antibodies binding system, in which the antibodies detect viral antigen or antibodies released in response to dengue infection. Commercially available lateral flow immunoassay for dengue diagnosis can detect viral antigen NS1, IgG or IgM. The sensitivity of commercial lateral flow immunoassay ranged from 50 – 80% (Castellanos and Coronel-Ruiz, 2014). Although the sensitivity of lateral flow immunoassay is not as high as ELISA, it is still the preferred method for dengue diagnosis due to its benefits which outweigh its disadvantages.

Dielectrophoresis (DEP)-based microfluidic system represents one of the lab-on-a-chip systems which has a potential for point-of-care testing. DEP refers to the movement of polarisable particles caused by the non-uniform electric field. The relative polarisability between the particle and the surrounding medium enables the manipulation of particles by trapping or sorting. DEP has been used in cancer research to isolate cancerous cells from non-cancerous cells due to the difference in the cells' dielectric properties. In addition, smaller biomolecules such as DNA or protein from the biological samples can also be detected using DEP (Rahman, Ibrahim and Yafouz, 2017). The DEP-based microfluidic system is useful for the detection of biomolecules that are present in small amounts or samples in small volumes (Viefhues and Eichhorn, 2017a).

1.2 Problem Statement and Hypothesis

The problem statements for this study were:

1) An ELISA kit for VEGF detection is available commercially but it is expensive and not suitable for point-of-care use.
2) Although many biomarkers have been shown to play important roles in the pathogenesis of dengue and severe dengue, it is still unclear how VEGF contributes to the vascular permeability that leads to severe dengue.
3) It is also unclear whether anti-VEGF therapy can reverse the effects of plasma leakage in severe dengue cases.

The hypothesis for this study were:

1) A rapid test for VEGF would be useful for screening and predicting severe dengue where laboratory facility is not readily available.
2) Lateral flow immunoassay can be used as a rapid test for the detection of the VEGF level equivalent in severe dengue patients.
3) VEGF and anti-VEGF can affect vascular permeability by the regulation of genes involved in vascular permeability or genes implicated in severe dengue.

1.3 Research Questions

1) Is it possible to develop a VEGF rapid test that can detect the level of VEGF present in the serum of a severe dengue patient?
2) To what extent does VEGF affect the permeability of human endothelial cells?
3) Can anti-VEGF therapy reverse the effects of VEGF-induced endothelial permeability?
4) Which genes are dysregulated during VEGF and anti-VEGF treatment on human vascular endothelial cells?

1.4 Objectives

1) To develop a rapid test for the detection of VEGF.
2) To study the effect of VEGF on the permeability of human endothelial cells *in vitro*.
3) To study the effect of anti-VEGF therapy on VEGF-induced endothelial permeability.
4) To investigate the gene expression profile of VEGF and anti-VEGF treated human pulmonary microvascular endothelial cells.

CHAPTER 2

LITERATURE REVIEW

2.1 Dengue Fever

Dengue fever is a viral disease characterised by the onset of fever and other symptoms and transmitted from human to human through mosquito vectors. The predominant species of mosquito that spread dengue is *Aedes aegypti* (World Health Organization, 2021). Any of the four distinct virus serotypes (dengue virus 1, 2, 3, or 4) may cause classical dengue fever and severe dengue, such as Dengue Haemorrhagic Fever (DHF) and Dengue Shock Syndrome (DSS).

Dengue fever has been endemic in more than 100 countries in tropical and sub-tropical areas. Unfortunately, the number of cases is commonly underreported and many are misclassified (World Health Organization, 2021). Bhatt *et al.* (2013) estimated the number of dengue cases worldwide to be 390 million per year, with 96 million patients showing dengue symptoms. These figures are several times higher than the WHO estimation of 50-100 million dengue infections per year (World Health Organization, 2009).

2.1.1 History & Epidemiology of Dengue Infection

The earliest record of dengue-like illness was dated back to 265 - 420 A.D. during the rule of the Chin Dynasty in China. The Chinese called it a “water poison” disease because it involved flying insects associated with water (Gubler, 1998). The dengue cases reported from 1780 to 1940 in Asia, Africa, and North America were intermittent but usually occurred as outbreaks. The global dengue pandemic started during World War II (from 1939 to 1945) when there was a huge number of human movements across different continents. The DHF epidemic was first reported in Manila, the Philippines, from 1953 to 1954 (Gubler, 1998), followed by an outbreak in Thailand in 1958 (World Health Organization, 2011). Before 1970, only nine countries had experienced dengue epidemics, mostly located in the Southeast Asia region (World Health Organization, 2021).

By 1970, dengue had spread throughout the Southeast Asian countries and then to other parts of the Asian continent. The reintroduction of the vector and new strains of dengue virus back to Central and South America had caused epidemics since the 1980s. Since the 1990s, outbreaks in the African continent were detected more frequently, especially in East Africa (Gubler, 1998). Currently, dengue is endemic in more than 100 countries, with America, Southeast Asia and Western Pacific regions being the most severely affected regions. For example, in 2016, the Philippines and Malaysia of the Western Pacific region experienced outbreaks, with more than 100 000 cases reported in each country. In 2016, more than 1.5 million dengue cases were reported in

Brazil, in which the number of dengue cases tripled compared to cases recorded in 2014. Dengue had also spread to European countries, where the first case was discovered in France and Croatia in 2010 (World Health Organization, 2021).

Dengue fever was first reported in Penang, Malaysia, in 1901, in a case imported from Singapore. The first case of DHF was reported in Penang in 1962. In 1973, a major outbreak of DHF occurred in Malaysia, with cases reported throughout the country (Poovaneswari, 1993). During the 1973 outbreak, a total of 969 cases and 54 deaths were reported (Pang and Loh, 2016). Since 1974, several periodic outbreaks were observed in 1978, 1982 and 1990 with a 4-year cycle outbreak trend (Muhammad Azami *et al.*, 2011). From 2000 onward, dengue cases increased except for a dip in 2011 (a 50% drop from 2010) and 2012. In 2014 and 2015, the number of cases doubled compared to 2013, with reported cases exceeding 100,000. The same trend in dengue cases occurred for dengue death. In 2014 and 2015, the death numbers increased to 215 and 336, respectively, from 92 deaths in 2013. In 2019, Malaysia recorded the highest number of dengue cases totalling 130,101, but the number of deaths was lower than the record death number in 2015 (336 deaths) (Figure 2.1) (Ministry of Health Malaysia, 2020).

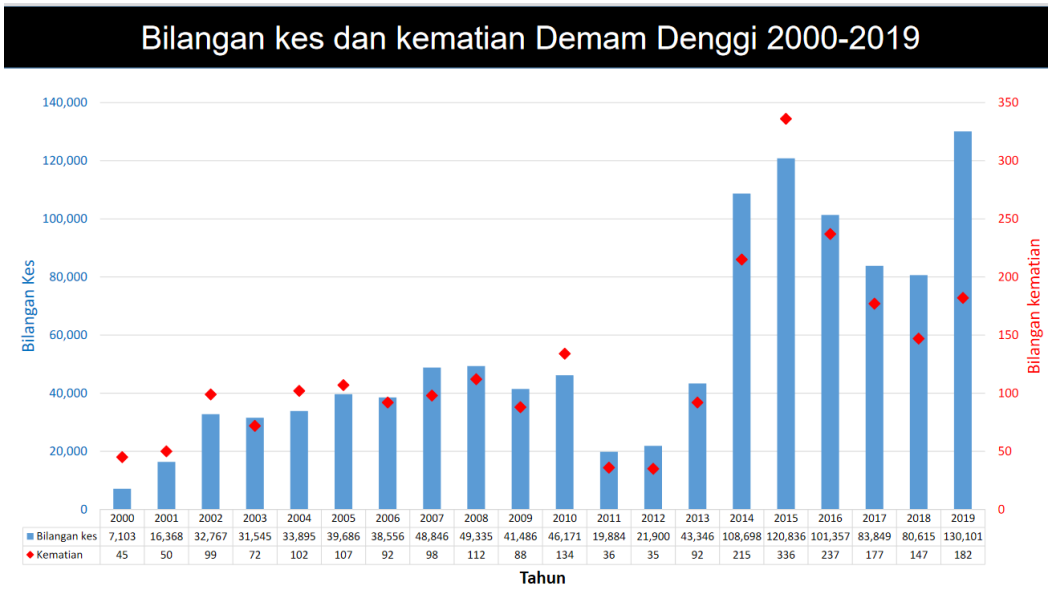

Figure 2.1 Dengue cases and death from 2000 – 2019 (Adapted from Ministry of Health Malaysia, 2020).

In the Malaysian paediatric (ages 0 – 18) population, the number of dengue cases has decreased since the 1990s, in contrast to the increase in the adult population. The majority (80%) of the paediatric dengue cases occurred in the more than 15 years age group (Cheah *et al.*, 2014), unlike the rest of the world, where the highest incidence is among children 5-14 years old (Stanaway *et al.*, 2016). It was believed that, in Malaysia, more cases were reported among children more than 15 years because children in this age group are usually active outdoors (either working, schooling, or playing) (Kim Teng and Satwant, 2001).

Many factors contributed to the rapid spread of the dengue virus to many countries. The first factor is the explosion of the global human population, which grew from 2.5 billion in 1950 to 7.8 billion in 2020 (Chamie, 2020).

Uncontrolled population growth might cause improper city planning, including overcrowding, unplanned housing development, and poor sewage and waste management. These problems create a perfect breeding ground for mosquitoes and the rapid spread of dengue infection between people (Gubler, 1998). The lack of an effective mosquito control method is a big issue. Fogging with insecticide is the only method used to kill mosquitoes but is ineffective in controlling the mosquito population. In addition, globalisation has led to more travel and transportation of goods to different parts of the world. Increased air travel carries mosquitoes and infected people to different countries, enabling the spread of dengue to countries with no previous reported dengue cases. Lastly, poor health infrastructure and lack of resources in many countries also lead to insufficient development of vector and disease prevention and control programs (Gubler, 1998, 2011).

2.1.2 Dengue Virus

Dengue virus serotypes 1 - 4 are closely related and share almost 60 – 70% similarity in their genomes (Sim and Hibberd, 2016). Dengue virus is a member of a group of viruses from the genus *Flavivirus* and the family Flaviviridae that includes West Nile virus, yellow fever virus, and Zika virus. Mosquito vectors spread the dengue virus through bites. After the mosquito bites a viraemic person (a person that already being infected with the dengue virus), the virus infects the midgut of the mosquito before moving to the salivary gland. Subsequently, the mosquito can infect another host when enough dengue virus is present in the mosquito saliva (Carrington and Simmons, 2014). After a

mosquito bite, there is an average incubation period of 4 - 7 days (during which the virus multiplies and is disseminated through the body) before the appearance of symptoms (Bhatt *et al.*, 2021). The common mosquito species involved in the dengue virus transmission among humans are *Aedes aegypti* and, less commonly, *Aedes albopictus* (Sim and Hibberd, 2016). *Aedes aegypti* is the predominant species that spread dengue because it breeds in an indoor or outdoor environment close to humans, while *Aedes albopictus* prefers outdoor, natural breeding sites (Kusumawathie, 2005).

Dengue virus is a positive, single-stranded RNA virus with 11 kilobases in genome size. It is spherical in shape with an outer layer originally from the host's lipid bilayer. The outer layer of the virus, known as the viral envelope, is made up of E and M proteins embedded in between the lipid bilayer. The mature virus particle is 50 nm in diameter and made up of three structural proteins, namely, C (capsid protein), M (membrane-associated protein), E (envelope protein), and its RNA genome (Figure 2.2) (Sim and Hibberd, 2016; Uno and Ross, 2018; Murugesan and Manoharan, 2020).

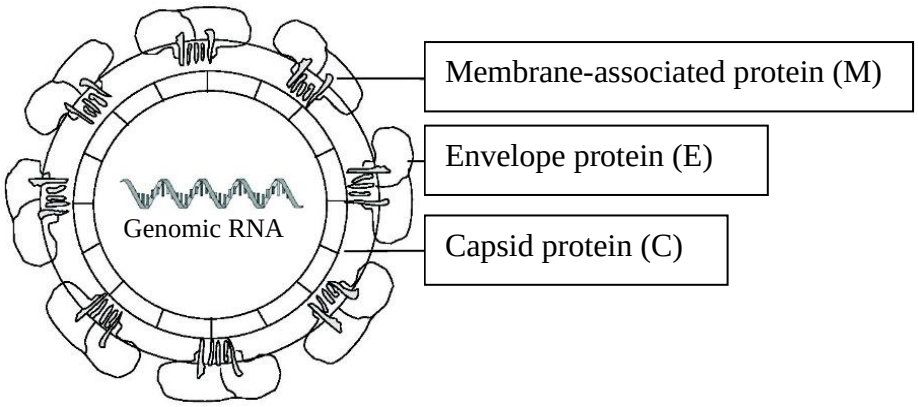

Figure 2.2 Structure of dengue virus. The mature virus particle is made up of three structural proteins, namely, C (capsid protein), M (membrane-associated protein), E (envelope protein), and its RNA genome (Modified from Roy and Bhattacharjee, 2021).

As the name implies, the C protein is the component for encapsidation of the virus' RNA genome. The M protein is involved in the arrangement and maturation of dengue virus particles. M protein is composed of 3 regions of pr molecule, M ectodomain, and TM region. The pr molecule function is to stop the newly produced virus from fusing back into the cell by covering the fusion loop of E protein. There are 180 copies each of E and M proteins, embedded in the membrane encapsulating the mature virion. The E protein acts as the viral attachment site and is transported through host membranes. One monomer of E protein is made up of three domains: central domain I, fusion domain II, and receptor binding domain III. Domains II and II are involved in the internalisation of the dengue virus into the cells (Murugesan and Manoharan, 2020).

The viral genome also encodes seven non-structural proteins, including NS1, NS2A, NS2B, NS3, NS4A, NS4B, and NS5 (Figure 2.3). NS1 is expressed within the cells, on the cell surface, or as circulating NS1 in the bloodstream. It assists in viral RNA replication together with other non-structural proteins. It is also involved in membrane bending and the development of nucleocapsid through its different domains (Scaturro *et al.*, 2015). The dimer form of NS1 has three domains: beta-roll domain, Wing domain, and beta-ladder domain (Dwivedi *et al.*, 2017; Murugesan and Manoharan, 2020). The beta-roll domain is involved in early events of RNA replication by associated with NS4A and NS4B. Wing domain assists in membrane bending, while the beta-ladder domain is involved in nucleocapsid development (Scaturro *et al.*, 2015). NS2 consists of two forms, NS2A and NS2B, which result from post-translational cleavage by NS2B-NS3 protease (Murugesan and Manoharan, 2020). NS2A is involved in viral RNA synthesis and virion assembly. NS2B acts as a cofactor to NS3 protease, forming the NS2B-NS3 protease. The protease complex is important for viral polyprotein processing, such as cleavage (Dwivedi *et al.*, 2017). Apart from forming protease complex with NS2B, NS3 has different enzymatic activities in RNA replication. The other functions of NS3 are RNA helicase, nucleoside 5’ triphosphatase (NTPase), and RNA 5’ triphosphatase (RTPase) (Murugesan and Manoharan, 2020).

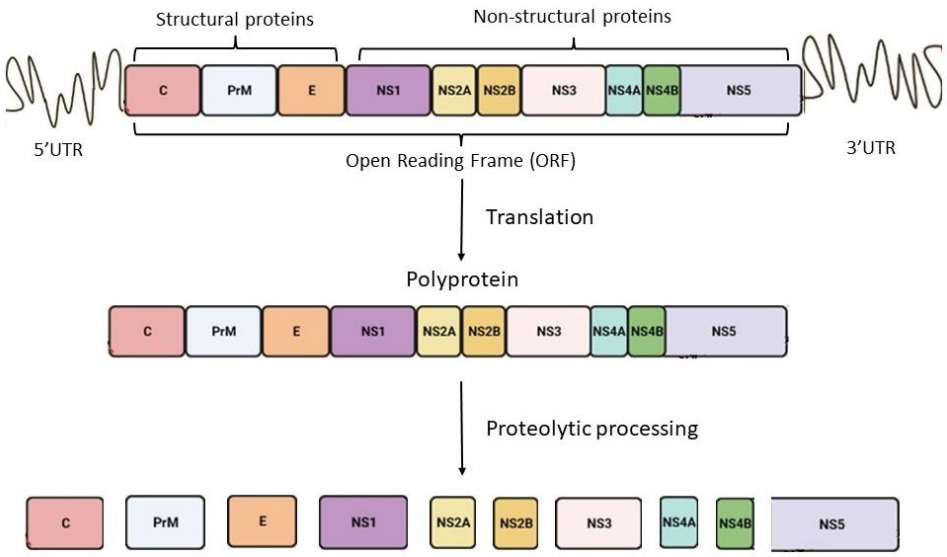

Figure 2.3 Genome of dengue virus. The viral RNA genome encodes 10 genes, namely, Capsid (C), Membrane (M), Envelope (E), NS1, NS2A, NS2B, NS3, NS4A, NS4B, and NS5. The genome is translated into polyprotein before cleaved into the structural and non-structural proteins (Modified from Nanaware et al., 2021).

Non-structural protein 4 (NS4) consists of two forms, NS4A and NS4B, which play important roles in dengue virus RNA replication and virus-host interactions. Both transmembrane NS4A and NS4B protein are part of the replication complex and interact with each other during viral RNA replication. NS4A also regulates the ATPase activity of the NS3 helicase, while NS4B promotes the dissociation of single-stranded RNA from NS3 after unwinding by the NS3 helicase (Dwivedi *et al.*, 2017; Elsen and Quek, 2021). NS5 is the largest and most conserved protein among all the dengue virus proteins. NS5 consists of two domains, Mtase and RdRp domain. The Mtase domain functions to cap the viral RNA and stabilise it, while the RdRp domain is involved in viral RNA synthesis during the initiation and elongation steps (Dwivedi *et al.*, 2017; Murugesan and Manoharan, 2020; Elsen and Quek, 2021). NS5 also helps to

evade the host's immune response by inhibiting STAT2 activated-type 1 IFN response which is effective in virus clearance (Uno and Ross, 2018).

2.1.3 Classification of Dengue

World Health Organization (WHO) classified dengue infection into classic dengue fever (DF), dengue haemorrhagic fever (DHF) and dengue shock syndrome (DSS) based on the 1997 Dengue Case Classification. DF was characterised as mild fever or sudden onset of high fever accompanied by signs and symptoms which included headache, pain behind the eyes, muscle ache, bone or joint pain, petechial rash, and leukopenia. DHF was divided into four categories of disease severity, namely, Grade I, II, III and IV. Grade I DHF was associated with high fever and haemorrhagic tendencies (petechiae, purpura, bleeding from mucosa or gastrointestinal tract, haematemesis), thrombocytopenia, and plasma leakage. The criteria for Grade II DHF were spontaneous bleeding in addition to the manifestations of Grade I DHF. The diagnostic criteria for grade III DHF were signs of circulatory failure (rapid and weak pulse and hypotension). Grade IV DHF was characterised by severe circulatory failure deteriorating into shock (DSS) with an imperceptible pulse, narrow pulse pressure (≤20 mmHg), lethargy, hypotension, cold, clammy skin, and restlessness (World Health Organization, 1997).

Due to many reports on the difficulties of classifying dengue cases using the 1997 Dengue Case Classification, the WHO produced a new guideline in 2009. Dengue was categorized into three groups: dengue with warning signs, dengue without warning signs, and severe dengue. The criteria for dengue diagnosis were nausea, vomiting, rash, aches, pains, leukopenia, and a positive tourniquet test. The warning signs listed in the guideline include abdominal pain, vomiting, clinical fluid accumulation, mucosal bleeding, lethargy, liver enlargement of more than 2 cm, and an increase of haematocrit. The criteria for severe dengue included severe plasma leakage (fluid accumulation, respiratory distress, deterioration into shock), severe bleeding, and severe organ involvement (high level of liver enzymes, impaired consciousness, and pathology in other organs) (World Health Organization, 2009).

The 1997 classification was too broad and required a more specific definition of warning signs stated in the classification. The limitations included the need to perform repetitive tests, the non-specificity of the tourniquet test used for DHF diagnosis, and overlapping case definitions between DF, DHF, and DSS (Hadinegoro, 2012). After the introduction of the new 2009 guideline, several studies have reported that the guideline increased the sensitivity for identifying severe dengue patients compared to the old guidelines. Furthermore, the 2009 guideline was more helpful for the management of dengue cases. Nevertheless, there were also a few issues regarding the 2009 classification, such as the inconsistency of using the guidelines in different countries and differences in the warning signs observed in patients in different countries (Barniol *et al.*, 2011;

Hadinegoro, 2012). The current guidelines was recommended to be improvised constantly for the accurate dengue or severe dengue diagnosis (Hadinegoro, 2012). For instance, to improve the diagnosis of severe dengue upon patient admission, suggestions have been made to use ultrasound to detect plasma leakage, to include decompensation of chronic disease, and thrombocytopenia <20,000 platelets/mm^3 in the diagnostic criteria (Ajlan *et al.,* 2019; Dussart *et al.*, 2020).

2.1.4 Dengue Diagnosis

In the management of suspected dengue cases, the medical practitioner will first diagnose the admitted patient based on clinical signs and symptoms. However, misdiagnosis of dengue as other viral or parasitic diseases such as malaria, Chikungunya, and Zika virus infection is common. Successful case management involves an early diagnosis based on clinical signs and symptoms in the guidelines provided by National or International bodies, followed by rapid confirmation based on diagnostic tools, and finally, appropriate supportive treatment (World Health Organization, 2012a). Dengue diagnosis based solely on clinical signs and symptoms can be unreliable and depends on the stage of infection (World Health Organization, 2012a; Harapan *et al.*, 2020). Dengue patients present with different symptoms throughout the stages of dengue. The viraemia or expression of viral antigen and antibodies against the dengue virus could also vary depending on the infection stage. Thus, some precautions need to be applied when using diagnostics tools for dengue detection.

The commonly used tests for dengue diagnosis are virus culture, molecular test, antigen detection and serological test. Antigen and nucleic acid tests are suitable for the early days of dengue infection (less than five days). The viraemia period during dengue infection is short. Samples, such as whole blood, serum, plasma, or tissue, not collected from patients during early infection might not contain any virus particles or antigens and thus, cannot be used for virus culture or isolation of viral nucleic acid. Serology for IgG and IgM detection comes in handy, especially for patients admitted after five days of infection. During primary dengue infection, IgM levels can be detected as early as day 3 and peak about two weeks after infection. On the other hand, IgG levels in primary dengue rise much slower and can be detected only after one week. However, during secondary infection, IgG levels rise as early as day 3, owing to the rapid expansion of memory B cells (Muller, Depelsenaire and Young, 2017; Harapan *et al.*, 2020). The clinical course of viraemia, NS1 antigen expression, and IgG and IgM during dengue virus infection are shown in Figure 2.4.

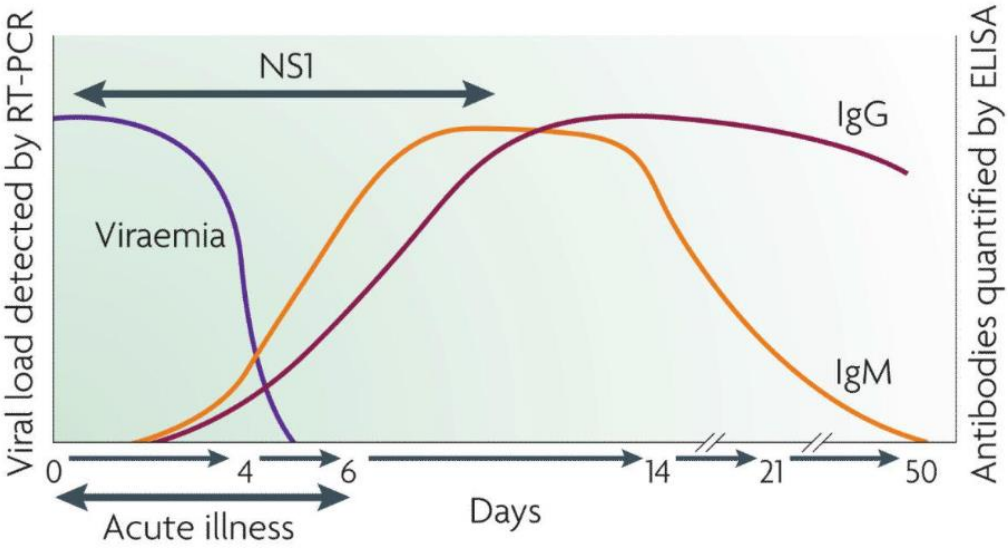

Figure 2.4 Clinical course of dengue. The viraemia during dengue infection is short and not detectable after five days. IgM levels can be detected as early as day 3 and peaks about 2 weeks after infection. On the other hand, IgG levels rise slower compared to IgM and are detectable after one week (Adapted from Guzman *et al.*, 2010).

2.1.4.1 Virus Culture

Dengue virus can be recovered from clinical specimens by inoculation into cell lines or mosquito larvae for viral propagation. The virus isolates or the RNA extracted from the virus can be confirmed with a dengue virus-specific immunofluorescence assay or real-time RT-PCR (Harapan *et al.*, 2020). Confirmation of dengue fever with this method is specific, but it could take days to weeks for the virus culture and confirmation assay. Another limitation is that virus culture has to be done within the first five days of illness onset as viable dengue virus is usually not detectable after the first five days (Muller, Depelsenaire and Young, 2017).

2.1.4.2 Molecular Identification

The molecular diagnosis uses RNA extracted directly from the clinical specimen without the need for prior culture. The RNA extracted is reverse-transcribed into cDNA or directly amplified for dengue identification by various assays, including the reverse transcription-PCR (RT-PCR) (Grobusch *et al.*, 2006), real-time RT-PCR (Mun *et al.*, 2019), and isothermal amplification (Kumar *et al.*, 2021). The molecular method is the most sensitive method for dengue diagnosis and is the only method to identify the dengue serotype. The sensitivity for PCR-based assays was around 83-100% (Gurukumar *et al.*, 2009; Najioullah, Viron and Césaire, 2014), which is in agreement with the guidelines published by WHO of around 80-100% (World Health Organization, 2009). The results from PCR-based methods can be obtained fast within 24 hours. However, many precautions are necessary to achieve reliable results. The primers used for amplification must be specific to dengue to prevent non-specific amplification. Specimen and reagent contamination can also cause false-positive results. The residual amplicons from previous amplifications have to be eliminated by using a stringent protocol during decontamination (World Health Organization, 2009). False-negative may occur due to primer-target mismatch, faulty sample collection and handling or low viral load in samples.

2.1.4.3 Antigen Detection

The antigen targeted for dengue detection is the dengue Non-structural 1 (NS1) antigen. NS1 can exist as membrane-bound or secretory form (Rosales Ramirez and Ludert, 2019). The secretory form of NS1, which is released by the

infected cells into the bloodstream, can be detected using either enzyme-linked immunosorbent assay (ELISA) or immunochromatographic strip test (rapid test) (Peeling *et al.*, 2010). The secreted NS1 can be detected in high concentrations, in clinical samples such as serum or plasma, for up to 9 days (Dussart *et al.*, 2006). NS1 can be detected in primary and secondary infections. However, NS1 levels in secondary dengue infection can only be detected over a shorter period due to active clearance by antibodies from the body (Muller, Depelsenaire and Young, 2017).

The sensitivity of the NS1 ELISA test was in the range of 56% to 89% (Dussart *et al.*, 2006; Aryati *et al.*, 2013). However, Aryati *et al.* (2013) found that NS1 detection sensitivity was as low as 4.2% when using a commercial NS1 ELISA kit. The authors hypothesised possible reasons for the large discrepancy observed to be due to geographical region, serotypes difference, and mishandling and storage of samples. Overall, the development of the NS1 rapid test has provided a useful method for early dengue diagnosis, which improves the management of dengue patients (World Health Organization, 2009; Muller, Depelsenaire and Young, 2017).

2.1.4.4 Serology

Dengue serology is based on the detection of IgG and IgM antibodies produced by the host against the dengue virus. Examples of serological assays include hemagglutination inhibition assay (HIA), enzyme-linked

immunosorbent assay (ELISA), complement fixation test, dot-blot assay, western blotting, indirect immunofluorescent antibody test, and plaque reduction neutralizing test (PRNT) (Muller, Depelsenaire and Young, 2017). Except for HIA and ELISA, the other methods are not routinely used due to their laborious and time-consuming procedures. Although IgG, IgM, IgA, and IgE are produced in response to dengue virus infection, only IgG and IgM are targets for routine laboratory testing (Peeling *et al.*, 2010). IgM can be detectable from the third day after the onset of symptoms, peaking about two weeks later. The IgG response is much slower, usually becoming detectable only after one week in primary infection. However, IgG levels may appear as early as the third day in secondary dengue infection (Muller, Depelsenaire and Young, 2017). After seroconversion, IgG levels remain detectable for several months. With both IgM and IgG levels, it is possible to determine a primary or secondary dengue infection (World Health Organization, 2009).

The haemagglutination inhibition assay (HIA) is a technique to detect the presence of dengue virus antigen based on the inhibition of red blood cells (RBCs) agglutination by anti-dengue antibodies. The agglutination is caused by the presence of the E protein of the dengue virus. The potency of inhibition is measured by the highest antibody dilution that prevents hemagglutination (World Health Organization, 2009; Harapan *et al.*, 2020). HIA has been routinely used for dengue diagnosis for a long time (Lukman *et al.*, 2016). Although HIA is simple and inexpensive, it has several limitations, such as unable to differentiate between dengue and other flaviviruses infection and

requiring sample pre-treatment to remove non-specific inhibitors of hemagglutination (Harapan *et al.*, 2020). Owing to these limitations, ELISA is replacing HIA as the preferred serology test for dengue diagnosis in the laboratory. The emergence of high-throughput ELISA and the availability of commercial ELISA kits have encouraged the use of ELISA for dengue diagnosis. While IgM antibody-capture ELISA is the preferred method for current infection diagnosis, the IgG antibody-capture ELISA enables current and past infection detection if paired acute and convalescent-phase sera can be collected (World Health Organization, 2009).

2.2 Pathogenesis of Severe Dengue

Pathogenesis is the development of diseases upon activation of the host's immune system by the pathogen. This complex pathogen-host interaction shows how invader and host adapt to each other. It will result in either the clearance of the pathogen or progression to severe manifestations of the disease in the host, which, in serious cases, might result in death due to overwhelming immune reactions towards the pathogen (*Nature Immunology*, 2007). Multiple theories of pathogenesis have been presented in the case of severe dengue, such as antibody-dependent enhancement, original antigenic sin, and cytokine storm (St. John, 2013).

2.2.1 Antibody Dependent Enhancement

Antibody-Dependent Enhancement (ADE) occurs when heterotypic antibodies bind to the dengue virus during secondary infection but fail to neutralise the virus. The sub-neutralising or non-neutralising heterotypic antibodies then assist the entry of the dengue virus into immune cells, such as monocytes, macrophages, and dendritic cells, via binding to the Fc receptor. Furthermore, the internalised viral-immune complex further suppresses the cellular innate immune response. The suppression of immune response leads to the massive production of viruses from the infected immune cells. The immune system counteracts the viruses by releasing inflammatory cytokines and vasoactive mediators, which causes plasma leakage and severe dengue (Kuczera *et al.*, 2018; Kulkarni, 2020). The sub-neutralising antibody of heterologous infection is low in avidity and has insufficient antibody concentration to trigger the threshold for inducing neutralisation. The mechanism of ADE in dengue infection is illustrated in Figure 2.5.

The protection provided against the same dengue serotype is lifelong or at least partially. Re-infection by homotypic dengue virus has been reported as well (Waggoner *et al.*, 2016). During homotypic dengue infection, memory B cells produce antibodies at a much faster rate and higher response than during primary infection, thus providing better protection (Balakrishnan *et al.*, 2011; Moi, Takasaki and Kurane, 2016). The severity of secondary dengue infection is dependent on the timing between primary and secondary infections. A longer time interval has been associated with more severe disease owing to the waning

broadly neutralising anti-dengue antibodies (Kulkarni, 2020). The early memory B cells (9-11 days after primary infection) are serotype-specific, while memory B cells detected after six months are serotype cross-reactive (Mathew *et al.*, 2011).

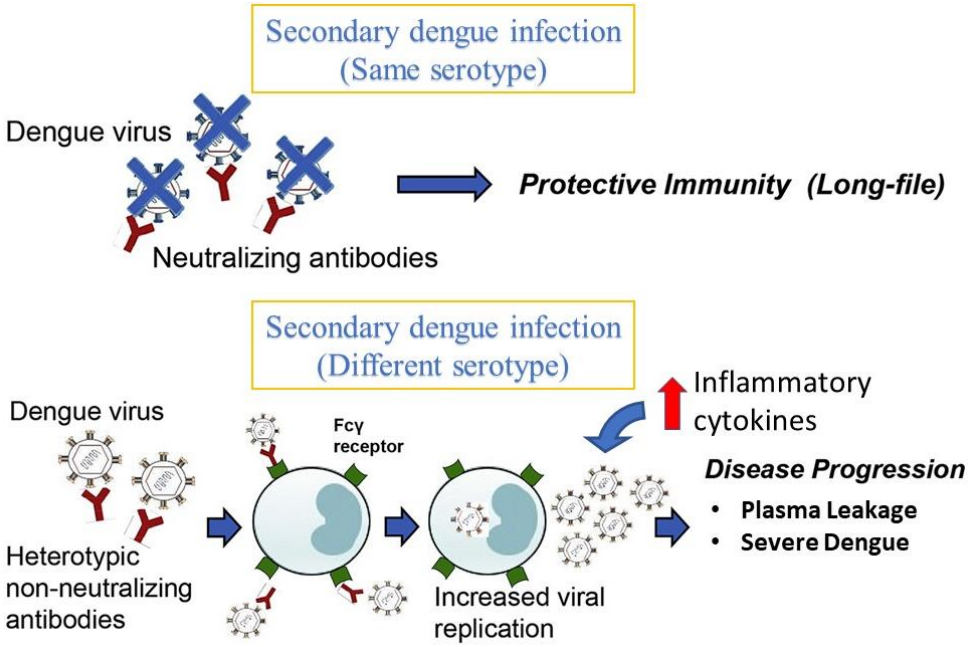

Figure 2.5 Antibody-dependent enhancement of dengue virus infection. Dengue infection from the same serotype of the dengue virus usually provides lifelong protection. Antibody-Dependent Enhancement occurs when heterotypic, non-neutralising antibodies bind to the dengue virus during secondary infection but fail to neutralise the virus. The non-neutralising antibodies then assist the entry of the dengue virus into immune cells via binding to the Fc receptor. The suppression of immune response leads to the massive production of viruses. The immune system counteracts the viruses by releasing inflammatory cytokines, which cause plasma leakage and severe dengue (Modified from Wang *et al.*, 2020).

Besides increasing the severity of secondary heterotypic infections, ADE is also involved in the pathogenesis of dengue in infants with acquired maternal dengue antibodies and dengue in the presence of cross-infection with other flaviviruses. In addition, it is a concern in the use of antiviral immunoglobulins and vaccination for dengue treatment and prevention, respectively (Kulkarni, 2020).

Infants passively acquire maternal anti-dengue antibodies from the mother during pregnancy and are protected up to 4 months old. On the other hand, infants infected with the dengue virus from 4 to 12 months are susceptible to ADE owing to the remaining maternal non-neutralising antibodies in the infants and the waning of neutralisation antibodies. The waning of neutralising antibodies could enhance dengue virus infection and increase the risk of severe dengue for older infants (Chau *et al.*, 2009).

Certain countries such as Brazil, Malaysia, and Singapore, have recorded simultaneous infections by different flaviviruses to the same person, for example, dengue virus and Zika virus infection. The same vector could possibly spread the different flaviviruses at the same time or in alternate outbreaks (Woon *et al.*, 2019). In Brazil, the vector mosquito (*Aedes aegypti*) spreads the dengue virus, Zika virus, and Chikungunya virus concurrently (Musso, Cao-Lormeau and Gubler, 2015). Consecutive infections by different flaviviruses may also trigger ADE. This could be due to the similarity of the amino acid sequence of

the envelope protein in different flaviviruses. The sequence difference between the dengue virus and the zika virus is only 41 - 46% (Dejnirattisai *et al.*, 2016). Katzelnick *et al.* (2020) found that children who had prior Zika virus had a 12.1% increased risk of dengue compared to only 3.5% for flavivirus-naive children.

Anti-viral immunoglobulin therapy has been used to treat severe dengue, but more effective immunoglobulin therapy is needed. Effective immunoglobulin therapy should be able to neutralise all four serotypes of the dengue virus. The antibodies should neutralise the dengue virus and should not bind to the Fc receptor on the immune cells (Chan, Ong and Ooi, 2013). The roll-out of vaccines to prevent dengue is facing a hurdle due to ADE. The dengue vaccination program by the Philippines government for school children faced a backlash when multiple deaths happened. The vaccine increased the risk of severe dengue in the seronegative individual who experienced natural dengue infection after vaccination (Thomas and Yoon, 2019). Thus, the Advisory Committee on Immunization Practices, US CDC, recommended vaccination for children (aged 9-16 years) with previous dengue infection and living in dengue-endemic areas (Paz-Bailey *et al.*, 2021).

2.2.2. Original Antigenic Sin

Original antigenic sin occurs when the second infection triggers strong antibody responses towards the previously infecting serotype than the currently

infecting serotype. After primary infection, memory B and T cells circulate in the bloodstream. After re-infection with a different dengue virus serotype, the activated memory B and T cells produce rapid immune responses. But, these responses might not be translated into the clearance of the virus from the host as the activated memory cells might not have optimal avidity against epitopes on the second different infecting serotype (Rothman, 2011). Memory B and T cells are also cross-reactive and will protect against all serotypes for a short period (around 2 - 3 months). After 2 - 3 months, the cross-reactive protection will wane and confer only serotype-specific protection (St. John and Rathore, 2019).

During the first infection with the dengue virus, naive CD4+ and CD8+ T cells are activated and differentiated into effector T cells to remove the dengue virus from the circulation through direct lysis of virus-infected cells or production of cytokines (Rothman, 2011). During secondary dengue virus infection, the body produces a stronger immune response against the previous infecting serotype compared to the current infecting serotype. Furthermore, the response to heterologous infection is serotype-specific, which leads to different effector functions by producing different cytokines and TCR signallings (Rothman, 2011). For example, when a full agonist peptide (same sequence as the first infecting serotype) is presented to the T cells, they respond by producing cytokines such as IFN-γ, TNF, and CCL4 and efficient lysis of infected cells. On the other hand, the T cell response when encountering a partial agonist peptide (with some sequence difference) is different with the production of high levels of CCL4, low levels of IFN-γ and TNF, and inefficient infected-cell lysis

(Rothman, 2011). The production of weak-affinity T cell responses is associated with severe dengue, as the T cells are inefficient at viral clearance and produce excess cytokines, which cause plasma leakage (St. John and Rathore, 2019).

Memory B cells mature against the infecting serotype with the highest specificity. Upon reinfection, the antibody response will produce much higher antibody titres and broader neutralisation of the four dengue virus serotypes. The titres of antibodies produced in the body against the first infecting serotype will be higher than the titres of antibodies against the currently infecting serotype (Rothman, 2011). Antibodies mediate dengue virus infection by neutralisation of the virally infected cells, antibody-dependent cell-mediated cytotoxicity, and antibody-dependent enhancement (Srikiatkhachorn, Mathew and Rothman, 2017). Antibodies usually recognise viral proteins such as E protein, precursor M, and NS1 proteins. During ADE, the binding to these proteins enhances the phagocytosis of the viral-antibodies complex into the cells with Fc receptors. Furthermore, the viral-antibodies complex suppresses the immune cell from secreting IFN-beta and IL-10, which promote viral replication (Ubol *et al.*, 2010). Activated B cells also secrete different cytokines such as IL-6, IFN-γ, TNF-α, IL-10 and IL-35. These cytokines are involved in the differentiation of memory T cells and negative regulation of immune responses, which further contribute to the pathogenesis of dengue infection (Srikiatkhachorn, Mathew and Rothman, 2017). Both innate and adaptive immune systems contribute to the pathogenesis of dengue and cause the overexpression of immune cells to secrete a large number of cytokines which leads to cytokine storm (Srikiatkhachorn,

Mathew and Rothman, 2017). The mechanism of the original antigenic sin of B and T cells in dengue infection is shown in Figure 2.6.

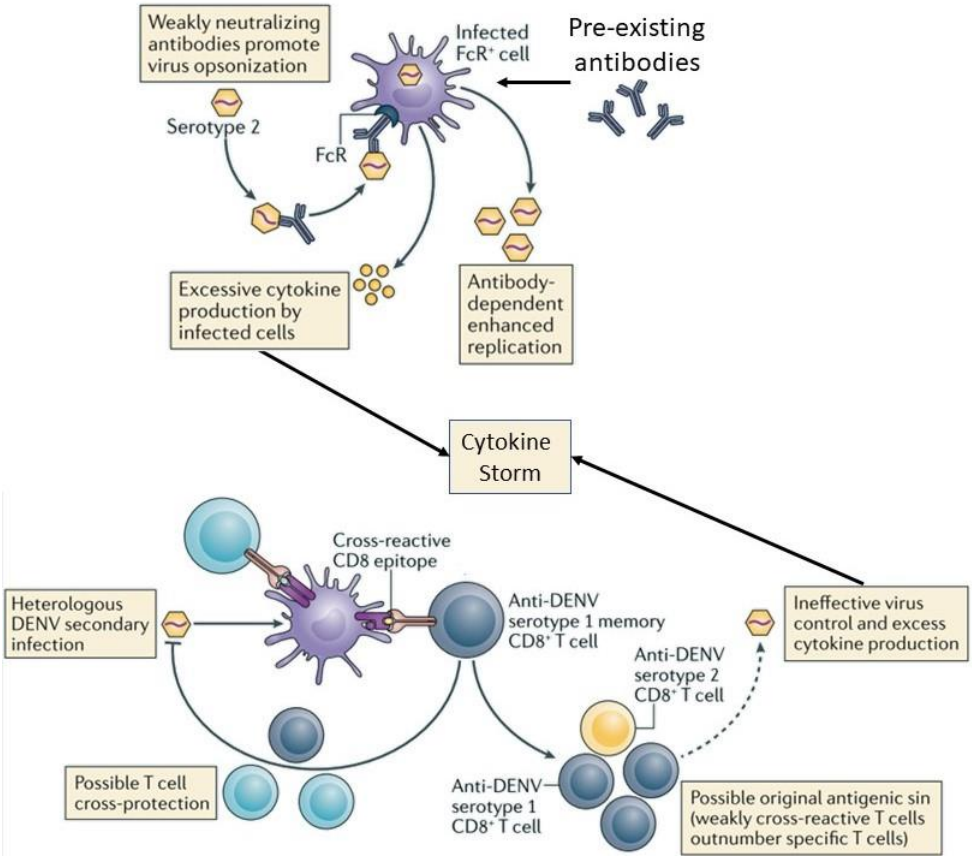

Figure 2.6: Original antigenic sin of dengue virus infection. Original antigenic sin occurs when the second infection trigger strong antibody responses toward the previously infecting serotype than the currently infecting serotype. After primary infection, memory B and T cells circulate in the bloodstream. After re-infection with a different dengue virus serotype, the activated memory B and T cells produce rapid immune responses. But, these responses might not be translated into the clearance of the virus from the host as the activated memory cells might not have optimal avidity against epitopes on the second different infecting serotype. The ineffective clearance of the dengue virus leads to excess production of cytokine situation called cytokine storm (Modified from St. John and Rathore, 2019).

Current literature is scarce on dengue pathogenesis. Most studies focused on *in vitro* cell culture models, animal models, and human clinical studies (Srikiatkhachorn, Mathew and Rothman, 2017). *In vitro* studies of dengue virus infection on different cell types such as endothelial cells, macrophages, and dendritic cells have shown that many cytokines are produced in response to the viral infection. Anti-viral cytokines that regulate immune cells or enhance vascular permeability all contribute to the pathogenesis of dengue. However, the findings from *in vitro* studies do not necessarily reflect the actual dengue pathogenesis *in vivo* (Bente and Rico-Hesse, 2006; Srikiatkhachorn, Mathew and Rothman, 2017).

Studies using animal models provide more details on dengue pathogenesis, but some animal models do not develop the clinical manifestations of dengue and do not support dengue virus replication as in humans (Zompi and Harris, 2012). Even with the use of some better representative mouse models, the findings in these studies still need to be validated because the mouse models still do not mimic severe dengue that occurs in humans (Srikiatkhachorn, Mathew and Rothman, 2017). In human studies, most investigators only identified biomarkers from the serum or plasma, where the levels of the biomarkers were expressed differentially during dengue and severe dengue (Srikiatkhachorn, Mathew and Rothman, 2017). Conflicting findings between studies were reported, which could be due to several factors such as differences in sample collection and storage, the timing of sample collection, and the

availability of clinical and laboratory data to support the case classification (Srikiatkhachorn, Mathew and Rothman, 2017).

2.3 Biomarkers

A biomarker is defined as an indicator of the medical state measured outside of the patient. The World Health Organization defines biomarker as "almost any measurement reflecting an interaction between a biological system and a potential hazard, which may be chemical, physical, or biological" (WHO International Programme on Chemical Safety, 1993; Strimbu and Tavel, 2010). In the context of severe dengue, an ideal biomarker should serves as an early indicator to identify severe dengue. Although the exact pathogenesis of severe dengue remains uncertain, the host immune responses are believed to be the main contributors to the development of severe dengue. This hypothesis is supported by the low viraemia in severe dengue, which indicates that the occurrence of severe dengue is related to immunopathology rather than the presence of the virus (John, Lin and Perng, 2015). In addition, the integrity of the endothelial cells remains intact, but the functionality is compromised by the secretion of various cytokines that increase the vascular permeability of endothelial cells. Thus, endothelial activation markers can be used as predictors of severe dengue (John, Lin and Perng, 2015).

2.3.1 Vascular Endothelial Growth Factors

Vascular endothelial growth factor (VEGF) is a signalling factor that promotes angiogenesis and the growth of vascular endothelial cells. VEGF is produced by different cell types such as macrophages, keratinocytes, and others (Johnson & Wilgus, 2014). It is also involved in normal body functions such as bone formation and development (Moghaddam et al., 2012). During wound repair, VEGF promotes the growth of vascular endothelial cells and the formation of new blood vessels, which are essential to support the newly formed tissue (Johnson & Wilgus, 2014). VEGF is encoded by a single VEGF gene whose product is alternatively spliced to produce different members of the VEGF family, including VEGF-A, VEGF-B, VEGF-C, VEGF-D, VEGF-E, VEGF-F, and PlGF (Hoeben et al., 2004).

VEGF is also known as the vascular permeability factor, which promotes microvascular hyperpermeability (Hoeben et al., 2004). Various studies reported elevated VEGF levels in DHF. VEGF also plays a role in plasma leakage in DHF, as in other viral diseases such as hantavirus pulmonary syndrome (Tseng et al., 2005; Srikiatkhachorn et al., 2006; Seet et al., 2009; Low et al., 2015; Thakur et al., 2016). Srikiatkhachorn *et al.* (2006) reported that VEGF regulates vascular permeability through binding to soluble VEGF receptor-2 (VEGFR-2) and concluded that the expression of soluble VEGFR-2 may be involved in DHF. On the other hand, Seet et al. (2009) reported that the level of circulating VEGF was lower in DF and DHF compared to controls, but the level of VEGFR-1 was higher in DHF than in DF. The authors suggested that the low level of circulating

VEGF could be due to the higher binding of VEGF to VEGFR-2 and that soluble VEGF receptor-1 (sVEGF-1) might be used as a predictive marker for DHF.

Tseng et al. (2005) reported that plasma VEGF in DHF patients was significantly elevated compared to dengue fever and non-febrile fever control groups. The authors further concluded that the activation of the fibrinolytic system involves the production of VEGF in dengue patients, which contributes to the pathogenesis of DHF (Tseng et al., 2005). In another paper by Thakur et al. (2016), the VEGF level in severe dengue patients was significantly higher compared to dengue patients and the healthy group. The authors grouped the levels of VEGF based on the day of collection and showed that the VEGF levels from Day 1 to more than nine days were increasing. The VEGF levels in severe dengue patients could be detected from Day 1 and were significantly higher than in the healthy controls. There was a huge increase in the VEGF levels from Day 4 (~50 pg/ml) to Day 5 (~350 pg/ml). This result showed that VEGF could be used as a predictive marker for progression to severe dengue (Thakur et al., 2016).

In another study on the diagnostic accuracy of VEGF in severe dengue patients admitted to Hospital Ampang and Serdang Hospital, Malaysia, the authors reported that it was statistically significant to use VEGF as a diagnostic marker on Day 2 and Day 3 of illness. The cut-off for VEGF levels was 19.03 - 50.53 pg/ml with a sensitivity of 80% - 100% and specificity of 76.47% - 80%, with the best cut-off to be used for VEGF diagnosis was 37.5 pg/ml (specificity

of 80% and sensitivity of 100%). The authors concluded that VEGF is best used as an additional parameter to support severe dengue diagnosis when used as a single biomarker (Low *et al.*, 2018).

2.4 Anti-VEGF Therapy

Anti-VEGF therapy is the treatment commonly used for treating cancer and ocular diseases (Meadows and Hurwitz, 2012; Khanna *et al.*, 2019). As its name implies, this therapy targets VEGF in several ways, such as binding to VEGF to block it from binding to the VEGF receptor, binding to the receptor to block initiation of signalling, and blocking the kinase activity of the receptors (Zirlik and Duyster, 2018). Examples of commonly used anti-VEGF are bevacizumab, pegaptanib, ramucirumab, sunitinib, and others. Bevacizumab is a recombinant humanized monoclonal antibody that functions as an anti-angiogenic by blocking the binding of VEGF-A to its receptor (Zirlik and Duyster, 2018). Bevacizumab is the approved treatment for colorectal cancer, breast cancer, glioblastoma and others (Meadows and Hurwitz, 2012).

From the literature search, only one paper studied the effects of anti-VEGF against severe dengue in a mouse model. AG129 mice were inoculated with dengue virus 2 to induce the severe dengue effects seen in humans, including capillary leakage and shock. The mice were treated with sunitinib (a VEGF receptor tyrosine kinase inhibitor) once or twice daily after infection. The results showed reduced mortality of mice treated with sunitinib compared to the

untreated mice. In addition, the authors showed that a combination of sunitinib and anti-TNF antibody provide protection from severe dengue infection and reduce vascular leakage. The survival rate of dengue virus-infected mice treated with both treatments was 80% on Day 8 compared to only 5% for untreated mice (Branche *et al.*, 2018).

2.5 Lateral Flow Immunoassay

Lateral flow immunoassay (LFIA or immunochromatographic strip test or rapid test) is a biosensing platform for the rapid detection of biomarkers (Koczula and Gallotta, 2016). The first commercial lateral flow immunoassay was the home pregnancy test kit in 1978 (National Institutes of Health, 2021). It is known for its rapid detection because it produces results within 5 – 30 minutes, and it is easy to be used by anyone without training. The World Health Organization (WHO) Sexually Transmitted Diseases Diagnostics Initiative (SDI) has identified the ideal rapid test criteria to be used in primary health care settings: ASSURED criteria (A: Affordable, S: Sensitive, S: Specific, U: User-friendly, R: Robust and rapid, E: Equipment-free, D: Deliverable to those who need them) (Peeling *et al.*, 2006). Although the use of LFIA is simple, the construction of the test kit is usually complicated because it requires knowledge of the use of suitable solid materials and biochemical reagents (Ching, 2015). Different biological samples could be used with LFIA, such as urine, serum, plasma, whole blood, and others (Koczula and Gallotta, 2016). This technology has been used for biomarkers detection in infectious diseases and other diseases,

toxic compounds detection, and monitoring of metabolites related to drug use (Liao and Li, 2010; Liu *et al.*, 2014; Ching, 2015).

2.5.1 Components of Lateral Flow Immunoassay

The lateral flow immunoassay strip is made up of different components such as a sample pad, conjugate pad, nitrocellulose membrane, where the test line and control line are, and an absorbent pad (Figure 2.7). Each component has its function according to the design of the test. The testing principle of lateral flow immunoassay starts with a testing material, a liquid sample containing the target analyte. The liquid sample will move across the different components of the strip through the capillary action and interact with multiple molecules dried on the strip. The test line is where the analytes conjugated to the molecules and produced a signal. The signal produced could be read as qualitative (read as positive or negative) or quantitative (measured by the colour intensity of the test line) (Posthuma-Trumpie, Korf and Van Amerongen, 2009).

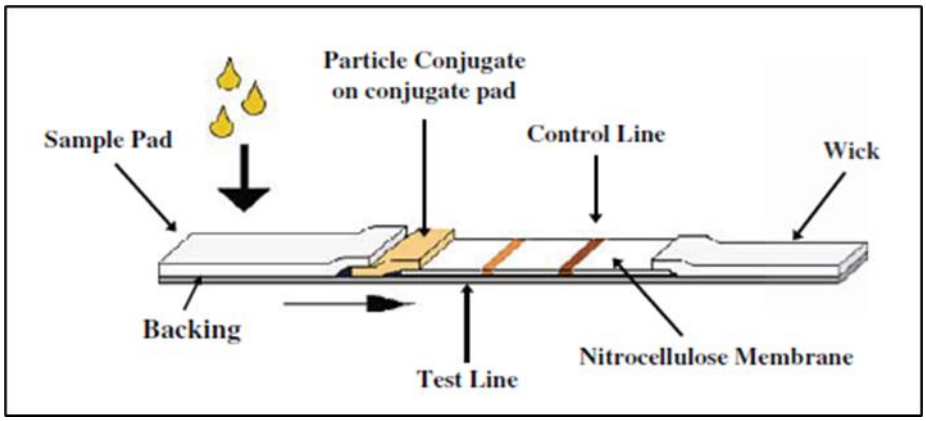

Figure 2.7 Lateral flow immunoassay strip. The lateral flow immunoassay strip is made up of different components such as a sample pad, conjugate pad, nitrocellulose membrane, where the test line and control line are, and absorbent pad (Adapted from O'Farrell, 2009).

The functions of the sample pad are receiving and ensuring the uniform distribution of the sample and controlling the rate of liquid entering the conjugate pad. The sample will migrate from the sample pad into the conjugate pad, where the captured reagent (usually antibody conjugated to coloured or fluorescent particles) will capture the analytes that pass through the conjugate pad. The analytes bound to the captured reagent migrate along the strip into the nitrocellulose membrane. The detection reagent is immobilised on the test line and the secondary antibody on the control line. The detection antibody on the test line will recognise the analytes bound to the captured antibody. The analytes will accumulate at the test line and produce a bright red signal (in the case of gold nanoparticles). The unbound captured antibody will bind to the secondary antibody on the control line. The remaining liquid and reagents will flow through the nitrocellulose membrane and be absorbed into the absorbent pad (Ching, 2015; Koczula and Gallotta, 2016).

As mentioned above, the signal produced from the lateral flow immunoassay can be detected qualitatively or quantitatively. Qualitative detection is by visual inspection of the test line. A positive result means the presence of the test line, and a negative result means the absence of the test line. The commonly used colour labels are gold nanoparticles (visible as red) and coloured latex (visible as different colours depending on the type of latex beads used). For quantitative detection, either a reader is used to record the colour intensity, or an image is taken before being analysed using imaging software. Many types of labels could be used for quantitative detection methods, such as colour labels (gold nanoparticles or coloured latex), fluorescent labels (quantum dots), and other labels (paramagnetic labels, enzymes labels, or carbon nanoparticles) (Koczula and Gallotta, 2016).

2.5.2 Applications of Lateral Flow Immunoassay

The importance of lateral flow immunoassay for dengue detection in dengue-endemic countries is undeniable. Due to the lack of diagnostic resources in many underdeveloped endemic countries, this rapid diagnostic test is crucial for the point-of-care dengue diagnosis. Lateral flow immunoassay is available commercially for dengue diagnosis to detect NS1 antigen, IgM, and IgG antibodies. Many dengue lateral flow immunoassay products are available worldwide, but some products suffer from poor quality in terms of low specificity and sensitivity. Popular products available in the market include Bioline Dengue Duo (Standard Diagnostics, USA), Panbio Dengue Duo Cassette (Alere, USA), and Standard QTM Dengue Duo (SD Biosensor, South Korea),

among others. Regrettably, the test performance quoted by the kit manufacturers is usually higher than the performance obtained in published studies. The sensitivity and specificity of the lateral flow immunoassay for dengue diagnosis in some comparison studies were in the range of 17.5 – 100% (Blacksell *et al.*, 2006; Hunsperger *et al.*, 2009; Pal *et al.*, 2015; Yow *et al.*, 2021).

During the early stage of LFIA usage, coloured particles were commonly used, such as coloured latex particles and gold nanoparticles (Amerongen *et al.*, 2018). Up until now, coloured particles are still commonly used in LFIA products due to their good detection performance, high sensitivity and can be used for either qualitative or quantitative detection (Calabria *et al.*, 2021). More recently, efficient label probes based on fluorescence or chemiluminescence have been used in the LFIA development. A few examples of efficient fluorescence probes used are dyes, quantum dots, and fluorescent nanoparticles. Commonly used chemiluminescence probes are HRP- 3,3',5,5'-tetramethylbenzidine (TMB) and HRP-luminol/H_2O_2. These probes are highly sensitive with low background and are suitable for quantitative measurement.

In a study by Parolo, Escosura-muniz, and Merkoci (2012), the authors compared different systems for the detection of IgG and determined the sensitivity of each system. For the lateral flow immunoassay, which uses the colour from the gold nanoparticles as the signal, the detectable signal was 50 ng/ml of human IgG with naked eyes. Different chemiluminescence HRP

substrates such as TMB, 3-amino-9-ethylcarbazole (AEC) and 3,3'-Diaminobenzidine tetrahydrochloride (DAB) were used as an enhancer to increase the detection signals. TMB and AEC were better substrates than DAB to enhance the detection limit. TMB and AEC substrate could detect human IgG signals at a limit of 5 ng/ml compared to 50 ng/ml when using the DAB substrate. The detection limit could be further enhanced when quantified using a portable strip reader. The signal read by the portable strip reader for gold nanoparticles was at a limit of 2 ng/ml. The limit of IgG detection with the use of enhanced substrate TMB, AEC and DAB was 200 pg/ml, 310 pg/ml and 1.6 ng/ml, respectively (Parolo, de la Escosura-Muñiz and Merkoçi, 2013). In another study, lateral flow immunoassay was used to detect cardiac troponin I (cTnI). The detection system was composed of HRP-conjugated gold nanoparticles, detection antibodies, and capture antibodies. The chemiluminescence reagents, luminol and H_2O_2 were added at the last step. The signal emitted was captured as an image. This detection system had a limit of detection of 5.6 pg/ml (Han and Kim, 2020).

2.6 Dielectrophoresis

Dielectrophoresis (DEP) is a technique that relies on electric fields to polarise bioparticles and manipulate their movement, including separating, focusing, trapping, and concentrating (Qian *et al.*, 2014; Rahman, Ibrahim and Yafouz, 2017). This technique has been used in medical science research, such as for isolation of cancerous from non-cancerous cells and manipulation of DNA and proteins. The advantages of this technique over others are that it is fast,

accurate, low-cost, requires small volumes of samples and can detect low concentration samples (Rahman, Ibrahim and Yafouz, 2017; Viefhues and Eichhorn, 2017b). The DEP technique could be used in a label-free condition, for example, to separate bacteria from yeast (Khoshmanesh *et al.*, 2012). Furthermore, DEP can be used in different systems with detection methods such as optical, electrochemical or microfluidic (Iswardy *et al.*, 2017).

Dielectrophoresis-based microfluidic is a technique that uses electric current to manipulate bioparticles or macromolecules present in liquid samples within a channel (Ramirez-Murillo, de los Santos-Ramirez and Perez-Gonzalez, 2021). A microfluidic system is referred to as the technique of fluid manipulation in the channel on a smaller (not necessary in micrometre) scale (Ramirez-Murillo, de los Santos-Ramirez and Perez-Gonzalez, 2021). Microfluidics is one of the main techniques used in the point-of-care (POC) test. Lateral flow immunoassay, as reviewed above, is also a technique based on a microfluidic system and is widely used worldwide in healthcare facilities and homes (Su *et al.*, 2015)

2.6.1 Theory of Dielectrophoresis

The DEP force is generated when a non-uniform electric field is applied on polarisable particles and creates a net force between the particles and the suspending medium (Figure 2.8) (Rahman, Ibrahim and Yafouz, 2017; Ramirez-

Murillo, de los Santos-Ramirez and Perez-Gonzalez, 2021). The DEP force is expressed by the following equation:

$$F_{DEP} = 2\pi r^3 \varepsilon_m \, Re[f_{CM}(\omega)] \, \nabla E^2,$$

where r is the particle radius, ε_m is the permittivity of the surrounding medium, $Re[f_{CM}(\omega)]$ is the real part of the Clausius–Mossotti (CM) factor and E is the electric field gradient. Clausius–Mossotti (CM) factor is expressed as:

$$f_{CM} = \frac{\varepsilon_p^* - \varepsilon_m^*}{\varepsilon_p^* + 2\varepsilon_m^*},$$

where ε_p^* is the complex permittivity of particles and ε_m^* is the complex permittivity of the surrounding medium. The frequency of the electric field can be altered to manipulate the effects of the permittivity. The relative polarisability between the particles and the surrounding medium will result in two different DEP forces, namely positive DEP (pDEP) and negative DEP (nDEP). pDEP occurs when the particle is more polarisable than the surrounding medium, and the particles will be attracted to the high electric field region. While for nDEP, the particle is less polarisable than the surrounding medium resulting in the particle being repelled from the high electric field region (Figure 2.9) (Cheng, Han and Chang, 2012).

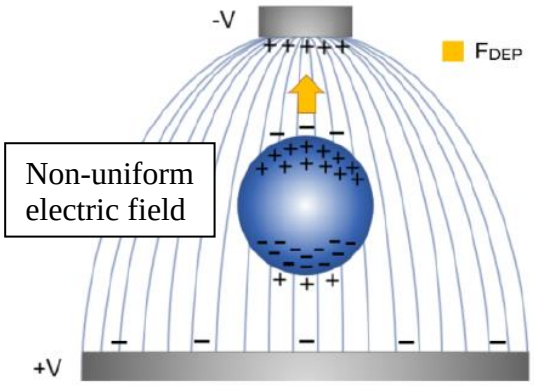

Figure 2.8 Theory of dielectrophoresis. The generation of DEP force occurs when a non-uniform electric field is applied on a polarisable particle and creates a net force between the particles and the suspending medium.

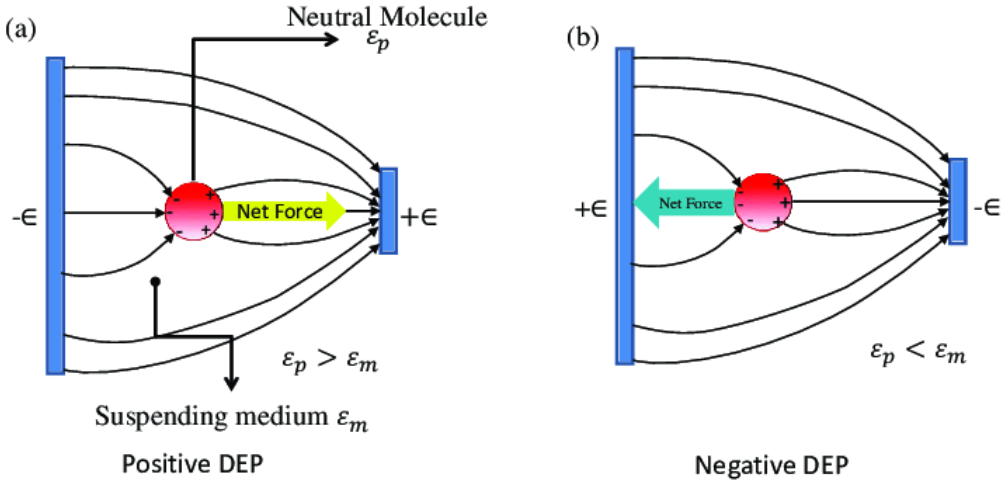

Figure 2.9 Movement of polarised particles after DEP response. Positive DEP ($\mathcal{E}_p > \mathcal{E}_m$) occurs when the particle is more polarisable than the surrounding medium and the particles will be attracted to the high electric field region. Negative DEP ($\mathcal{E}_p < \mathcal{E}_m$) is when the particle is less polarisable than the surrounding medium resulting in the particle being repelled from the high electric field region (Adapted from Manocha, Chandwani and Das, 2020).

2.6.2 Applications of Dielectrophoresis-based Microfluidics

There are various applications of DEP in the medical science field that have been explored, such as the detection of biomarkers, viruses, extracellular vesicles, bacteria, cancer cells, stem cells and DNA. Sanghavi *et al.* (2014) used frequency-selective DEP to preconcentrate neuropeptide Y and Orexin A by trapping them in the nanochannel before detection of the biomarkers using the electrochemical method. Negative DEP was applied for 10 seconds with the following parameter: 300 V_{pp}/cm at 3 MHz with 1.5 VDC/cm to trap the biomarkers away from the constriction and onto the nanochannel with fabricated electrodes for electrochemical detection. This platform can detect neuropeptide Y and Orexin A with high sensitivity and require small volumes of samples. The sensitivity for neuropeptide Y was 4 pM and for Orexin A was 22 pM (Sanghavi *et al.*, 2014).

In another study, the authors used a 3D DEP-based microfluidic chip for dengue virus detection. The microfluidic system, coupled with an optical detection device, used fluorescence-labelled antibodies to detect the presence of the dengue virus. Anti-flavivirus antibodies were conjugated on the silica beads before being trapped inside the microchannel using negative DEP force (Voltage: 15 V_{pp}/cm, frequency: 1 MHz). Once the silica beads were trapped within the tip of the electrode, the second injection consisted of an anti-dengue virus antibody and dengue virus was injected into the channel. As the antibody-virus conjugate flowed through the channel, it bound to the trapped silica beads, producing the fluorescence signal, which accumulated over time. The images of

the fluorescence signal observed under a fluorescence microscope were captured and analysed using imaging software for the intensity value. The technique used was able to detect the dengue virus rapidly within 5 minutes and detect dengue virus as low as 10^4 PFU/mL (Iswardy *et al.*, 2017).

Song et al. (2015) used a continuous-flow microfluidic DEP-based device to separate human mesenchymal stem cells (hMSCs) from their differentiated cells (i.e., osteoblasts). The device consisted of one cell sample inlet, one running buffer inlet, two outlets, and interdigitated electrode array within the channel. The DEP force was applied at an AC field of 7.2 V_{pp} and frequency of 3 MHz with a flow rate of 1.8 µl/min. The alternating, on-off electric field was used to produce the DEP effect. The osteoblasts experienced stronger pDEP forces and migrated laterally when the AC field was on and then forward, producing a zig-zag migration pattern towards the lower outlet. On the other hand, the undifferentiated hMSCs migrated on a straight course without any deflection towards the upper outlet. This method was able to purify hMSCs up to 84% and osteoblasts for up to 87% (Song *et al.*, 2015).

CHAPTER 3

MATERIALS & METHODS

3.1 Overview

This work is an extension of previous studies on biomarkers expression in dengue patients (Low, Gan and Ho, 2015; Low et al., 2018), supported by a UTARSRF grant (Programme title: Study on Traditional Chinese herbal compound, RIsk association from an epidemiological and psychosocial aspect and Predictive Efficacy of biomarkers in Dengue [STRIPED Study]), and UTARRF grant (Project title: Development of VEGF detection system based on electrochemical aptasensor, lateral flow immunoassay, and bead aggregation assay for comparison in rapid detection of severe dengue). The first part is to develop a rapid test for VEGF detection. Two methods were developed for VEGF detection, namely lateral flow immunoassay and 3D DEP microfluidic assay. The second part is to study the effects of VEGF and anti-VEGF on pulmonary microvascular endothelial cells using permeability assay and microarray gene expression study. This second part of the study was conducted to support the use of VEGF as a biomarker for the detection of severe dengue. It is necessary to study whether VEGF is one of the biomarkers responsible for the increase in endothelial permeability. In addition, the gene expression study using microarray could further confirm the effect of VEGF in the regulation of the genes involved in vascular permeability and relate VEGF with other biomarkers which are involved in increasing the permeability of endothelial cells. Based on

the hypothesis that anti-VEGF can reverse VEGF-induced permeability, the effects of anti-VEGF were studied using endothelial permeability assay and microarray genes expression study. The overall workflow in this study is illustrated in Figure 3.1.

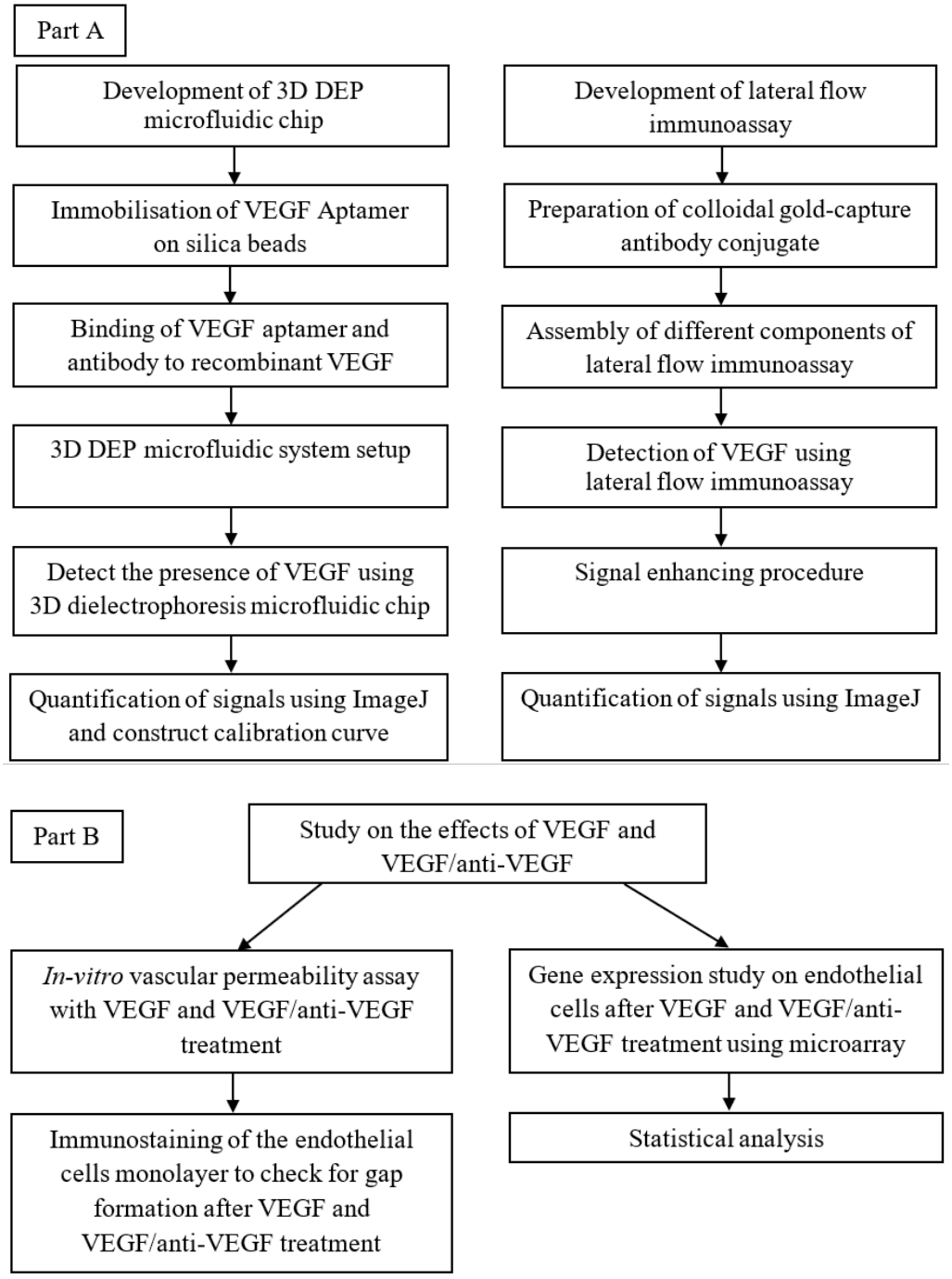

Figure 3.1 Flow chart of research methodology in this study.

3.2 Lateral Flow Immunoassay

3.2.1 Conjugation of VEGF Antibody to Gold Nanoparticles

All reagents were warmed to room temperature. The stock antibody of human VEGF monoclonal antibody (R&D Systems, USA) was diluted with the antibody diluent provided to 0.1 mg/ml. For each reaction, 42 µl of reaction buffer was added into a clean microcentrifuge tube, followed by 12 µl of the diluted antibody from the previous step, and the tube was thoroughly mixed. Forty-five microlitre of the mixture was transferred to a vial of gold nanoparticles and reconstituted by gently pipetting up and down. The mixture was allowed to stand at room temperature for 10 minutes. Five microlitres of Quencher was added to the mixture and mixed gently. The 50 µl of 20 OD gold-VEGF monoclonal antibody conjugate is then ready to be used. This protocol was recommended in the Goldlink Rapid Conjugation Kit's (BBI Solutions, UK) instruction manual.

3.2.2 Setting Up the Component of the Lateral Flow Immunoassay

Immunoassay strips were assembled using four components: sample pad, conjugate pad, nitrocellulose membrane and absorbent pad. The dimension of each component of the lateral flow immunoassay is shown in Figure 3.2. The sample pad was saturated with 0.01 M phosphate-buffered saline (PBS) solution (pH 7.4) containing 0.2% Tween-20 before being dried for 2 hours at 37^{o}C. The conjugate pad was saturated with a blocking solution consisting of 0.01 M PBS containing 2% bovine serum albumin (BSA), 0.5% sucrose, 0.5% Tween-20,

and 0.5% polyvinylpyrrolidone K30. The pad was then dried for 30 minutes at 37^{o}C.

After the sample and conjugate pad pre-treatment, 15 µl of gold- VEGF monoclonal antibody (concentration: 20 OD) and 40 µl of VEGF biotinylated antibody (concentration: 10 µg/ml) were jetted onto the conjugate pad and sample pad, respectively. Both pads were then dried for 2 hours at 37^{o}C. A drop (~2 µl) of Streptavidin (concentration: 1 mg/ml) and mouse polyclonal antibody (concentration: 1 mg/ml) were dispensed onto the test and control line, respectively, before drying for 2 hours at 37^{o}C. After drying, all components were stored in a closed petri dish with silica gel at 4^{o}C. Lastly, all three components (sample pad, conjugate pad, and absorbent pad) were assembled onto the nitrocellulose membrane strip, which comes with adhesives and plastic backing (Figure 3.3). This protocol was modified from Hou *et al.* (2015).

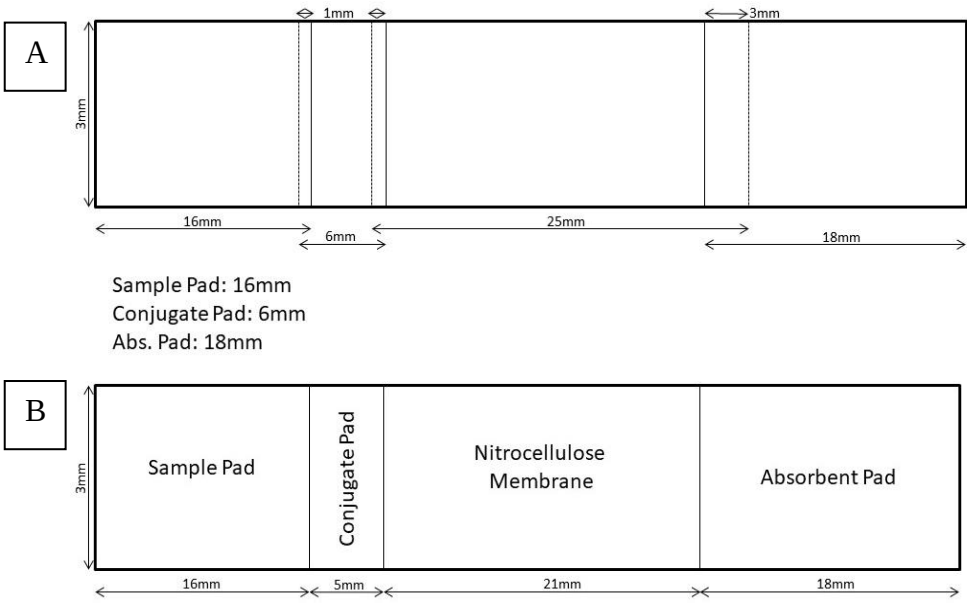

Figure 3.2 Design of the lateral flow immunoassay. (A) The setup of the lateral flow immunoassay with the measurements. There was some overlapping between segments to promote smooth flow from the sample pad toward the absorbent pad. (B) Final appearance of the lateral flow immunoassay inclusive of the overlapping measurement.

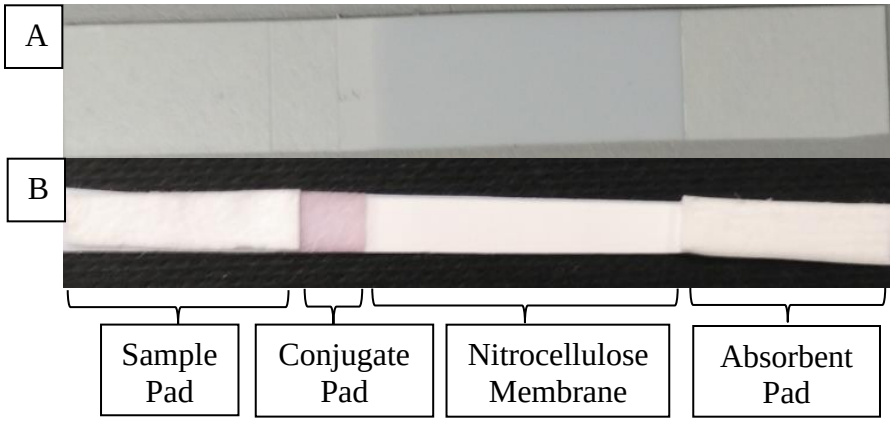

Figure 3.3 Lateral flow immunoassay (LFIA) strip. (A) The nitrocellulose membrane strip with adhesive and plastic backing. The adhesive cover can be peeled off, and different components of the LFIA can be placed on it. (B) The image of the self-assembled LFIA strip, consisted of four components: sample pad, conjugate pad, nitrocellulose membrane and absorbent pad (from left to right).

3.2.3 Samples Detection

Around 60 µl of recombinant VEGF at different concentrations (250, 100, 10, 1, 0.1 ng/ml) and PBS control was dispensed onto the fully assembled lateral flow immunoassay strip. The result was visible within 15 minutes. After 15 minutes, a red colour signal was seen on the test and control lines for samples. For the control, only the control line is visible. Each strip was subjected to a signal enhancing procedure using the silver enhancing kit as described in the section below. The image of the strips with signal were captured using a scanner (Canon, Japan). The images were then processed using ImageJ to produce intensity value.

3.2.4 Signal Enhancing Procedure

The test and control lines produced on the lateral flow immunoassay were enhanced using Silver Enhance Kit (Sigma, USA). Solution A and Solution B were mixed immediately before use at a ratio of 1:1. The gold-labelled section of the test and control lines was covered with the solvent mixture and stained for 5-10 minutes. After being stained, the strip was rinsed with distilled water. The strip was then fixed in sodium thiosulfate solution for 2 – 3 minutes before being rinsed again.

3.3 3D Dielectrophoresis Microfluidic Chip

The 3D DEP microfluidic chip for VEGF detection was developed during my 1-year research collaboration with Prof. Chang Hsien-Chang

(Biosensor Laboratory, Department of Biomedical Engineering, National Cheng Kung University, Taiwan) under TEEP@AsiaPlus Scholarship provided by the Ministry of Education, Taiwan. This work was used to apply for collaboration under the President's Forum of Southeast and South Asia and Taiwan Universities (SATU)'s 2018 Joint Research Scheme. This technique was previously used for yeast species identification (Cheng, Han and Chang, 2012) and dengue virus detection (Iswardy *et al.*, 2017).

3.3.1 Immobilisation of VEGF Aptamer on Silica Beads

One hundred microlitres (concentration: 1 mg/ml) of 1 µm silica beads was transferred from the stock solution into a 1.5 ml microcentrifuge tube with 1 ml distilled water. The silica beads were centrifuged at 6000 rpm for 5 minutes before removing the supernatant. One millilitre MES buffer (20 mM, pH 5.8) was added into the tube and vortexed. The silica beads were centrifuged at 6000 rpm for 5 minutes before removing the supernatant. While centrifuging the beads, 5 mM EDC/NHS mixture was prepared. After centrifuging the beads, 500 µl of EDC/NHS mixture was added to the silica beads and transferred to a 0.5 ml microcentrifuge tube. The tube contents were mixed using a rotation spinner for 30 minutes. Next, 300 µl of VEGF aptamer 1 (concentration: 1000 nM) (Sequence: NH_2-5'-TGT GGG GGT GGA CGG GCC GGG TAG A-3') were added into the beads and mixed by rotation spinner for 2 hours. After 2 hours, the mixture was centrifuged for 5 minutes at 6000 rpm, and the supernatant was removed. The mixture was washed with 1 ml of 0.05% BSA in PBS for 5 minutes at 6000 rpm. The silica beads were blocked with 0.05% BSA

for 30 minutes at room temperature. After blocking, the mixture was centrifuged for 5 minutes at 6000 rpm. The mixture was then washed with 1 ml PBS and centrifuged for 5 minutes at 6000 rpm. The silica beads were resuspended in 1 ml of PBS and stored at 4°C before being used. The schematic illustration of the immobilisation protocol is shown in Figure 3.4.

The efficiency of immobilisation of VEGF aptamer on silica beads was tested using the protocol described above, except that VEGF Aptamer 2 with fluorescence conjugate was used instead of VEGF Aptamer 1. The VEGF aptamer 2 with fluorescence conjugated to silica beads was run with the DEP microfluidic chip, and the beads were collected at the capturing electrode. The presence of a fluorescence signal at the tip of the electrode indicates the success of the immobilisation.

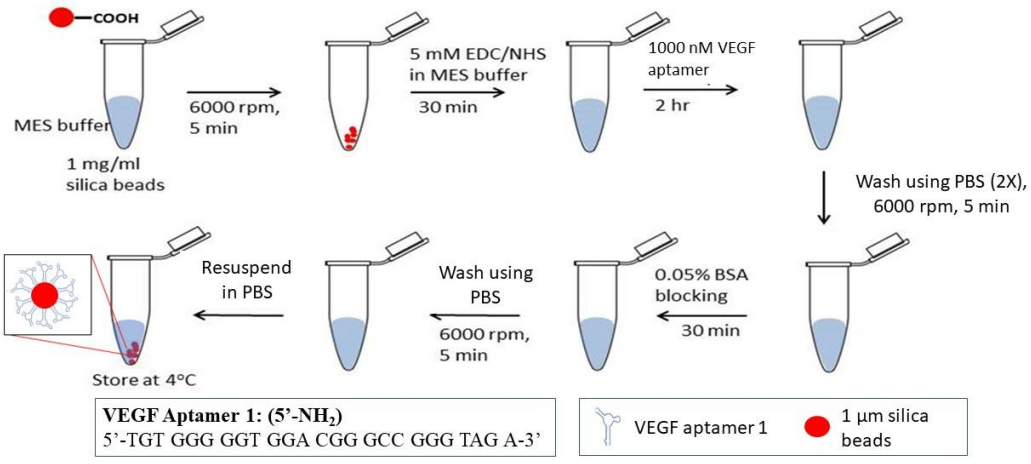

Figure 3.4 Immobilisation of VEGF aptamer on silica beads. The starting material was 1 µm silica beads with functional group -COOH (carboxylic group). The carboxylic-functionalised silica beads were modified with EDC/NHS to produce amine-reactive NHS ester, which reacted with the amine-functionalised VEGF aptamer 1 to produce VEGF aptamer 1-silica bead conjugate.

3.3.2 Binding of VEGF Aptamer and VEGF Antibody to Recombinant VEGF

VEGF Aptamer 2 (concentration: 500 nM) (Sequence:5'-ATACCAGTCTATTCAATTGGGCCCGTCCGTATGGTGGGTGTGCTGGCCAGATAGTATGTGCAATCA-3') was added to 200 µl of different concentrations of recombinant VEGF (5, 10, 50, and 100 pg/ml) and incubated for 2 hours at 37°C. After 2 hours, the mixture was stored at 4°C until further use. For antibody system, human VEGF antibody (concentration: 25 µg/ml) (R&D Systems, USA) was added to 200 µl of different concentrations of recombinant VEGF (5, 10, 50, and 100 pg/ml) and incubated for 30 minutes at 37°C. After 30 minutes, the mixture was stored at 4°C until further use. The schematic illustration of the binding protocol is shown in Figure 3.5.

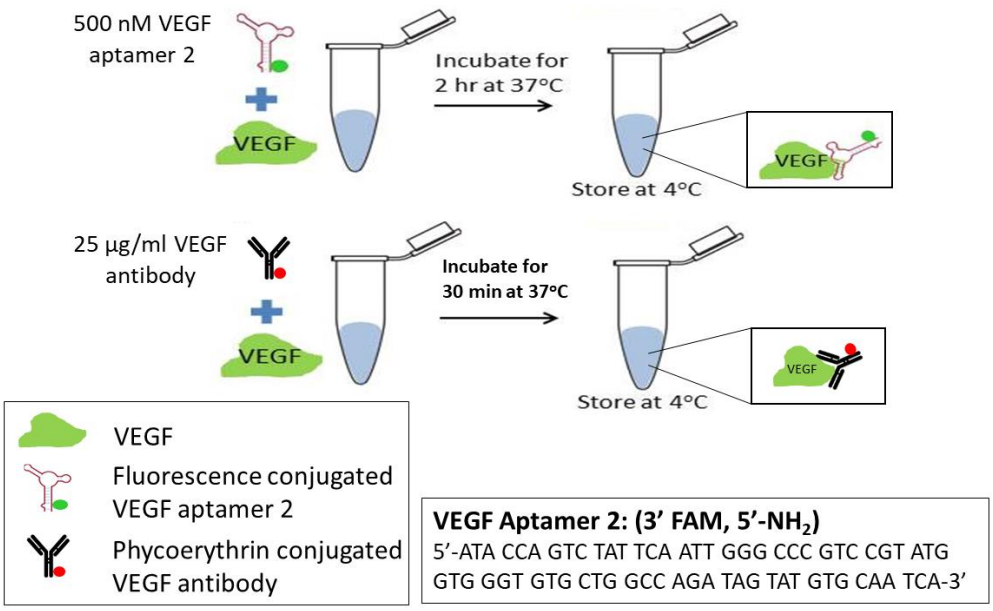

Figure 3.5 Binding of VEGF aptamer and antibody to recombinant VEGF (rVEGF). VEGF aptamer or VEGF antibody was added to rVEGF and allowed to react for either 30 minutes or 2 hours. The mixture can be used directly or kept at 4°C for future use.

3.3.3 3D DEP Microfluidic System Setup

The system was set up as shown in Figure 3.6A. The conductivity of all buffers was adjusted to 1 mS/cm before use. The first step was blocking the channel of the 3D DEP microfluidic chip using 1% BSA in PBS for 30 minutes. After 30 minutes, the BSA and bubbles formed in the channel were removed by running PBS through the channel. When the chip was ready, the sample was loaded into a glass syringe and placed on the syringe pump to control the flow rate of the sample injection. A flow rate of 0.4 µl/min was used for both samples injection. After setting up the flow rate, the syringe pump was turned on to start the injection of the first sample into the DEP microfluidic chip. The first injection consisted of silica beads conjugated with VEGF aptamer 1. When the beads reached the capturing electrode, the functional generator was switched on to supply the current at 15 V_{pp} and 1 MHz. Next, the guiding electrode was turned on to stop the conjugated silica beads from continuously being collected at the capturing electrode. The first injection was stopped before starting the second injection. The second injection consisted of conjugated VEGF aptamer 2 and VEGF. The silica beads collected at the capturing electrode will bind any VEGF aptamer 2-VEGF conjugates that flowed through. The fluorescence signal produced at the capturing electrode could be quantified from the image captured using a camera attached to the fluorescence microscope. The captured images were uploaded into ImageJ for fluorescence signal quantification.

3.3.4 Fluorescence Signal Quantification using ImageJ

The captured images were uploaded into ImageJ. Background subtraction was performed on the images using a built-in rolling stone algorithm. The area of interest was selected and used for all images for consistency. Then, the images were converted into a binary image and a threshold value was set so that the real signal could be differentiated from the background signal. The area of the fluorescence signal was measured, and the signal area against the concentration of VEGF was plotted (Figure 3.6C).

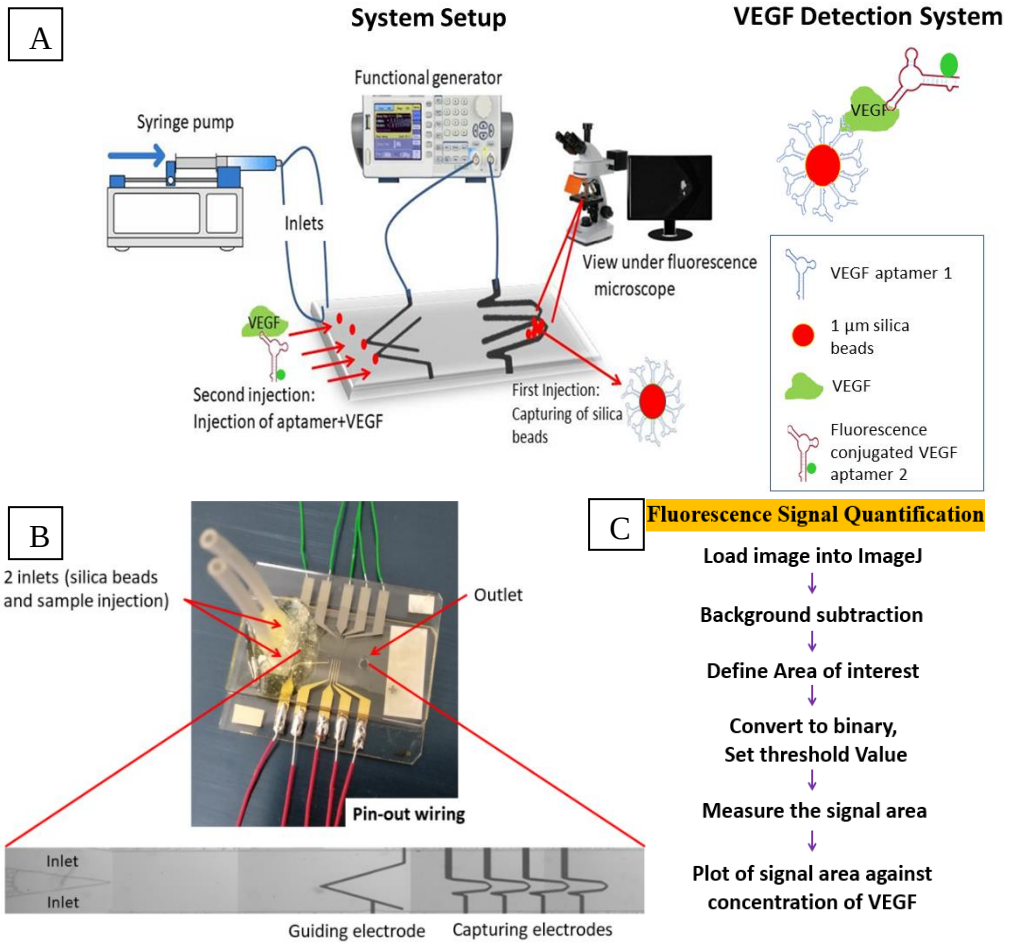

Figure 3.6 3D DEP Microfluidic Chip for detection of VEGF. (A) The image shows the setup of the instruments needed for the detection of VEGF. The function of the syringe pump was to inject the aptamer conjugated silica beads and aptamer conjugated VEGF into the 3D microfluidic chip. The functional generator supplied electrical current to the electrode to produce the dielectrophoretic effect. Parameters used to generate DEP were voltage: 15 Vpp, frequency: 1 MHz, and flow rate: 0.3 µl/min. When signals were produced from the interaction, the fluorescence microscope captured the generated signals into images. The image on the right shows the schematic reaction of binding that occurred after VEGF was captured by the aptamer at the tip of the electrode. (B) The image of the 3D DEP microfluidic chip and the design inside the channel. (C) The steps to quantification of the fluorescence signal using ImageJ.

3.4 Cell Culture & Maintenance

3.4.1 Culture of Human Pulmonary Microvascular Endothelial Cells

Human Pulmonary Microvascular Endothelial Cells (HPMECs) were primary cells isolated from the lung of a single donor. HPMEC was purchased from PromoCell (Germany). This primary cell was delivered as the first passage and in a cryopreserved form. The revived HPMEC was maintained in a Nunc tissue culture flask (Thermo Fisher, USA) containing Endothelial Cell Growth Medium MV2 (Promocell, Germany) and placed in an CO_2 incubator at 37^{o}C, 5% CO_2.

3.4.2 Thawing of Cryopreserved Human Pulmonary Microvascular Endothelial Cells

The recommended seeding density of HPMEC is 10,000 - 20,000 cells per cm^2. At least 9 ml of growth medium was added to each of the two T_{25} culture flasks. The flasks were placed in an incubator (37^{o}C, 5% CO_2) for 30 minutes to warm up the medium. The cryovial containing the cells was removed from the liquid nitrogen container. Then, the cryovial was immersed in a water bath (37^{o}C) up to the screw cap for 2 minutes. It was thoroughly rinsed with 70% ethanol under a laminar flow bench to disinfect the exterior. Then, 500 µl of the cell suspension was transferred to each culture flask containing the pre-warmed medium, and the flasks were placed in a CO_2 incubator (37^{o}C, 5% CO_2) for cell attachment. The medium was replaced after 16 - 24 hours and every two to three days. The cells were sub-cultured once they have reached 70 - 90% confluency.

3.4.3 Subculture of Human Pulmonary Microvascular Endothelial Cells

0.05% Trypsin-EDTA was placed in the water bath to warm up the reagent. The medium was carefully removed from the culture flask, and 1 ml PBS was added to the flask to wash the cells with the flask agitated for 15 seconds. PBS was removed from the culture flask, after which 3 ml 0.05% Trypsin-EDTA solution was added to the T_{75} culture flask (or 1 ml for the T_{25} flask). The cells were detached at room temperature and constantly examined under a microscope. The flask was tapped gently on the side to loosen the remaining cells when the cells started to detach. After the cells had detached, 3 ml Trypsin Neutralization Solution (TNS) was added to the flask surface. The flask was gently agitated to spread the TNS evenly. The cell suspension was carefully removed and transferred to a centrifuge tube. The cells were spun down for 3 minutes at 220 x g. The supernatant from the tube was discarded before 1 ml of the growth medium was added to the cell pellet. The cells were resuspended by carefully pipetting up and down. The cells were plated according to the recommended seeding density in a new culture flask containing a pre-warmed growth medium. Then, the flask was placed in an incubator (37^{o}C, 5% CO_2), and the media was changed every two to three days.

3.4.4 Cryopreservation of Human Pulmonary Microvascular Endothelial Cells

The HPMECs were sub-cultured according to the steps described in Section 3.4.3 until the cell pellet was obtained. Then, 1 ml of Freezing Medium Cryo-SFM (PromoCell, USA) was added to the cell pellet, and the cells were

resuspended gently. After being resuspended, the cell suspension was transferred into a cryovial. The cryovial was stored immediately in a Mr. Frosty Freezing Container (Nalgene, USA) at -80^{o}C overnight. The cryovial was transferred to liquid nitrogen tank the next day.

3.5 *In vitro* Permeability Assay

3.5.1 *In vitro* Permeability Assay using Cell Culture Insert Method

An *in vitro* permeability assay was performed as described elsewhere (Martins-Green, Petreaca and Yao, 2008). Human Pulmonary Microvascular Endothelial Cells (HPMECs) were cultured to 80% confluence before the cells were used for seeding on the cell culture inserts (Falcon, USA) placed in the wells of a 24-well microtiter plate. Before seeding, the inserts were coated with diluted Matrigel (Corning, USA) (at 3:1 ratio with cold DMEM culture medium), the bulk of which were immediately removed after coating. The insert with a thin film of Matrigel was then incubated at 37^{o}C for 30 minutes to solidify the Matrigel. Two hundred thousand endothelial cells in 100 µl medium were seeded on each insert. After 30 minutes of incubation at 37^{o}C, another 200 µl of culture medium was added to the insert, and 1 ml of culture medium was added to the well of the microtiter plate. The whole microtiter plate was then incubated in a CO_2 incubator at 37^{o}C for 24 hours. At the end of this incubation, another 2 x 10^5 cells were seeded into each insert. The cells were incubated in a CO_2 incubator at 37^{o}C for 24 hours before performing the vascular permeability assay.

The VEGF used in the permeability assay was recombinant VEGF protein (Merck, Germany), while the anti-VEGF was a human VEGF monoclonal antibody (R&D Systems, USA). In VEGF treated wells, only VEGF was added into the upper and lower chambers to a final concentration of 200 pg/ml. In anti-VEGF treated wells, both VEGF and anti-VEGF were added into the upper and lower chambers to a final concentration of 200 and 400 pg/ml, respectively. Next, FITC-Dextran (3kD, Sigma-Aldrich, USA) was added to the lower chamber to a final concentration of 10 µg/ml. Triplicates were prepared for treated and untreated wells. At different time intervals (0, 5, 15, 30, 45, 60, 120, and 180 minutes after treatment), 10 µl of culture medium from the upper chamber was removed and diluted with 90 µl water for transfer to a 96-well plate. After removing the medium from the last time point, the fluorescence intensity of each sample was quantified using a fluorescence microplate reader (Tecan, Switzerland) with excitation wavelength at 485 nm and emission wavelength at 535 nm. The permeability of endothelial cells was measured based on the FITC-dextran signal that passed through the endothelial cells. The higher the fluorescence signal, the higher the permeability of endothelial cells in allowing FITC-Dextran to pass through the endothelial cells to the upper chamber. The in vitro permeability assay procedures are illustrated in Figure 3.7.

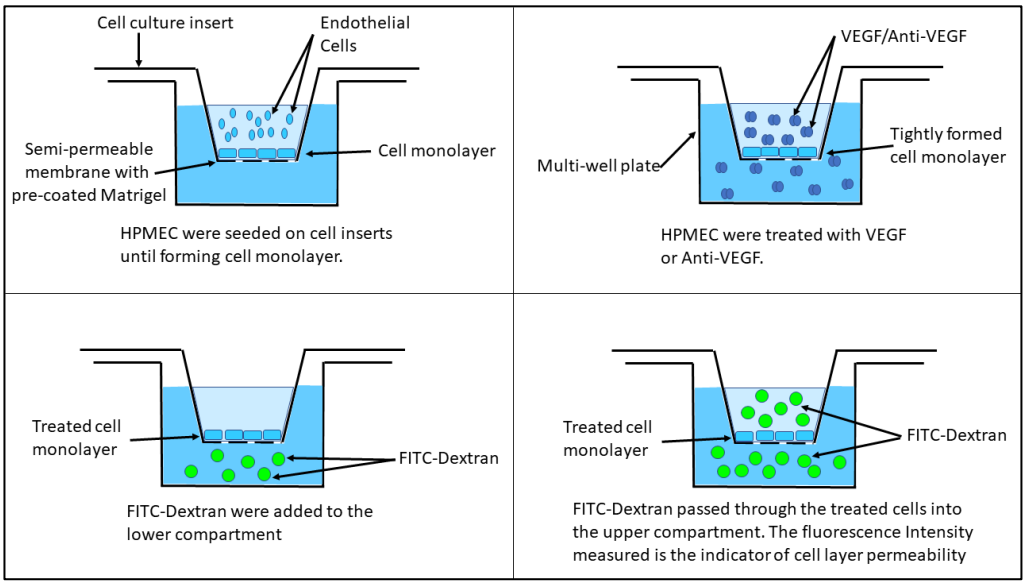

Figure 3.7 *In vitro* permeability assay using cell culture insert method. HPMEC were seeded on cell culture inserts coated with Matrigel and formed a monolayer of cells covering the surface of the whole insert. Three types of treatments (untreated, VEGF treatment, and VEGF/anti-VEGF treatment) were used in this assay. After 24 hours from the last seeding, the cells were ready to be used for permeability assay. The treatments were added before the FITC-Dextran. After each time interval (0, 5, 15, 30, 45, 60, 120, and 180 minutes), 10 µl of media were transferred out into a 96-well plate and diluted with 90 µl of distilled water. The fluorescence intensity of the media removed from each treatment and time point was read using a microplate reader.

3.5.2 Immunofluorescence Staining of the Treated and Untreated HPMEC

An immunofluorescence staining procedure was performed as described elsewhere (Martins-Green, Petreaca and Yao, 2008). HPMECs were plated onto Matrigel-coated cell culture inserts and treated with VEGF, VEGF/anti-VEGF or left untreated, as described above. First, the culture medium was removed from the upper and lower chambers of the inserts. Each insert was rinsed twice with PBS. Then, the cells were fixed for 30 minutes with 4% paraformaldehyde in PBS and then washed twice with PBS for 5 minutes each time. The cells were incubated in 0.1 M glycine in PBS for 10 minutes to quench free paraformaldehyde radicals and then washed twice with PBS for 5 minutes each

time. Next, the cells were permeabilised with diluted Perm/Wash solution (BD Biosciences, New Jersey) for 15 minutes at room temperature. The cells were incubated for 30 minutes in 10% goat serum (100 µl/well) to block non-specific binding of the secondary antibody and further incubated for 1 hour with 1:200 anti-PECAM mouse antibody in PBS containing 0.1% BSA. The cells were washed three times with PBS containing 0.1% BSA before staining for 1 hour with 1:100 goat anti-mouse FITC in PBS containing 0.1% BSA. Three more washes were made with PBS containing 0.1% BSA to remove any remaining antibodies. Cell nuclei were stained with DAPI for 30 minutes at room temperature. After DAPI staining, the same washing steps with PBS were performed. Lastly, the permeable membrane was removed from the cell culture insert with a clean scalpel and placed with cells facing up onto a clean glass slide. The glass slide was mounted with a fluorescence mounting medium (Dako, Denmark) for cell visualisation under an inverted fluorescence microscope (Carl Zeiss, Germany).

3.6 Gene Expression Study of VEGF and Anti-VEGF Treatment on Endothelial Cells

3.6.1 Ribonucleic Acid (RNA) Extraction

The RNAs from HPMECs treated with VEGF, VEGF/anti-VEGF and untreated were extracted using Ribospin II RNA Purification Kit (GeneAll, South Korea). The cells were harvested using a cell scraper and pelleted by centrifugation at low speed (below 800 x g) for 5 minutes. After discarding the supernatant, 350 µl of buffer RAL were added to the tube and the sample was

lysed by pipetting up and down. Seventy percent ethanol (350 µl) was added to the lysate and mixed well by pipetting. The mixture was transferred to a mini spin column (Type F). The column was centrifuged at 10,000 x g for 1 minute at room temperature. The pass-through was discarded, and the mini spin column was reinserted back into the collection tube. Buffer RW (350 µl) was added into the column, and centrifuged for 30 seconds at 10,000 x g. The pass-through was discarded, and the mini spin column was reinserted back into the collection tube. DNase I reaction mixture (70 µl) was pipetted onto the centre of the spin column membrane and incubated for 10 minutes at room temperature. Buffer RW (350 µl) was added into the column and centrifuged for 30 seconds at 10,000 x g. The washing procedure was repeated twice with 500 µl of buffer RSW, after which the column was centrifuged at full speed (10,000 x g) for 1 minute to remove any residual wash buffer. The mini spin column was then placed into a new 1.5 ml microcentrifuge tube. Nuclease-free water (50 µl) was pipetted onto the centre of the membrane in the mini spin column. The column was left to stand for 1 minute and then centrifuged at 10,000 x g for 1 minute at room temperature.

3.6.2 Assessment of Concentration, Purity, and Integrity of Extracted RNA

The concentration, purity, and integrity of the extracted RNAs were determined before being subjected to microarray analysis. The concentration and purity of RNA samples were determined using the Nanophotometer UV/VIS spectrophotometer (Implen, Denmark). The quality of RNA was determined by gel electrophoresis and 2100 Bioanalyzer (Agilent, USA). For RNA gel electrophoresis, 1.5% agarose gel was prepared in 1X TAE buffer. Five hundred

nanogram of sample was loaded into one well. One microgram of single-stranded RNA (ssRNA) ladder (New England Biolabs, USA) was loaded onto the gel with the samples. The gel electrophoresis was run at 40 V for 70 minutes in 1X TAE buffer. At the end of the electrophoresis, the gel was stained with GelRed (Biotium, USA), visualised, and photographed under a UV transilluminator (Analytik Jena, USA).

3.6.3 Gene Expression Study on Treated and Untreated HPMEC using Microarray

The RNA extracted from untreated and treated HPMEC cells were subjected to microarray analysis using SurePrint G3 Human Gene Expression v2 8x60K Microarray (Agilent, USA) with 50,599 probes covering 24,588 genes available in RefSeq. For this analysis, 10 – 200 ng of total RNA were used to reverse transcribed to cDNA. Then, the cDNA was amplified and labelled with Cy3 fluorescence to produce a final product of Cy3 labelled-complementary RNA (cRNA). The cRNA was then purified using RNeasy Mini Kit (Qiagen, Germany), fragmented at 60^{o}C for 30 minutes and then loaded onto the microarray slide for hybridisation at 65^{o}C for 17 hours. After hybridisation, the slide was washed with Gene Expression Wash Buffer I and II to remove any non-hybridised cRNA. Then, the slide was slotted into the holder and scanned immediately using Agilent SureScan Microarray Scanner and Agilent Scan Control 9.1.3 software. The microarray scan image was extracted using the Agilent Feature Extraction Software. The extracted txt files were then analysed using GeneSpring software Version 14.9.

The txt files loaded into the software were normalised using quantile normalisation to reduce the variation in the distribution of samples. The next step was to filter by expression to remove saturated or background signals. The cut-off was set at 20 – 100%. After pre-processing of the data, statistical analysis was performed on the data. The One-way ANOVA test was chosen to compare the three samples, namely, Untreated, VGEF treated, and VEGF/anti-VEGF treated. The fold change pairing options for comparison were as follows: VEGF/anti-VEGF treated vs Untreated, and VEGF treated vs Untreated. Subsequently, the results were presented as fold change. Lastly, processed data were subjected to Gene Ontology and DAVID analysis to find out the set of gene sets that contributed to certain functions.

3.6.4 Validation of Differentially Expressed Genes in Microarray Analysis using qRT-PCR

3.6.4.1 Complementary Deoxyribonucleic Acid (cDNA) Conversion

The RNA extracted from treated and untreated cell samples were converted to cDNA before being used for validation using qRT-PCR. cDNA conversion was performed using AffinityScript QPCR cDNA Synthesis Kit (Agilent, USA). The cDNA synthesis reaction was prepared in a microcentrifuge tube by adding in order the components shown in Table 3.1. After each reaction tube was prepared, the tube was placed in a Veriti™ 96-well thermal cycler (Applied Biosystems, USA) with the conditions shown in Table 3.2.

Table 3.1 The reagents used in cDNA conversion.

Components	**Volume**	**Final Concentration**
2x First strand master mix	10.0 µl	1x
oligo(dT) primer (100 ng/µl)	1.7 µl	170 ng
random primers (100 ng/µl)	0.3 µl	30 ng
AffinityScript RT/ RNase Block enzyme mixture	1.0 µl	-
Total RNA	x µl	1 µg
RNase-free water	Top up to total 20 µl	-

Table 3.2 Thermal cycler conditions used for cDNA synthesis.

Steps	**Temperature**	**Time**
Primer Annealing	25°C	5 minutes
Reaction	42°C	15 minutes
Termination	95ºC	5 minutes
Hold	4ºC	∞

3.6.4.2 Quantitative Real-Time Polymerase Chain Reaction (qRT-PCR)

The converted cDNA from treated and untreated cell samples were used for the validation of the upregulated and downregulated genes indicated in the microarray. Random genes were selected from the top 20 upregulated and downregulated genes for validation. One microgram of RNA from each treated cell sample was reverse transcribed as described above. The cDNA obtained was used to perform qRT-PCR using the primers for the following genes: CXCL2, CSF3, IL23A, CSF2, SELE, F3, CXCL3, TRIL, CH25H, and PDK4. GAPDH was used as the housekeeping gene. The primer sequences are listed in Table 3.3. Each qRT-PCR reaction was prepared in a microcentrifuge tube by adding the components in order as listed in Table 3.4. After they were prepared, the tubes were mixed gently without creating bubbles and centrifuged briefly. The tubes were placed in the StepOnePlus Real-Time PCR machine (Applied Biosystems, USA). The cycling conditions for qRT-PCR were set up as shown in Table 3.5. This protocol was according to the manufacturer's instruction manual. CT value was obtained for each sample, and $2^{-\Delta\Delta Ct}$ method was used to determine the relative changes in gene expression for the samples (Livak and Schmittgen, 2001).

Table 3.3 List of primers used in qRT-PCR.

Primers	**Forward Primer**	**Reverse Primer**	**Reference**
CH25H	5’-TCC TGT TCT GCC TGC TAC TCT TC-3’	5’-GGT ACA GCC AGG GCA CCT T-3’	(Tuohimaa *et al.*, 2013)
CSF2	5'-AGA AAT GTT TGA CCT CCA GGA-3'	5'-TTG CAC AGG AAG TTT CCG-3'	(Sjölinder *et al.*, 2012)
CSF3	5'-GCT TGA GCC AAC TCC ATA GC-3'	5'-TTC CCA GTT CTT CCA TCT GC-3'	(Sjölinder *et al.*, 2012)
CXCL2	5'-AAC CGA AGT CAT AGC CAC AC-3'	5'-AGG AAC AGC CAC CAA TAA GC-3'	(Mai *et al.*, 2016)
CXCL3	5'-CGC CCA AAC CGA AGT CAT AG-3'	5'-GCT CCC CTT GTT CAG TAT CTT TT-3'	(Afshari *et al.*, 2019)
F3	5'-GCC AGG AGA AAG GGG AAT-3'	5'-CAG TGC AAT ATA GCA TTT GCA GTA GC-3'	(Mälarstig *et al.*, 2003)
IL23A	5'-GAC ACA TGG ATC TAA GAG AAG AG-3'	5'-AAC TGA CTG TTG TCC CTG AG-3'	(Jiang *et al.*, 2016)
PDK4	5'-TCC ACT GCA CCA ACG CCT-3'	5'-TGG CAA GCC GTA ACC AAA A-3'	(Edge *et al.*, 2015)
SELE	5'-AGC CCA GAG CCT TCA GTG TA-3'	5'-CTC CAA TAG GGG AAT GAG CA-3'	(Giebe *et al.*, 2017)
TRIL	5'-CCT CGG CGG CAA CTT CAT AA-3'	5'-AGA GCG GAT CTG GTT GTA CTG-3'	-*
GAPDH	5’-GAA ATC CCA TCA CCA TCT TCC AGG-3’	5’-GAG CCC CAG CCT TCT CCA TG-3’	-*

*The primer sequences were verified with Primer-Blast shown to be specific to the gene. Primer-Blast results are shown in Appendix F.

Table 3.4 The reagents used in qRT-PCR.

Reagents	**Volume (µl)**	**Final Concentration**
2× SYBR green QPCR master mix	10	1x
Forward primer	0.5	250 nM
Reverse primer	0.5	250 nM
Diluted reference dye*	0.3	300 nM
cDNA (5ng/µl)	2.0	10 ng
RNase-free H_2O	6.7	-
Total	20	

*Reference dye was diluted in 1:50 using nuclease-free PCR-grade water and was prepared fresh each time before use.

Table 3.5 Thermal cycler conditions used for qRT-PCR

Steps	**Temperature**	**Time**	**Cycle**
Initial Denaturation	95°C	3 minutes	1
Denaturation	95°C	5 seconds	40
Annealing/Extension	60°C	10 seconds	
Melt Curve	95°C	15 seconds	1
	60°C	1 minute	
	60-95°C	15 seconds	+2ºC/cycle

3.7 Statistical Analysis

For lateral flow immunoassay, the statistical difference between the signal intensity of different concentrations of VEGF and control was calculated using one-way ANOVA with Dunnett's post-hoc test. P-values of less than 0.05 were considered statistically significant. Statistical difference between untreated and treated cells in the permeability assay was calculated using student t-test. P-values of less than 0.05 were considered statistically significant. The statistical analyses were carried out using GraphPad Prism7, and the graphs were drawn using Microsoft Excel.

CHAPTER 4

RESULTS

4.1 Lateral Flow Immunoassay for Detection of VEGF

The setup for VEGF detection using lateral flow immunoassay with different reagents is shown in Figure 4.1. The reaction started once the VEGF sample was applied to the sample pad. The human VEGF biotinylated antibodies on the sample pad captured any VEGF it encountered. The VEGF-VEGF biotinylated antibodies moved towards the conjugate pad via capillary action. At the conjugate pad, the VEGF-VEGF biotinylated antibodies bound to the gold-VEGF monoclonal antibodies upon contact. The mobile phase carried the VEGF-antibody conjugates along the nitrocellulose membrane. The VEGF-VEGF antibodies bound to the streptavidin in the test line and remained there. The gold-VEGF monoclonal antibodies that did not bind to VEGF passed through the test line and were bound to the mouse IgG polyclonal antibodies at the control line. The remaining reagents and unbound molecules were carried along to the absorbent pad.

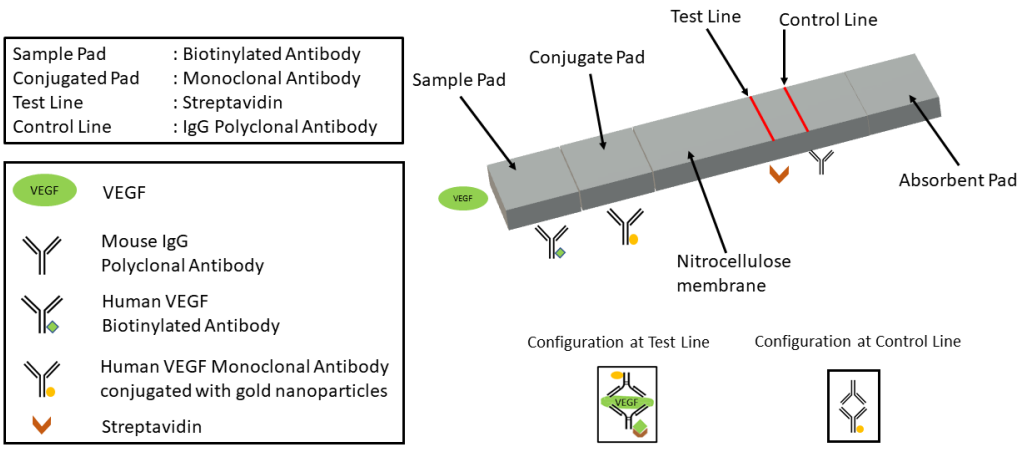

Figure 4.1 The setup of lateral flow immunoassay for the detection of VEGF. The different compartments of lateral flow strip and the different reagents used or dried on the strip. The configuration of VEGF, VEGF antibodies and streptavidin at test line and configuration of antibodies at control line are shown above.

Different concentrations of VEGF (0.1, 1, 10, 100, 250 ng/ml) were used. PBS was included as a control. The signal at the test and control line was further enhanced by using silver kit staining. After enhancement, the sample pad, conjugate pad, and absorbent pad were removed before scanning the strip into an image. The images were analysed using ImageJ to get the intensity value. Based on the signal intensity observed from the lateral flow strips, the test detected VEGF concentrations from 10 ng/ml and above (Figure 4.2). Using the quantitative method, the lowest VEGF concentration that could be differentiated from the control was 100 ng/ml.

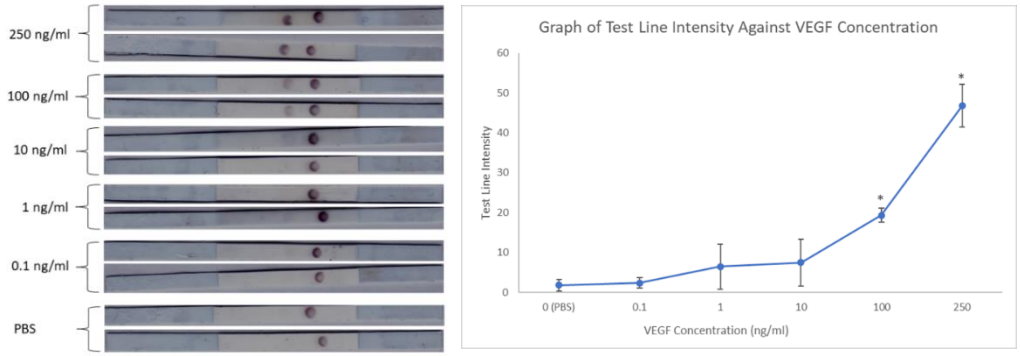

Figure 4.2 Lateral flow immunoassay for the detection of VEGF. Five different concentrations of VEGF (250, 100, 10, 1, and 0.1 ng/ml) and 0 ng/ml (PBS) as control were used. The left image shows lateral flow immunoassay strips with signal enhanced with silver enhancing kit. The right image shows the graph plotted for test line intensity against different VEGF concentrations. Statistical analysis was performed using One-way ANOVA with Dunnett's post-hoc test. *denotes significance increased compared to control, $p<0.05$.

4.2 3D Dielectrophoresis Microfluidic Chip

The first step in 3D DEP dielectrophoresis microfluidic assay was to inject the silica beads conjugated with a VEGF aptamer. Once the silica beads reached the electrode, the electric field was turned on. Negative DEP force was generated at the electrode and repelled any silica beads. At the same time, hydrodynamic drag force from the sample buffer flow was generated and pushed the silica beads forward. When both DEP and hydrodynamic force were at equilibrium, the beads were trapped at the tip of the electrode (Figure 4.3). When the second injection started, the VEGF-aptamer conjugate flowed through the channel and bound to the silica beads. A stronger electric field had built up at the front part of the collected beads. When VEGF flowed through the channel, it would be absorbed into the assembled beads and bound to the aptamer immobilised on the beads. The fluorescence signal accumulated over time as more VEGF bind to the aptamer.

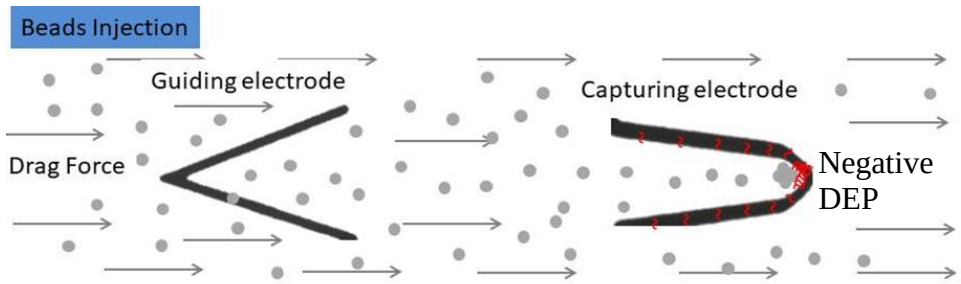

Figure 4.3 The beads collected at the tip of the electrode. The silica beads from the first injection were collected at the tip of the electrode due to the negative DEP force (repulsion force from the electrode) and the hydrodynamic drag force from the buffer flow.

Before the detection of VEGF, the effectiveness of the binding between the VEGF aptamer and silica beads was tested. The VEGF aptamer 2 (used to bind VEGF in the second injection) silica beads conjugates were ran on the 3D DEP chip. The silica beads collected at the tip of the electrode showed a fluorescence signal (Figure 4.4B). It means that the aptamers were successfully immobilised on the silica beads. The unbound aptamers were eliminated after washing during the immobilisation procedures. The 3D DEP chip with unconjugated beads did not show any non-specific signal (Figure 4.4A). Hence, the fluorescence signal was coming from the fluorescence-conjugated aptamer. This successful binding between the VEGF aptamer and silica beads indicated it was safe to proceed to run the samples using the 3D DEP microfluidic chip.

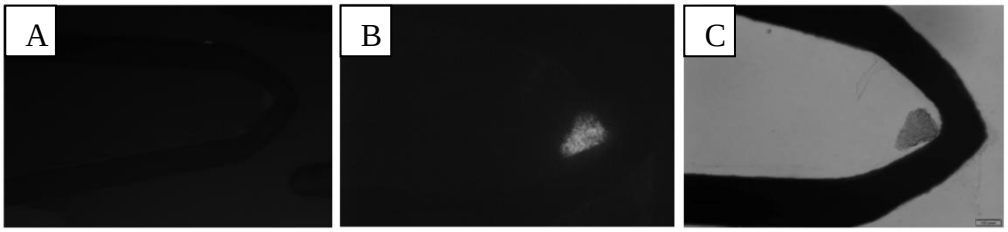

Figure 4.4 Testing the effectiveness of the binding between the VEGF aptamer and silica beads. The sample used was VEGF aptamer 2-immobilised silica beads. Parameters used to run the beads in a 3D DEP chip were voltage of 15 V_{pp}, frequency of 1 MHz, and sample flow rate of 0.4 µl/min. (A) The fluorescence image of the unconjugated silica beads collected at the tip of the electrode showed no unspecific fluorescence signal. (B) The fluorescence image showed VEGF aptamer 2-silica beads collected at the tip of the electrode producing a fluorescence signal. (C) Brightfield image of VEGF aptamer 2-immobilised silica beads collected at the tip of the electrode.

The optimisation of the first injection was performed to get a suitable amount of silica beads collected at the tip of the electrode. The number of beads increased from 0 – 40 seconds and stabilised after 40 seconds (Figure 4.5). The time to turn on the guiding electrode was 5 seconds after the beads started to collect at the tip of the electrode. After turning on the guiding electrode, there were still silica beads moving towards the electrode. The amount of silica beads was sufficient to bind the VEGF-Anti VEGF aptamer 2 conjugates. After the beads stabilised, the second injection was injected at a flow rate of 0.4 µl/min.

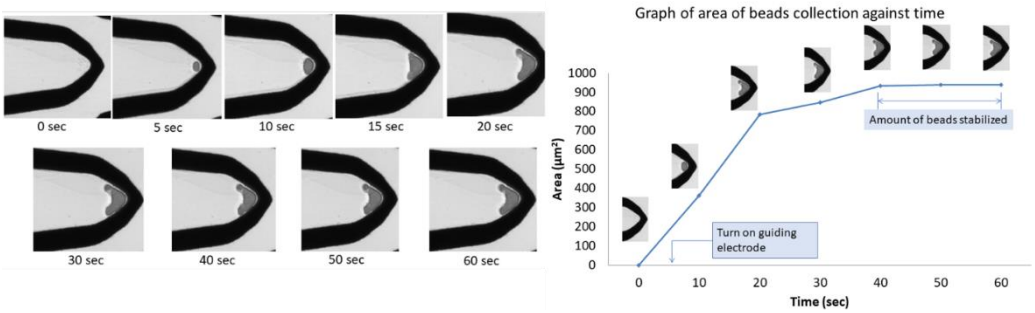

Figure 4.5 Optimisation of the time for the collection of silica beads at the tip of electrode. The guiding electrode was turned on at 5 seconds interval after the beads started to collect at the tip of the electrode. The total amount of silica beads collected stabilised at 40 seconds. Parameters used: Voltage of 15 V_{pp}, frequency of 1 MHz, and sample flow rate of 0.4 µl/min.

The complete experiment was performed with the first and second injections. The collection of VEGF aptamer 1-silica beads was performed for 40 seconds, followed by a second injection consisting of VEGF aptamer 2-VEGF conjugates. The second injection was run for at least 10 minutes to check for the presence of fluorescence signal. For the double aptamer system, there is no fluorescence signal detected at the end of each run of different VEGF concentrations (Figure 4.6A).

Since there was no VEGF detected using the double aptamer system, the VEGF aptamer 2 (with fluorophore) was substituted with PE conjugated-VEGF antibody. The VEGF-VEGF antibody conjugates (second injection) bound to the VEGF aptamer-silica beads to produced fluorescence signal (Figure 4.6B). Different VEGF concentrations (5, 10, 50, 100, 200 pg/ml) were run using the 3D DEP microfluidic chip. The images of the fluorescence signal were captured using a microscope and analysed using ImageJ.

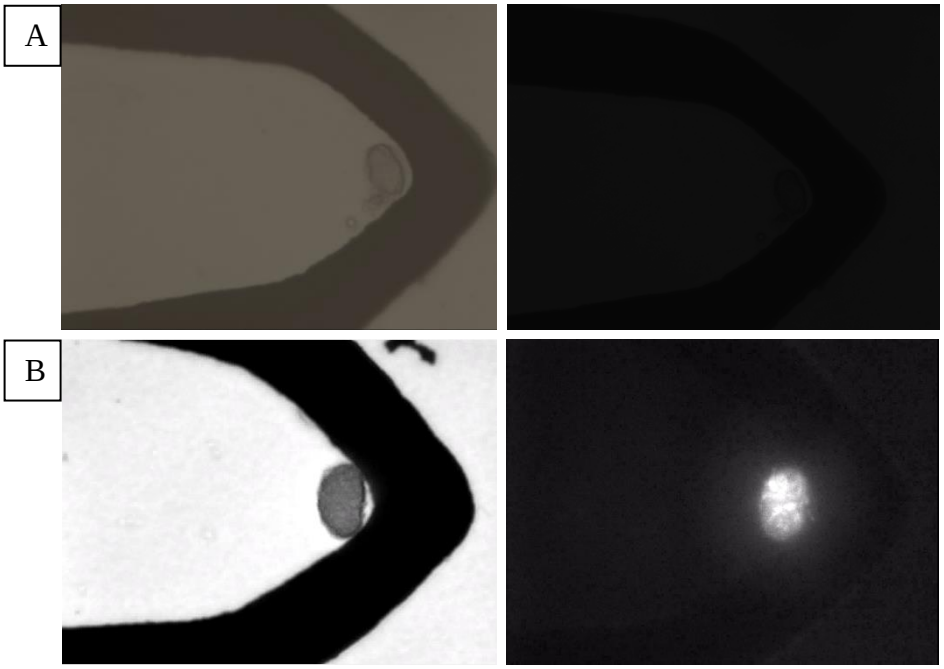

Figure 4.6 Detection of VEGF using 3D DEP microfluidic chip. (A) Representative images of VEGF detection using a double aptamer system. The left image showed beads collected at the tip of the electrode before reaction with the VEGF-VEGF aptamer conjugate (second injection). The right image showed the VEGF aptamer-silica beads conjugate unable to capture VEGF-VEGF aptamer conjugate. Thus, no fluorescence signal was seen in the fluorescence image. (B) Representative images of VEGF detection using the aptamer-antibody system. The left image showed the VEGF aptamer-silica beads collected at the tip of the electrode. After running the VEGF-VEGF antibody conjugate, the bound VEGF-VEGF antibody conjugate produced fluorescence as more and more VEGF was captured.

Based on the graph, 10 minutes was selected as the optimum time to run the second injection so that enough VEGF could bind to the VEGF aptamer-silica beads. A longer time was not selected because a sufficient signal could be seen for each VEGF concentration, and a long time may produce non-specific signals. The area of fluorescence at different detection time points (up to 10 minutes) for different VEGF concentrations is shown in Figure 4.7. After selecting the optimum reaction time, the same experiments were repeated by

running different concentrations of VEGF using the 3D DEP microfluidic chip. A calibration curve was constructed using the area of fluorescence against VEGF concentrations. A calibration curve was drawn with a linear range of 5 - 200 pg/ml and a coefficient of determination of 0.9825. The next step was to test the calibration curve using a random sample (100 pg/ml VEGF concentration). The mean fluorescence signal obtained from the random sample in triplicate was 487 μm^2. This value was substituted into the linear equation, y=5.7577x + 22.278, to obtain the VEFG concentration of the random sample. The recovery rate was calculated by comparing the VEGF concentration obtained from the linear equation to the original VEGF concentration. The sample recovery for the random sample was 81% (Figure 4.8).

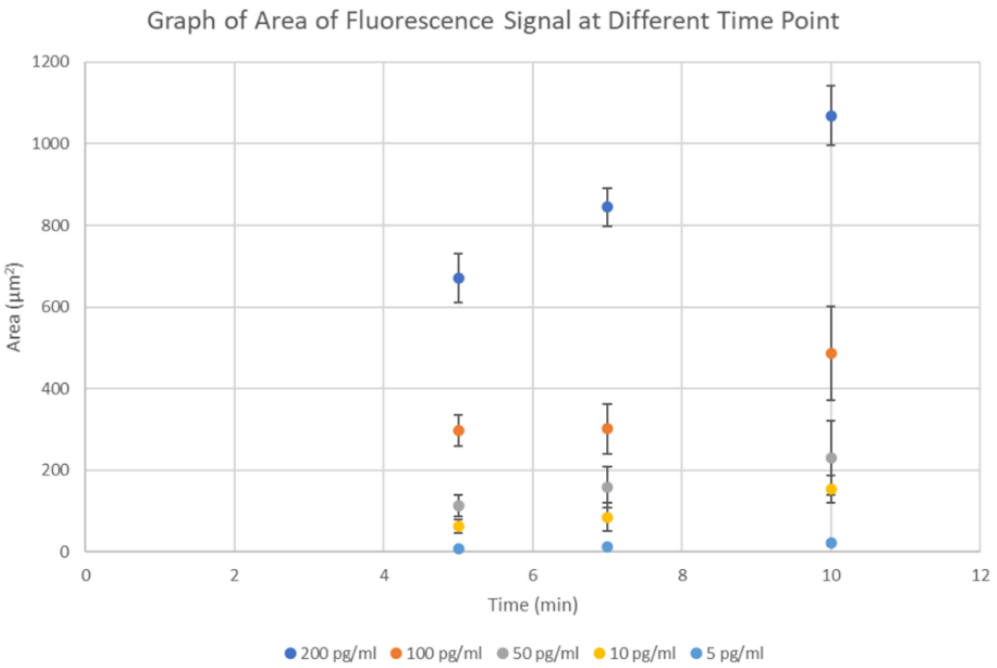

Figure 4.7 Optimisation of the detection time. The fluorescence signal increased with time for all 4 different concentrations of VEGF used. A detection time of 10 minutes was selected as the optimum time for the binding of VEGF to the VEGF aptamer-silica beads conjugates.

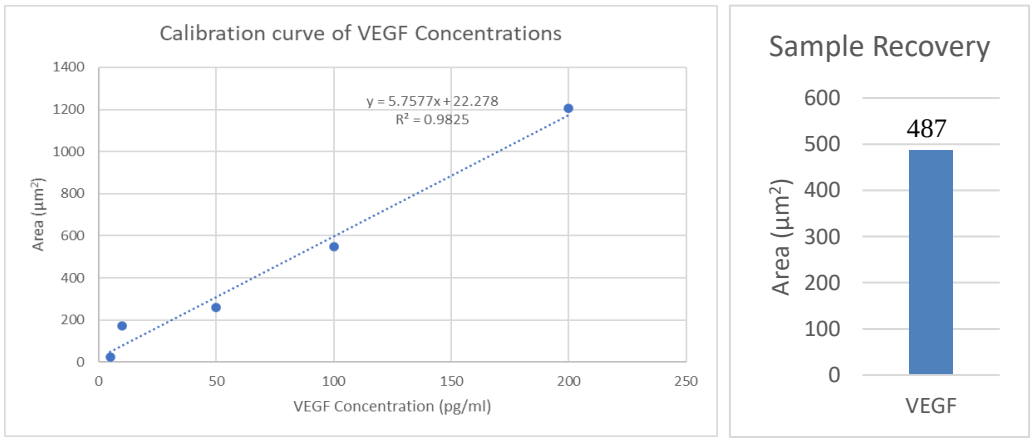

Figure 4.8 Calibration curve of VEGF detection. Calibration curve for VEGF detection. The left graph shows the calibration curve for the VEGF detection with a linear range from 5 - 200 pg/ml. The bar chart (right) shows the sample recovery of a random sample (100 pg/ml VEGF) by substituting the y-value (487 μm^2) into the linear equation, y=5.7577x + 22.278. The recovery rate was calculated by comparing the VEGF concentration obtained from the linear equation to the original VEGF concentration. The sample recovery rate was 81%.

4.3 *In vitro* Permeability Assay

In this study, human pulmonary microvascular endothelial cell (HPMEC) (Figure 4.9), having formed a monolayer, was used to test the permeability inducing effect of VEGF and to study whether treatment with anti-VEGF could reduce the permeability of FITC-Dextran across the endothelial cell monolayer. From the results, the wells treated with VEGF showed higher movement of FITC-Dextran across the cells. The fluorescence reading at 120 and 180 minutes for VEGF wells showed a significant increase compared to untreated wells. For wells treated with VEGF/anti-VEGF, the movement of FITC-Dextran across the monolayer were lower compared to VEGF-treated well but slightly higher compared to the untreated well. Only at 120 and 180 minutes did the VEGF/anti-VEGF treatment led to a statistically significant signal reduction compared to the VEGF treatment (Figure 4.10).

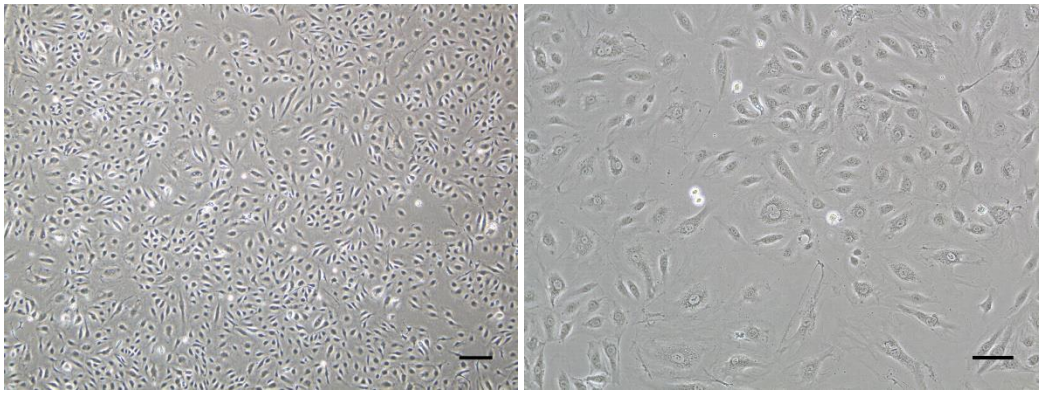

Figure 4.9 Morphology of human pulmonary microvascular endothelial cells (HPMECs). Images of HPMEC at different magnifications. Scale bar: 200 µm (left) and 100 µm (right).

After the fluorescence intensity recording, the treated cells were stained with PECAM-1 antibody. PECAM-1 is one of the major components of the endothelial cell intercellular junction that is present in high amounts (Newman, 1997). PECAM-1 appears in the immunofluorescence image as the boundary between cells and reveals any paracellular gap formation (Martins-Green, Petreaca and Yao, 2008). The endothelial cells treated with VEGF showed more gap formation between cells (~45 gaps, n=3) compared to the untreated cells (~5 gaps, n=3) or cells treated with VEGF/anti-VEGF (~20 gaps, n=3) (Figure 4.11). As the endothelial cells treated with VEGF showed more paracellular gap formation, the rate of FITC-Dextran across the cell monolayer also increased. The untreated cells showed the lowest leakage rate because the tight linkage between endothelial cells prevented movement of FITC-Dextran across the cell-cell junctions. The trend of endothelial cell permeability shown in the graph (Figure 4.10) was supported by fluorescence images of gap formation (Figure 4.11). In VEGF/anti-VEGF treated cells, the number of gaps formed between cells were less than those in the VEGF-treated cells. This suggests that treatment with anti-VEGF could reduce the gaps or leakage caused by VEGF.

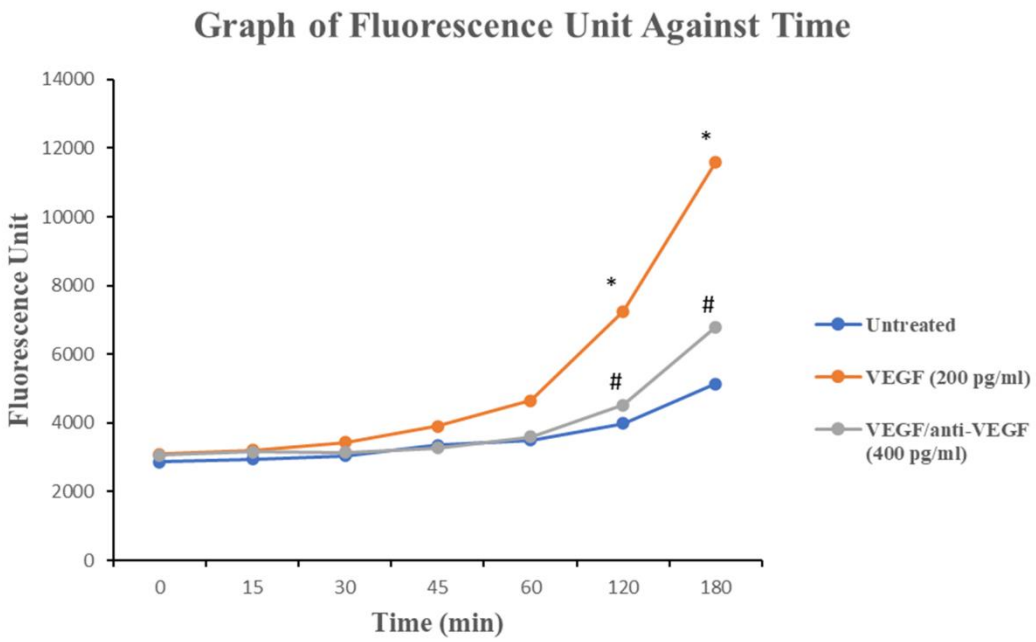

Figure 4.10 The graph of FITC-Dextran fluorescence signal measured against time. In the permeability assay, the FITC-Dextran measured represents the degree of permeability. The higher the FITC-Dextran intensity means more FITC-Dextran were able to pass through the monolayer, and it also represents higher permeability of the endothelial monolayer. Statistical analysis was performed using student t-test. * represents a significant increase of signal from VEGF-treated cells against untreated cells, $p<0.05$. $^{\#}$ represents a significant reduction of signal from VEGF/anti-VEGF-treated cells against VEGF-treated cells, $p<0.05$.

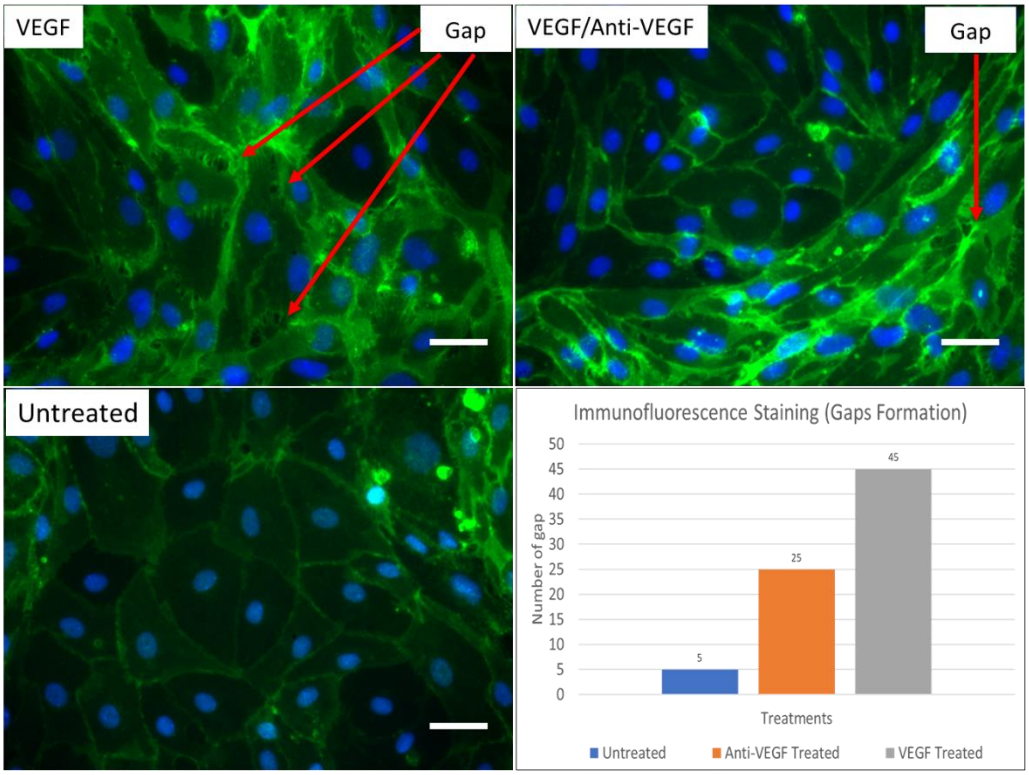

Figure 4.11: Immunofluorescence staining images of untreated and treated cells stained with PECAM-1 (green). The formation of gaps between the endothelial cells allows molecules to cross the monolayer. The number of gaps formation for different treatments is illustrated in the bar chart. The endothelial cells treated with VEGF showed more gaps formation between cells (~45 gaps, n=3) compared to the untreated cells (~5 gaps, n=3) or cells treated with VEGF/anti-VEGF (~20 gaps, n=3). Scale bar: 25 µm.

4.4 Gene Expression Study of VEGF and Anti-VEGF Treatment on Endothelial Cells

Before microarray analysis, the concentration and purity of the RNAs were measured using a nanodrop spectrophotometer. The purity of the nucleic acid is commonly determined using the A260/A280 and A260/A230 ratios. The low A260/A280 ratio indicates the presence of contamination proteins, while a low A260/A230 ratio indicates contamination by an organic compound such as Triton X or EDTA during the nucleic acid extraction processes. The pure RNA

has a value of 2.0 for the A260/A280 ratio and 2.0 - 2.4 for the A260/A230 ratio (Wilfinger, Mackey and Chomczynski, 1997; Farrell, 2017). The RNA purity for all the samples in this study was within the recommended ranges (Table 4.1).

RNA integrity can be easily checked in any laboratory using native gel electrophoresis. RNA appears as 1.9 kb and 5 kb bands in the gel electrophoresis representing the 28S rRNA and 18S rRNA, respectively, with the intensity of the 28S band roughly double the 18S band. In the gel image obtained in this study (Figure 4.12), In the gel image, all samples had distinct two bands, but not all 28S bands were twice as intense as the corresponding 18S bands. Nevertheless, none of the bands showed smearing. The presence of smearing would indicate RNA degradation due to RNase, which is commonly present in the environment.

The more accurate way to check the concentration and integrity of the RNA is by using a bioanalyzer. The RNA integrity number (RIN) is a scale from 1 – 10, with a scale 1 for completely degraded RNA and 10 for fully intact RNA. The recommended RIN for RNA samples suitable for downstream applications such as microarray or next-generation sequencing is RIN 7 and above. All RNA samples in this study ranged from 9.5 – 9.8 (Table 4.1), showing their suitability for microarray analysis. The intensity of the 28S rRNA band for all samples was twice the intensity of the corresponding 18S rRNA band (Figure 4.13).

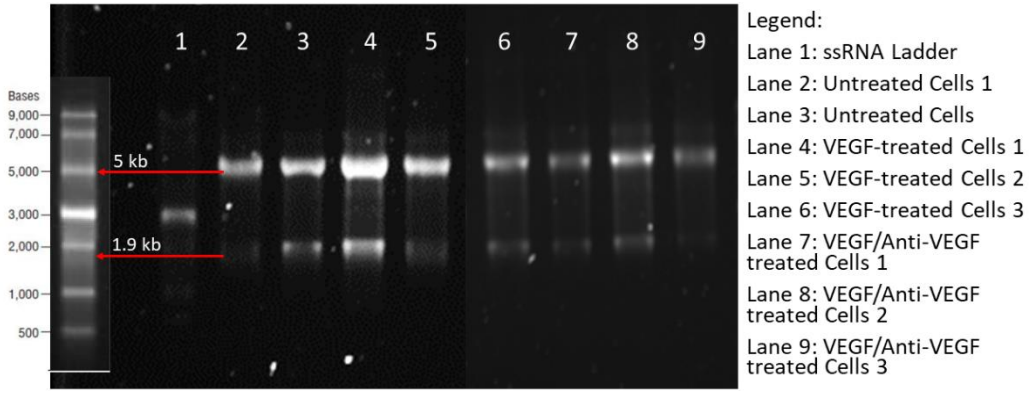

Figure 4.12 RNA gel electrophoresis. The intact RNA run on gel electrophoresis will yield 2 bands, which are 28S rRNA and 18S rRNA. The size for 28S is around 5 kb and 18S is around 1.9 kb, with the intensity of 28S rRNA band twice more intense than the 18S rRNA band.

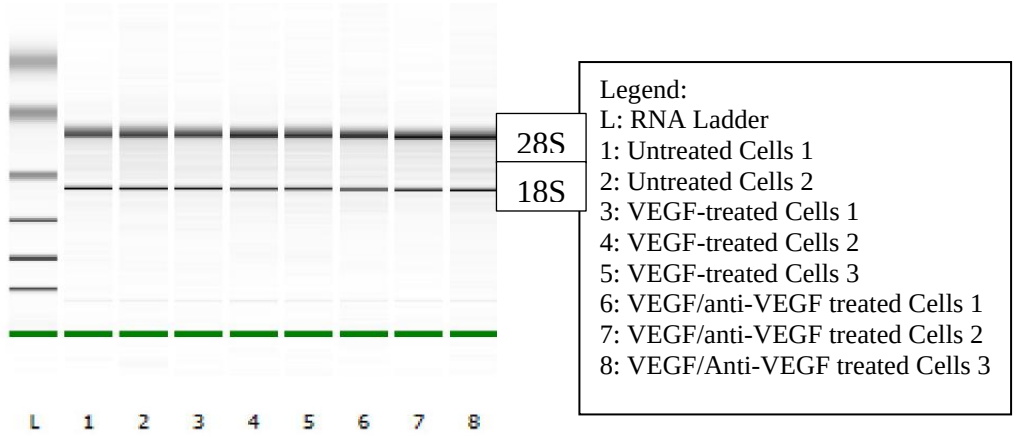

Figure 4.13 Assessment of RNA integrity using Bioanalyzer. The intact RNA consists of 2 bands, namely 28S rRNA and 18S rRNA. The intensity of the 28S rRNA band is twice as intense as the 18S rRNA band. The RIN for all samples were in the range of 9.5 – 9.8, meaning all the samples were of good quality and suitable for microarray analysis.

Table 4.1 Concentration, purity, and integrity of RNA extracted from untreated and treated endothelial cells. The concentration and purity of RNA were obtained from Nanophotometer, while the RNA integrity was obtained from 2100 Bioanalyzer.

Sample	**Concentration (ng/µl)**	**Ratio 260/230**	**Ratio 260/280**	**RNA Integrity Number (RIN)**
Untreated Cells 1	197.6	1.91	2.15	9.6
Untreated Cells 2	205.12	2.00	2.15	9.8
VEGF-treated Cells 1	193.76	1.88	2.14	9.6
VEGF-treated Cells 2	124.08	2.23	2.13	9.6
VEGF-treated Cells 3	162.16	1.98	2.13	9.6
VEGF/anti-VEGF treated Cells 1	139.36	2.20	2.11	9.5
VEGF/anti-VEGF treated Cells 2	127.76	1.96	2.16	9.5
VEGF/anti-VEGF treated Cells 3	106.48	1.91	2.14	9.5

The genome-wide microarray analysis featured 50,599 probes covering 24,588 genes. After VEGF treatment, 111 genes showed more than 2-fold differential expression, of which 103 genes were upregulated and 8 downregulated. Following VEGF/anti-VEGF treatment, 118 genes showed more than 2-fold differential expression compared to untreated endothelial cells. Of these, 106 genes were upregulated, and 12 genes downregulated. Table 4.2 shows the top 10 upregulated and downregulated genes for both types of treated endothelial cells. When analysed using unsupervised hierarchical clustering, the treated and untreated HPMEC samples were grouped into three different clusters. The two treated samples formed two separate clusters but were grouped closer to each other than to the untreated cells (Figure 4.14).

Table 4.2 Top 10 upregulated genes and downregulated genes for VEGF and VEGF/anti-VEGF treated HPMEC after statistical analysis using One-way ANOVA ($p<0.05$, $FC \geq 2$).

VEGF vs Untreated	Fold Change	Regulation	VEGF/anti-VEGF vs Untreated	Fold Change	Regulation
F3	330.17	Up	CSF2	425.06	Up
CSF2	299.61	Up	F3	256.10	Up
LIF	191.54	Up	TNF	252.29	Up
TNF	180.82	Up	LIF	242.85	Up
CXCL3	175.95	Up	CXCL3	201.89	Up
CSF3	92.73	Up	CSF3	140.07	Up
C2CD4A	85.62	Up	IL23A	95.34	Up
IL23A	68.99	Up	C2CD4A	89.70	Up
IL1B	66.47	Up	CXCL2	86.34	Up
CXCL2	57.75	Up	SELE	66.96	Up
OR9A2	-2.90	Down	CH25H	-4.45	Down
TRIL	-2.83	Down	CUL4A	-3.49	Down
TBX1	-2.61	Down	PDK4	-3.43	Down
RAB37	-2.24	Down	TRIL	-3.35	Down
SLC2A12	-2.17	Down	OR9A2	-3.10	Down
TACC3	-2.16	Down	TBX1	-2.80	Down
BRD3	-2.08	Down	ADAMST12	-2.41	Down
NRDE2	-2.00	Down	DDIT4L	-2.39	Down
			RAB37	-2.28	Down
			BRD3	-2.22	Down

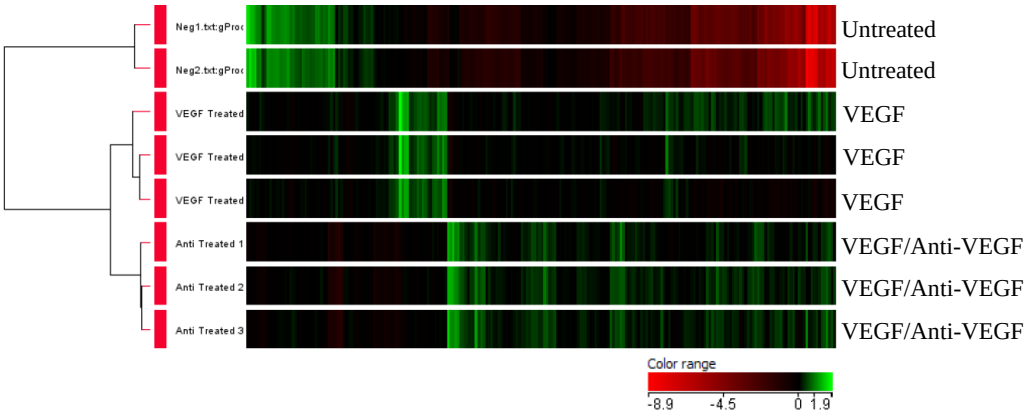

Figure 4.14 Unsupervised hierarchical clustering of untreated and treated human pulmonary microvascular endothelial cells. The treated and untreated HPMEC samples were grouped into 3 distinct clusters. The colour bar shows the range of fold change red represents downregulated genes and green represents upregulated genes.

Gene ontology (GO) describes the functions of genes and groups them under three main categories: molecular functions, biological processes, and cellular components (The Gene Ontology Consortium *et al.*, 2000). In this study, the GO enrichment analysis of differentially expressed genes showed 387 GO terms satisfying the corrected p-value cut-off of 0.05 (Figure 4.15), grouped under biological processes (46.5%), molecular functions (46.1%), and cellular components (7.5%). Under biological processes, there were 12 sub-categories topped by biological regulation (17.3%), response to stimuli (14.3%), and cellular process (13.2%). The molecular function category had only binding (78.8%) and molecular function regulator (21.2%), while four sub-categories were listed in the cellular component category, namely, cell (29.2%), cell part (29.2%), membrane (20.8%) and membrane part (29.2%).

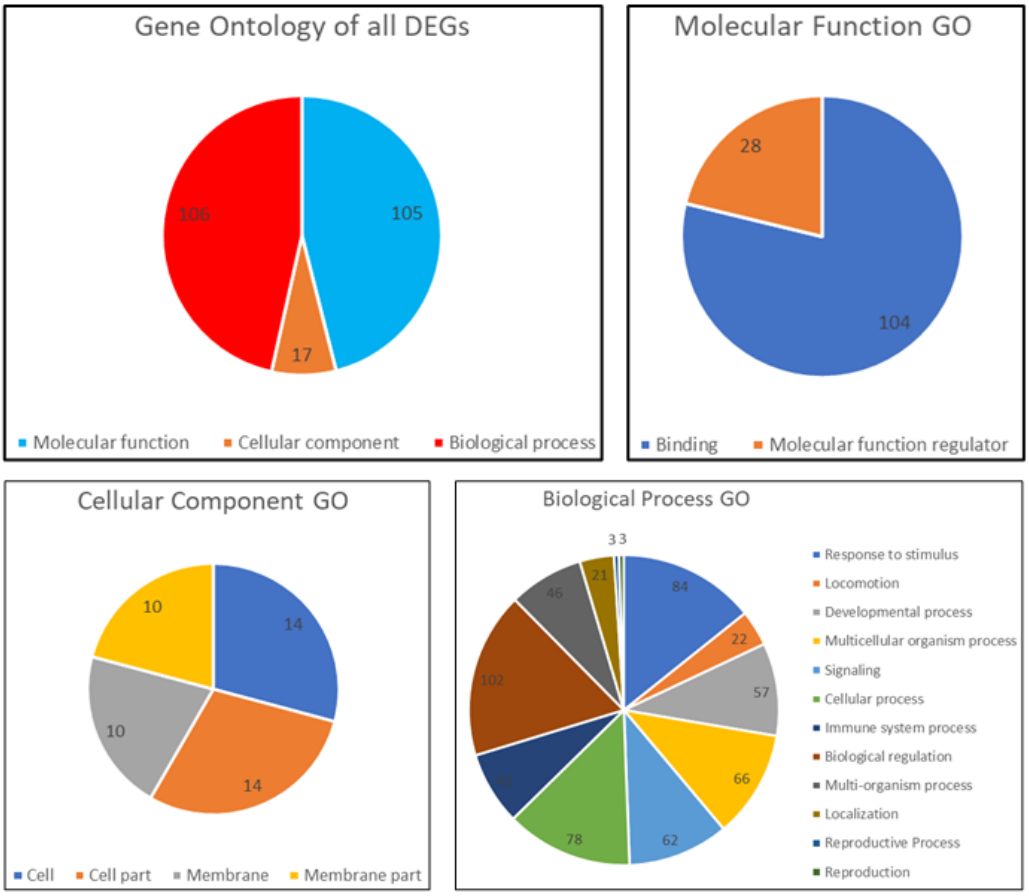

Figure 4.15 Gene Ontology (GO) enrichment analysis on the differentially expressed genes (DEG) of untreated and treated endothelial cells. The DEGs were divided into 3 GO categories, namely molecular function, cellular component, and biological process. The percentage of genes enriched in the following terms were as follows: biological processes (46.5%), molecular function (46.1%), and cellular component (7.5%).

The Database for Annotation, Visualization and Integrated Discovery (DAVID) enrichment analysis showed the upregulated genes in VEGF-treated cells were enriched in inflammatory response, regulation of endothelial barrier, regulation of angiogenesis, regulation of nitric oxide biosynthesis, and NOD-like receptor signalling pathway (Table 4.3). The fold change for the upregulated genes of VEGF and VEGF/anti-VEGF treated cells were compared. The genes, which showed a lower fold change for the VEGF/anti-VEGF treated cells compared to the VEGF treated cells, were then subjected to DAVID enrichment analysis. This analysis showed that the genes that showed lower fold change in VEGF/anti-VEGF treated cells were enriched in the regulation of angiogenesis, regulation of cytokine secretion, and cytokine-mediated signalling pathway (Table 4.4). In VEGF-treated and VEGF/anti-VEGF-treated cells, there were no enriched functions among the downregulated genes after DAVID analysis.

Table 4.3 Enriched functions in upregulated genes in VEGF-treated cells ($p<0.05$, $FC\geq2$).

Regulation of endothelial barrier (Fold enrichment: 51.6)	
Gene	Fold Change
TNF	180.82
IL1B	66.47
Regulation of angiogenesis (Fold enrichment: 7.85)	
F3	330.17
IL1B	66.47
CX3CL1	15.31
ZC3H12A	9.01
ETS1	3.53
Regulation of nitric oxide biosynthesis (Fold enrichment: 29.39)	
TNF	180.82
IL1B	66.47
IL6	42.33
PTGS2	12.99
SOD2	4.82
ICAM1	4.49
SMAD3	2.36
NOD-like receptor signalling pathway (Fold enrichment: 21.55)	
TNF	180.82
IL1B	66.47
CXCL2	57.75
IL6	42.33
NOD2	33.84
BIRC3	20.46
TNFAIP3	15.88
CXCL1	12.21
NFKBIA	4.21
CCL2	2.82

Inflammatory response (Fold enrichment: 9.53)	
Gene	Fold Change
TNF	180.82
CXCL3	175.95
IL23A	68.99
IL1B	66.47
CXCL2	57.75
SELE	44.25
IL6	42.33
CXCL6	20.11
TNFAIP3	15.88
BDKRB1	15.62
PTGS2	12.99
CXCL1	12.21
BMP2	10.53
ZC3H12A	9.01
NFKBIZ	8.32
TLR2	3.58
CXCL5	3.44
CSF1	3.19
CCL2	2.82
TNFRSF11B	2.38

Table 4.4 Enriched functions in upregulated genes for VEGF/anti-VEGF treated cells which showed reduction in fold change compared to the VEGF-treated cells ($p<0.05$, $FC\geq2$).

Regulation of cytokine secretion (Fold enrichment: 138.78)	
Gene	Fold Change
SOCS1	20.43
TLR2	3.39
Regulation of angiogenesis (Fold enrichment: 19.91)	
F3	256.10
IL1B	56.56
ETS1	3.26
Cytokine-mediated signaling pathway (Fold enrichment: 17.48)	
F3	256.10
IL1B	56.56
SOCS1	20.43

4.5 Validation of Differentially Expressed Genes from Microarray Analysis

Random genes from the upregulated and downregulated genes were selected for validation using qRT-PCR. From the validated results, all the genes selected for validation (i.e., CXCL2, CSF3, IL23A, CSF2, SELE, F3, CXCL3, TRIL, CH25H, and PDK4) showed expression pattern that were similar in both qRT-PCR and microarray. The validation data for VEGF-treated cells and VEGF/anti-VEGF treated cells are shown in Figures 4.16 and 4.17.

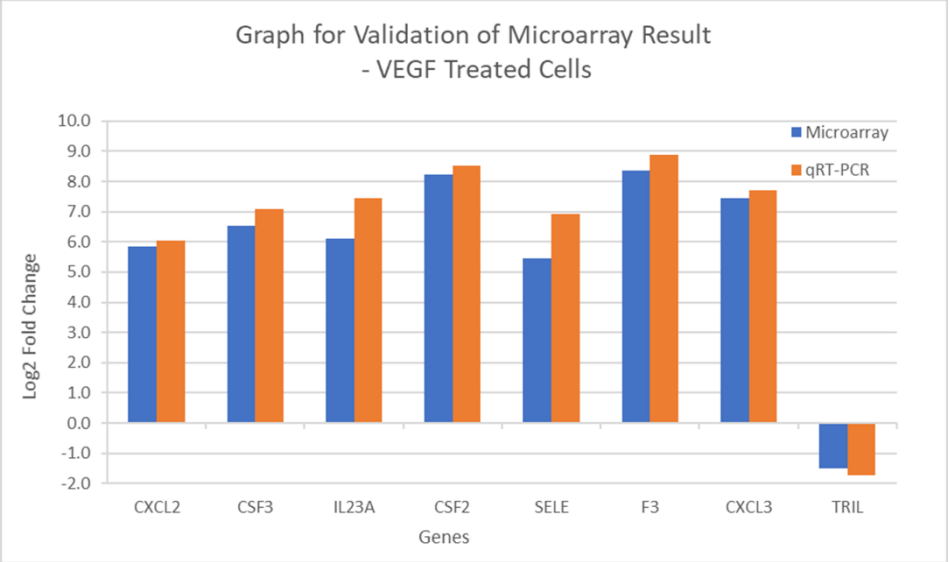

Figure 4.16 Validation of microarray data for dysregulated genes in VEGF-treated cells with qRT-PCR. CXCL2, CSF3, IL23A, CSF2, SELE, F3, CXCL3, and TRIL, from differentially expressed genes in VEGF-treated cells, were selected for validation. All the genes showed similar expression patterns in qRT-PCR with microarray results.

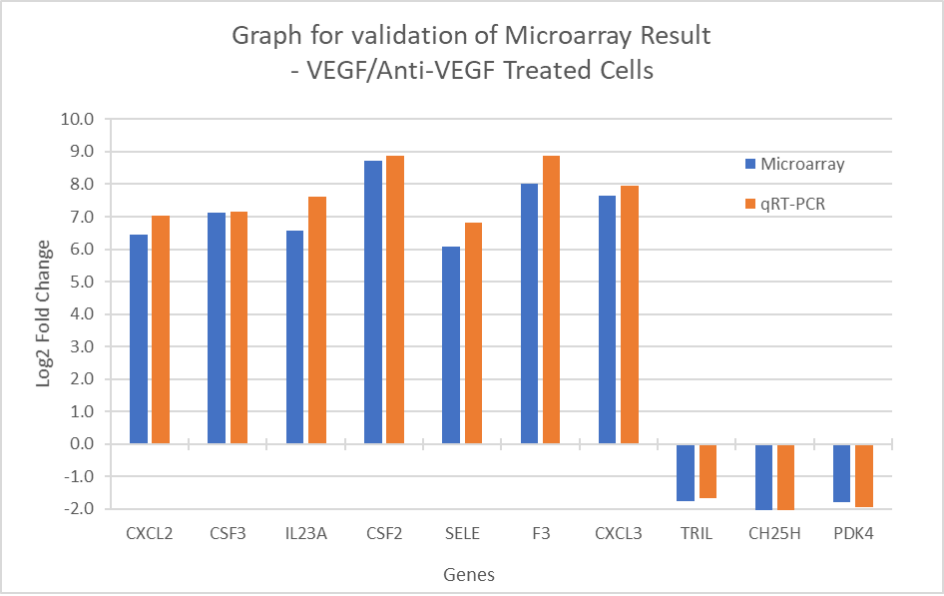

Figure 4.17 Validation of microarray data for dysregulated genes in VEGF/anti-VEGF treated cells with qRT-PCR. CXCL2, CSF3, IL23A, CSF2, SELE, F3, CXCL3, TRIL, CH25H, and PDK4, from differentially expressed genes in VEGF/anti-VEGF treated cells, were selected for validation. All the genes showed similar expression patterns in qRT-PCR with microarray results.

CHAPTER 5

DISCUSSION

5.1 Rapid Test for Detection of VEGF

Since the dengue virus targets the microvascular endothelium, endothelial dysfunction is the main finding seen in severe dengue cases. Dengue virus causes endothelial dysfunction through the action of secreted cytokines to increase vascular permeability. Thus, plasma leakage is commonly seen in severe dengue patients due to the leaky microvessel (Spiropoulou and Srikiatkhachorn, 2013). VEGF was initially identified as a vascular permeability factor (Senger *et al.*, 1983). Due to the roles of VEGF on endothelial cells and vasculature, it is vital to study vascular permeability caused by increased VEGF levels. VEGF acts by binding to the transmembrane tyrosine kinase receptor, mainly through VEGFR2. Furthermore, VEGFR2 is found abundantly on endothelial cells, which make up the blood vessels. VEGFR2 is involved in the regulation of vascular permeability by activating the pathways that regulate the endothelial junctions (Claesson-Welsh, Dejana and McDonald, 2021).

Based on a literature search, VEGF have been associated with other clinical parameters such as aspartate transaminase (AST), Alanine aminotransferase (ALT), haematocrit, platelet, and leukocyte. Thakur et al. (2016) correlated the VEGF level to liver enzymes found in severe dengue

patients. VEGF-induced angiogenesis and fibrogenesis lead to abnormal liver circulation and liver damage. The raised haematocrit level might be caused by the VEGF-induced vascular permeability and leakage of plasma into the peritoneal and abdominal cavities (Thakur *et al.*, 2016). The negative correlation between VEGF level and platelet level might be due to increased platelet binding to endothelial cells, thus lowering the circulating platelets (De Azeredo, Monteiro and De-Oliveira Pinto, 2015).

VEGF is suitable to be used as a detection marker for progression to severe dengue (Goutam, Saha and Mukhopadhyay, 2019; Mukherjee, Saha and Tripathi, 2022). During dengue infection, the febrile stage lasts for 2 - 7 days after the onset of fever (Anoopkumar and Aneesh, 2021). After the febrile stage, the dengue patient either recovers or progresses to the critical stage. During the critical stage, the patient develops a high risk of severe plasma leakage, which lasts for 24 - 48 hours. The patient who does not receive appropriate treatment may risk developing shock that could lead to death (Anoopkumar and Aneesh, 2021). The mortality rate of severe dengue is less than 1% if supportive treatment is given on time (World Health Organization, 1997). From the literature search, the increase in VEGF levels coincides with the progression of the disease from the febrile stage to the critical stage, usually around the third or fourth day (Thakur *et al.*, 2016; Goutam, Saha and Mukhopadhyay, 2019). With a VEGF detection kit, the patient with a high risk of developing severe dengue could be tested frequently and provided with necessary treatment. Owing to the short

timing of dengue progression to severe dengue, multiple testing with a rapid test is beneficial.

In this study, the methods chosen for VEGF detection were lateral flow immunoassay and DEP-based microfluidic assay. Lateral flow immunoassay is a well-established method for many commercial products, such as the detection of dengue NS1 antigen and antibodies against the dengue virus (Kabir, Zilouchian and Younas, 2021). On the other hand, DEP-based microfluidic assay is a newer method used in medical research. There is no product that has been commercialised based on this assay. The DEP-based assay offers several advantages in medical research for disease diagnosis (Rahman, Ibrahim and Yafouz, 2017). Furthermore, no study utilises lateral flow immunoassay or DEP-based microfluidic assay for VEGF detection.

Several steps were introduced in the lateral flow immunoassay development, such as using sandwich VEGF antibodies and biotin for the high binding affinity of the VEGF-antibodies sandwich complex to the streptavidin on the test line. After adding VEGF to the sample pad, the VEGF was bound to the VEGF biotinylated antibodies and then flowed into the conjugate pad. The VEGF-VEGF antibody conjugates bound to the gold-conjugated VEGF antibodies on the conjugate pad. The two VEGF antibodies recognise different epitopes on the VEGF. Thus, there is no competition for the same binding site. The VEGF-VEGF antibodies complex is captured at the test line through the

interaction of biotin on the VEGF antibody with streptavidin immobilised on the test line. Streptavidin has a high affinity toward biotin; biotin and streptavidin binding is the strongest non-covalent bond with a dissociation constant of 1×10^{-15} M (Green, 1963; Liu, Zhang and Mei, 2016).

In this study, a range of VEGF concentrations, from 0.1 ng/ml - 250 ng/ml, were run using the lateral flow immunoassay. The positive signal produced at the test lines observed using the naked eye was for a VEGF concentration of 10 ng/ml and above. To date, no other rapid test has been used for dengue detection except for dengue NS1 detection. Furthermore, there is no test or biomarker for the detection of severe dengue. Although the sensitivity and specificity of the dengue rapid test kit are inconsistent between different manufacturers, ranging from 71 - 100%, the benefits of using a rapid test kit still outweigh its disadvantages (Kabir, Zilouchian and Younas, 2021). Lateral flow immunoassay fulfils the ASSURED criteria for a point of care diagnosis platform, such as rapid detection time, low-cost, user-friendly, equipment-free, acceptable sensitivity and specificity, and suitability for use in limited resources setting (Peeling *et al.*, 2006).

In a study by Tran *et al.* (2019), he authors developed a magneto-enzyme lateral flow immunoassay for dengue NS1 detection. The detection limit for their lateral flow immunoassay was 1.4 ng/ml NS1 from DENV1, 0.7 ng/ml NS1 from DENV2, 1.4 ng/ml NS1 from DENV3, and 6.6 ng/ml NS1 from DENV4. The

authors used biotinylated monoclonal antibody (mab)-coated magnetic nanoparticles to react with NS1 from the serum of patients. The NS1-mab-magnetic nanoparticles complex binds to the capture antibody on the test line, while any complex that does not bind to NS1 was captured at the control line. In another study, the authors used NS1 antibody-HRP to detect dengue NS1 protein in a lateral flow immunoassay. The NS1-NS1 antibody-HRP complex that reached the absorbent pad reacts with the luminol-H_2O_2 substrate to produce a chemiluminescence signal. An image of the signals was captured using a camera. The lowest NS1 concentration detected using this system was 5 ng/ml (Axelrod, Eltzov and Marks, 2020). The comparison of detection limit in this study to the two studies mentioned above is at least 2-15 times higher. But the sensitivity is still not enough for VEGF detection in clinical samples, which often have VEGF levels as low as 55 pg/ml (Thakur *et al.*, 2016).

DEP-based microfluidic has the potential for use in disease diagnosis. This technique offers an accurate, fast, low-cost, and label-free method for the detection of various proteins or separation based on cell types (Rahman, Ibrahim and Yafouz, 2017). This led to the development of DEP-based microfluidic assay for VEGF detection in this study. DEP utilises the ability to polarise particles or cells by applying electric current to manipulate the particles or cells by attracting or repelling them. The silica beads used in this study are polarisable particles and can be trapped using DEP force at the tip of the electrode. In the DEP test, the silica beads experienced negative DEP and were repel by the strong electric field at the electrode. There was another force, drag force, acting on the beads in

the direction of the flowing solution, trapping the beads at the tip of the electrode and preventing backflow (Cheng, Han and Chang, 2012; Iswardy *et al.*, 2017).

The colourimetric detection method was chosen to be coupled with the DEP microfluidic detection system because it is easy to design the detection system and capture the signals produced from positive results (Dehghani *et al.*, 2018). In this study, the fluorescence signal represents the amount of VEGF present in the sample. VEGF was detected using 3D DEP microfluidic chip through the aptamer-antibody system, with a linear range of VEGF concentration from 5 – 200 pg/ml. In another study that used colourimetric as a detection method, the microfluidic porous microgel based assay coupled to Alexa Fluor 488-conjugated antibody as the signal reporter was used to detect VEGF. The detection limit reported was as low as 0.9 pg/ml (Zhao *et al.*, 2015). In clinical settings, the range of VEGF levels detected in patients was around 55 – 430 pg/ml (Tseng *et al.*, 2005; Low, Gan and Ho, 2015; Thakur *et al.*, 2016). Thus, the detection limit of at least 5 pg/ml is sufficient for VEGF detection. This showed that the colourimetric method is a sensitive method for the detection of low levels of target in clinical samples.

The initial design of the VEGF detection system was based on the aptamers sandwich method, in which VEGF was captured by two aptamers at two different binding sites. Unfortunately, no signal is detected when running the VEGF samples using the aptamers sandwich method. Several reasons that

contributed to no signal being detected were the choice of aptamer or photobleaching of the fluorophore conjugated to the aptamer. Aptamers were used in the DEP-based microfluidic system because they offer better stability and can detect a wider range of target molecules compared to antibodies (Guo *et al.*, 2020). However, there are precautions to consider when choosing aptamers as a detection analyte, such as interference of surface to aptamer folding, the density of aptamer immobilisation on the bead surface, and competition for the same binding site by two aptamers in the sandwich-based assay (Nonaka, Abe and Ikebukuro, 2012; Urmann *et al.*, 2017). It has been reported that both the aptamers used in this study did not compete for the same binding site (Nonaka, Abe and Ikebukuro, 2012). The interference due to aptamer folding and aptamer density is not the concern in this study because signals were detected when using the aptamer-antibody detection system. It means that the aptamer folding is not affected or has no steric hindrance due to the high aptamer density, which will affect the detection system. The reaction time for the VEGF detection in the microfluidic channel was 10 minutes. The continuous exposure of 6-carboxyfluorescein (FAM)-aptamer to the excitation light from the fluorescence microscope could cause photobleaching since fluorescein-based dyes are susceptible to photobleaching and sensitive to an acidic environment (Mottram *et al.*, 2006).

Of the two methods used in this study, lateral flow immunoassay provides a more cost-effective way for rapid testing and is suitable for self-testing. Based on the data presented in this study, a DEP-based microfluidic chip

is preferable compared to a lateral flow immunoassay for VEGF detection due to its sensitivity. DEP-based microfluidic chip with colourimetric detection provides better advantages than others such as electrochemical, surface plasmon-based technique, or surface-enhanced Raman spectroscopy. The limitations of the other methods are sensitive to the sample's environment, such as pH, the requirement for a cleanroom for fabrication, susceptibility to nonspecific binding, low repeatability and high-cost reader (Campuzano *et al.*, 2020; Kabir, Zilouchian and Younas, 2021).

Metal electrodes are commonly used in DEP devices. Although metal is susceptible to fouling, the reason metal electrode is used during the development stage is that they can be used to study over wide ranges of frequency, and the DEP effect can be applied through the depth of the channel around the electrodes (Viefhues and Eichhorn, 2017a; Zhang, Chang and Neuzil, 2019). On the issue of production cost, it is possible to reduce the production cost of a microfluidic chip. The first way is to use non-metal electrodes such as carbon or polymer-based electrode such as PDMS. The cost of such electrodes is much cheaper compared to the metal electrode. Using non-metal electrodes, this could solve the metal fouling problem too. In a paper by Zhu *et al.* (2015), the authors used the screen-printing method to construct the DEP microfluidic chip and printed the electrode using carbon paste. The second way is by fabricating the microfluidic chip in 2D. The electrodes are fabricated on one side of the chip surface, thus reducing the cost. Furthermore, the 2D chip also does not require extra steps to align both sides of the chip, as in the case of a 3D chip (Zhang,

Chang and Neuzil, 2019). Furthermore, it is possible to develop the DEP microfluidic chip to be used in the clinical setting with minimal training and the availability of portable functional generators and fluorescence readers (Bhavanishankar and Manikandan, 2021; Shin, Teresa Gutierrez-Wing and Choi, 2021).

5.2 Effects of VEGF and Anti-VEGF on the Permeability of Endothelial Cells

In this study, the effects of VEGF and anti-VEGF treatment on the permeability of endothelial cells were investigated and gene profiling of the untreated and treated cells was performed using microarray gene expression study. Based on the permeability assay, the treated cells showed a higher detectable FITC-Dextran fluorescence signal which means higher permeability across the endothelial cell monolayer. Although the fluorescence signal for untreated and treated cells showed some degree of signal increased, the VEGF-treated cells still showed the highest degree of leakage. These findings were consistent with the observations of Monaghan-Benson and Burridge (2009) who showed that VEGF regulates microvascular permeability by regulating the integrity of the adhesion molecules. Visible gaps were seen between adjacent endothelial cells which provide the route for the passage of macromolecules. The authors further added that the largest permeability changes occurred in the microvessel (Monaghan-Benson and Burridge, 2009).

The binding of anti-VEGF to VEGF would stop it from inducing increased endothelial permeability. This anti-permeability effect was demonstrated by Peters *et al.*, 2007, who used Bevacizumab, an anti-VEGF monoclonal antibody, on choroidal endothelial cells. The results in this study also showed a decrease in endothelial cells permeability after anti-VEGF treatment, based on the reduced movement of FITC-Dextran across the endothelial cells. In addition, the increased endothelial cell permeability after VEGF treatment in our study was supported by the immunostaining images that showed the formation of many gaps between the endothelial cells after VEGF treatment but fewer gaps after VEGF/anti-VEGF treatment.

When the primary HPMEC were stained with VE-cadherin antibody, the expression of VE-cadherin was not detected (data not shown). Based on the product description from the manufacturer, HPMEC expresses both von Willebrand factor and PECAM-1 markers. Based on literature search, PECAM-1 is more commonly used as a characterisation marker for microvascular endothelial cells (Lou *et al.*, 1998; Krump-Konvalinkova *et al.*, 2001; Comhair *et al.*, 2012). According to the manufacturer, the source of HPMEC was from the capillaries of a human lung. Based on a study on VE-cadherin expression in human lungs, the authors found that VE-Cadherin was highly expressed in arteries, arterioles, and capillaries but not in veins and venules (Herwig, Müller and Müller, 2008). Thus, it could be that the HPMEC was isolated from venules rather than capillaries which explains why there is no expression of VE-cadherin in HPMEC.

5.3 Gene Expression Study of VEGF and Anti-VEGF Treatment on Endothelial Cells

The distinct clustering for treated cells and untreated cells indicated that there was a difference in the differentially expressed genes between the two groups of cells. Although VEGF-treated cells showed closer clustering to VEGF/anti-VEGF treated cells compared to untreated samples, the two treated cells were still clustered into different groups. With the use of Gene Ontology, a wide range of GO terms was identified for the genes being dysregulated for all the samples. The more notable ones involved the regulation of cytokines and chemokines, humoral and innate immune responses, inflammatory response, and regulation of cell adhesion.

From the DAVID enrichment analysis, several enriched functions in upregulated genes for VEGF treatment were listed in Table 4.3. One of the enriched functions in upregulated genes for VEGF treatment was inflammatory response. TNF, CXCL3, IL23A, IL1B, and CXCL2 were among the top 10 upregulated genes in the inflammatory response function. Many of the genes involved in the inflammatory response were cytokines and chemokines that were also overexpressed in the immune response function. IL23A is paired with IL12B to make the heterodimer IL23 which activates T helper 17 (T_H17) lymphocytes to produce IL17 and IL22. These interleukins are known to stimulate the production of diverse cytokines and chemokines during inflammation (Gaffen *et al.*, 2014; Kortlever *et al.*, 2017). CXCL2 and CXCL3 are involved in inflammation response by attracting leukocytes to endothelial

cells to fight infection (Loganathan *et al.*, 2020), and leukocytes are known to promote microvascular leakage (Wedmore and Williams, 1981; Owen-Woods *et al.*, 2020).

TNF and IL1B are linked to the regulation of endothelial barrier function. TNF is a potent pro-inflammatory cytokine produced by monocytes, macrophages, T lymphocytes, B cells, T cells and NK cells to carry out mediator functions in immune responses (Fitzgerald *et al.*, 2001; Josephs *et al.*, 2018). Increased levels of TNF have been detected in sera from DHF and DSS patients (Kittigul *et al.*, 2000). This cytokine induces the production of IL6 in endothelial cells that could lead to vascular leakage (Maruo *et al.*, 1992; Anderson *et al.*, 1997). In a study on TNF-induced vascular endothelial hyperpermeability, TNF overexpression was found to reduce the expression of tight junction protein, ZO-1. The reduction of ZO-1 causes the increase of endothelial permeability (Zhang *et al.*, 2017). Pan *et al.* (2019) have demonstrated that IL1B induced vascular leakage in HUVEC after IL1B overexpression and in interferon-alpha/beta receptor 1 deficient mice after dengue virus infection. In an earlier study by Du et al. (2015), IL1B treatment caused an increase in endothelial permeability of HUVEC monolayer and decreased VE-cadherin level. Thus, the IL1B treatment disrupts the endothelial integrity and further increases the permeability of HUVEC (Du *et al.*, 2015).

Another overrepresented function was the regulation of nitric oxide biosynthesis. The upregulated genes represented in this function were TNF, IL1B, and IL6. All three had been shown to induce the secretion of nitric oxide (NO) (Zamora, Vodovotz and Billiar, 2000; Kim *et al.*, 2008), which is known to enhance vascular endothelial permeability *in vivo* and *in vitro* (Fukumura *et al.*, 2001; Yang *et al.*, 2015). Furthermore, endothelial nitric oxide synthetase (eNOS)-induced NO has been shown to mediate VEGF-induced angiogenesis and vascular permeability (Fukumura *et al.*, 2001). NO acts on vascular smooth muscle cells by inducing vasodilation, increased blow flow and pressure within the vessels. These actions promote increased permeability of vessels and extravasation of fluid and solutes (Curry and Adamson, 2010; Claesson-Welsh, Dejana and McDonald, 2021).

NOD-like receptors (NLRs) act as a sensor for pathogens recognition and subsequent triggering of the immune response (Strober and Watanabe, 2011). The upregulated genes in this function include TNF, IL1B, CXCL2, IL6, NOD2, and BIRC3. NOD2 is activated by the presence of viral genomes and metabolites. It interacts with other anti-viral proteins to limit the replication of dengue viruses during early infection (Dominguez-Martinez *et al.*, 2021). BIRC3 was involved in maintaining cell proliferation or inflammatory response of endothelial cells (Okada et al., 2006). As for BIRC2, BIRC3 might also be involved in the regulation of vascular integrity and endothelial cell survival through the activation of NF-KB pathway (Santoro *et al.*, 2007).

Among many others, some potential genes such as TNF, IL1B, and IL6 were highly expressed in VEGF-treated endothelial cells and have been reported to be involved in increasing vascular permeability. Furthermore, three of these genes were highly expressed in severe dengue patients and associated with thrombocytopenia (Bozza *et al.*, 2008; Meena *et al.*, 2020; Tuyen *et al.*, 2020; Puc *et al.*, 2021). From all the evidence collected, TNF, IL1B, and IL6 have the potential to be used as multiple biomarkers for the diagnosis of severe dengue.

The genes upregulated after VEGF treatment but showing a lower fold change after VEGF/anti-VEGF treatment were enriched in the regulation of angiogenesis, regulation of cytokine secretion, and cytokine-mediated signalling pathway. The genes involved included IL1B, F3, ETS1, SOCS1, and TLR2. The schematic of enriched functions of the genes that showed a reduction in fold change after VEGF/anti-VEGF treatment is shown in Figure 5.2. IL1B plays a procoagulant role by inducing F3 (tissue factor) to promote angiogenesis (Puhlmann *et al.*, 2005), which precedes vascular permeability. In addition, IL1B also induce the expression of VEGF and VEGFR-2 (Maruyama *et al.*, 1999; Fahey and Doyle, 2019). On the other hand, VEGF was shown to induce the expression of tissue factor in endothelial cells (Mechtcheriakova *et al.*, 1999). The reduction of both IL1B and F3 might be caused by the inhibition from anti-VEGF.

ETS1 is a transcription factor that induces the endothelial cells angiogenic response through stimulation of VEGF (Chen *et al.*, 2017). ETS1 reduction could be due to inhibition of VEGF by anti-VEGF. SOCS1 is the main negative regulator of several cytokines involved in the inflammatory response. Virus infection upregulates the expression of SOCS1 for the virus to overcome the host immune response (Flores-Mendoza *et al.*, 2017). TLR2 is known to participate in immunity upon pathogens exposure by inducing the secretion of T helper 1 and T helper 2 cytokines (Schaub *et al.*, 2004). SOCS1 and TLR2 might not have directly been affected by anti-VEGF treatment but rather by the levels of expression of other cytokines.

In this study, a VEGF/anti-VEGF combination was used on endothelial cells to mimic the *in vivo* conditions in severe dengue patients in whom VEGF levels are most likely high when anti-VEGF treatment is prescribed. Clinically, anti-VEGF is approved for use in cancer treatment, but it can also be used to treat eye diseases such as age-related macular disorders. Bevacizumab is used to treat AMD with an intravitreal injection dosage of 1.25 mg, while for cancer treatments, a dosage of 5 - 15 mg is used (Arevalo *et al.*, 2008; Garcia *et al.*, 2020). For the *in vitro* permeability study, it was significant that the treatment with anti-VEGF did reverse the permeability induced by VEGF. But, in terms of gene expression after anti-VEGF treatment, the pattern is almost the same as after VEGF treatment. The incomplete neutralization of VEGF by anti-VEGF could be explained by partial blocking of VEGF-induced effects by the small dose of anti-VEGF. Peters *et al.* (2007) used 1 mg/ml of Bevacizumab to

completely block 100 ng/ml of VEGF-induced permeability, whereas, in this study, only 400 pg/ml of anti-VEGF antibody were used to neutralize the effects induced by 200 pg/ml of VEGF, with the same incubation time. So, the gene expression from the microarray study needs to be treated with caution since there were effects of anti-VEGF on permeability assay. Thus, for future work in the animal model, more prior work needs to be done on the anti-VEGF concentration, period of treatment, and timing to harvest the sample after treatment.

5.4 Limitations of the Study

The limitations of using VEGF as the diagnostic marker for severe dengue are the difficulty to determine the cut-off VEGF level for severe dengue and the non-specific nature of VEGF expression. Although many studies have reported higher VEGF levels in severe dengue patients compared to dengue patients or controls, the difference in the reported VEGF levels makes it difficult to determine the cut-off level for severe dengue that is applied worldwide. Many reasons contributed to the inconsistency in reported VEGF levels. These are the differences in blood collection methodology (serum or plasma), storage of blood samples during transportation or at a laboratory, study design, and sample size (Thakur *et al.*, 2016). Thus, the VEGF level cut-off for severe dengue needs to be determined in each country to obtain an acceptable cut-off value. The standardisation of the factors that contributed to the inconsistency, as mentioned above, needs to be addressed. Furthermore, many pathological conditions such as cancer and arthritis also expressed higher VEGF levels (Ozgonenel *et al.*,

2010; Wang *et al.*, 2016). Thus, VEGF can be used for confirmed dengue patients who have no diseases associated with increased VEGF levels.

The method of adding VEGF and Anti-VEGF at the same time as co-treatment could have affected the results in this study. The partial neutralisation of Anti-VEGF on the VEGF-induced permeability was reflected in the microarray gene expression study. There was an insignificant difference in the differential gene expression for VEGF and Anti-VEGF treated endothelial cells. The main reason for using VEGF/anti-VEGF as co-treatment was to mimic the in vivo condition in severe dengue patients in whom VEGF levels are most likely high when anti-VEGF treatment is prescribed. Thus, another treatment method that can give a better picture of the gene expression study should be explored.

CHAPTER 6

CONCLUSION

In conclusion, two methods, lateral flow immunoassay and 3D DEP microfluidic chip, were developed in this study to detect VEGF. It is the first time any study has ever utilised lateral flow immunoassay or DEP-based microfluidic assay for VEGF detection. The lowest detected VEGF level for lateral flow immunoassay was 10 ng/ml. Further adjustment or optimisation are needed to increase the sensitivity of lateral flow immunoassay for VEGF detection in future work since the VEGF level present in the patient samples is much lower in the picogram level. 3D DEP microfluidic chip based on the aptamer-antibody sandwich system was shown to be able to detect as low as 5 pg/ml of VEGF, comparable to other microfluidic studies. This 3D DEP microfluidic chip has the potential to be designed to be more user-friendly and applicable in clinics. The use of DEP microfluidic chip can be improved with screen-printing method to print out the chip and electrode. Besides reducing the cost of production, this will also simplify the chip production procedures.

Furthermore, it was shown that VEGF treatment increased permeability across endothelial cells while the addition of anti-VEGF reduced the degree of leakage caused by VEGF. The upregulation of genes after the treatment with VEGF protein was involved in the inflammatory response, regulation of

endothelial barrier, regulation of nitric oxide synthesis, regulation of angiogenesis, and the NOD-like receptor signalling pathway. Many of these genes are encoded for proteins that have been implicated in severe dengue. It is hoped that further studies on the role of these genes in the pathophysiology of severe dengue would yield information that is useful for diagnosis and patient management. Even though the genes expressions across VEGF and VEGF/anti-VEGF treatments were not significantly different in this study, further in-depth analysis is likely to uncover more differences between the two treatments at the gene level. The prospect of using anti-VEGF antibodies to neutralise VEGF gives hope for future effective therapy to stop the progression of dengue into severe dengue.

Future Studies

VEGF is still one of the important markers for dengue diagnosis. The involvement of VEGF or related biomarkers in the pathogenesis of severe dengue should be further elucidated. Nevertheless, the role of VEGF receptors, especially VEGFR2 should not be ignored. In a study by Srikiatkhachorn *et al.*, (2006), the authors showed that VEGFR2 plays a role as a regulator of VEGF. In future studies, VEGF and its receptors (especially VEGFR2) should be studied in a mouse model or dengue-inflicted mouse model for their role in vascular permeability. Genomic studies such as next-generation sequencing (NGS) could identify potential gene targets responsible for vascular permeability, followed by gene knockdown studies to study the function of the targets. In addition, multiple biomarkers could be identified for severe dengue

diagnosis. Since several factors are involved in the control of vascular leakage, potential biomarkers could be those involved as endothelial cell receptors, adherens junctions, permeability factors, and immune complexes (Dalrymple and MacKow, 2012).

The treatment of severe dengue using anti-VEGF should be studied extensively *in vitro* and *in vivo* to find out the effects of anti-VEGF on vascular permeability and plasma leakage. Before embarking on animal studies, more prior work needs to be done on the concentration of anti-VEGF and the duration and timing of treatment before harvesting the post-treatment sample for testing. With more extensive studies inclusive of genomic and proteomic studies, it is hoped that more conclusive results will be produced to show the beneficial effects of using anti-VEGF to reduce vascular permeability.

Since the 3D DEP microfluidic assay tested in this study was able to detect VEGF, the next plan is to use this assay to test the samples obtained from the dengue and severe dengue patients. Either serum or plasma from the patient's whole blood can be used as the testing material. It is important to test using a patient's sample because there are a lot of proteins present in the serum or plasma that could interfere with the results. The validation of the 3D DEP microfluidic assay will be carried out next. Validation parameters such as specificity, precision, accuracy, stability, the limit of detection, and limit of quantification will be performed to find out whether this assay can specifically detect VEGF at

the tested level, the stability of the reagents/antibodies used in the assay, and the lowest amount of detectable VEGF. Specificity tests could be carried out using other biomarkers obtained from microarray studies such as TNF, IL1B or IL6 to test whether the detection system can specifically detect VEGF and no other biomarkers present in the sample.

After the validation process, the VEGF detection kit can be used on patients' sample to find out the effectiveness of this kit to detect severe dengue. Furthermore, the cut-off value of VEGF in dengue and severe dengue can be determined using the clinical samples. When the effectiveness of the kit is validated and the cut-off value of VEGF is determined, it is possible to integrate the other potential biomarkers, if necessary, as part of the multiple biomarkers detection system for severe dengue diagnosis. Among the potential biomarkers are TNF, IL1B, and IL6. For instance, TNF is a pro-inflammatory cytokine involved in inflammatory response, regulation of endothelial barrier function, and regulation of nitric oxide biosynthesis. These functions play major roles in increased vascular permeability and plasma leakage in severe dengue patients.

LIST OF REFERENCES

Afshari, A. R. *et al.* (2019) 'Auraptene-induced cytotoxicity mechanisms in human malignant glioblastoma (U87) cells: Role of reactive oxygen species (ROS)', *EXCLI Journal*, 18, pp. 576–590. doi: 10.17179/excli2019-1136.

Ajlan, B. *et al.* (2019) 'Assessment of the new World Health Organization's dengue classification for predicting severity of illness and level of healthcare required', *PLoS Neglected Tropical Diseases*, 13(8), pp. 1–16. doi: 10.1101/516229.

Amerongen, A. Van *et al.* (2018) 'Lateral Flow Immunoassays', in Vashist, S. K. and Luong, J. H. T. (eds) *Handbook of Immunoassay Technologies*. Elsevier Inc., pp. 157–182. doi: 10.1016/B978-0-12-811762-0.00007-4.

Anderson, R. *et al.* (1997) 'Activation of endothelial cells via antibody-enhanced dengue virus infection of peripheral blood monocytes', *Journal of virology*, 71(6), pp. 4226–4232. doi: 10.1128/jvi.71.6.4226-4232.1997.

Anoopkumar, A. N. and Aneesh, E. M. (2021) 'Environmental epidemiology and neurological manifestations of dengue serotypes with special inference on molecular trends, virus detection, and pathogenicity', *Environment, Development and Sustainability*, 23(8), pp. 11217–11239. doi: 10.1007/s10668-020-01161-7.

Apte, R. S., Chen, D. S. and Ferrara, N. (2019) 'VEGF in signaling and disease: beyond discovery and development', *Cell*, 176(6), pp. 1248–1264. doi: 10.1016/j.cell.2019.01.021.

Arevalo, J. F. *et al.* (2008) 'Primary intravitreal bevacizumab for subfoveal choroidal neovascularization in age-related macular degeneration results of the Pan-American Collaborative Retina Study Group at 12 months follow-up', *Retina*, 28(10), pp. 1387–1394. doi: 10.1097/IAE.0b013e3181884ff4.

Aryati, A. *et al.* (2013) 'Performance of commercial dengue NS1 ELISA and molecular analysis of NS1 gene of dengue viruses obtained during surveillance in Indonesia', *BMC Infectious Diseases*, 13(1). doi: 10.1186/1471-2334-13-611.

Axelrod, T., Eltzov, E. and Marks, R. S. (2020) 'Capture-Layer Lateral Flow Immunoassay: A New Platform Validated in the Detection and Quantification of Dengue NS1', *ACS Omega*, 5(18), pp. 10433–10440. doi: 10.1021/acsomega.0c00367.

De Azeredo, E. L., Monteiro, R. Q. and De-Oliveira Pinto, L. M. (2015) 'Thrombocytopenia in dengue: Interrelationship between virus and the imbalance between coagulation and fibrinolysis and inflammatory mediators', *Mediators of Inflammation*, 2015. doi: 10.1155/2015/313842.

Balakrishnan, T. *et al.* (2011) 'Dengue virus activates polyreactive, natural IgG B cells after primary and secondary infection', *PLoS ONE*, 6(12). doi: 10.1371/journal.pone.0029430.

Ballmer-Hofer, K. (2018) 'Vascular Endothelial Growth Factor, from Basic Research to Clinical Applications', *International Journal of Molecular Sciences*, 19(12), p. 3750. doi: 10.3390/ijms19123750.

Barniol, J. *et al.* (2011) 'Usefulness and applicability of the revised dengue case classification by disease: Multi-centre study in 18 countries', *BMC Infectious Diseases*, 11, pp. 1–12. doi: 10.1186/1471-2334-11-106.

Bente, D. A. and Rico-Hesse, R. (2006) 'Models of dengue virus infection', *Drug Discovery Today: Disease Models*, 3(1), pp. 97–103. doi: 10.1016/j.ddmod.2006.03.014.

Bhatt, P. *et al.* (2021) 'Current Understanding of the Pathogenesis of Dengue Virus Infection', *Current Microbiology*, 78(1), pp. 17–32. doi: 10.1007/s00284-020-02284-w.

Bhatt, S. *et al.* (2013) 'The global distribution and burden of dengue.', *Nature*, 496(7446), pp. 504–507. doi: 10.1038/nature12060.

Bhavanishankar, H. and Manikandan, J. (2021) 'Design and development of low-cost portable function generator', in *2021 IEEE Mysore Sub Section International Conference*. IEEE, pp. 692–696. doi: 10.1109/mysurucon52639.2021.9641085.

Blacksell, S. D. *et al.* (2006) 'The comparative accuracy of 8 commercial rapid immunochromatographic assays for the diagnosis of acute dengue virus infection', *Clinical Infectious Diseases*, 42(8), pp. 1127–1134. doi: 10.1086/501358.

Bozza, F. A. *et al.* (2008) 'Multiplex cytokine profile from dengue patients: MIP-1beta and IFN-gamma as predictive factors for severity', *BMC Infectious Diseases*, 8. doi: 10.1186/1471-2334-8-86.

Brady, O. J. *et al.* (2012) 'Refining the Global Spatial Limits of Dengue Virus Transmission by Evidence-Based Consensus', 6(8). doi: 10.1371/journal.pntd.0001760.

Branche, E. *et al.* (2018) 'Synergism Between the Tyrosine Kinase Inhibitor Sunitinib and Anti-TNF Antibody Protects Against Lethal Dengue Infection', *Antiviral Research*, 158, pp. 1–7. doi: 10.1016/j.antiviral.2018.07.022.

Calabria, D. *et al.* (2021) 'Recent Advancements in Enzyme-Based Lateral Flow Immunoassays', *Sensors*, 21(10), pp. 1–19. doi: https://doi.org/10.3390/s21103358.

Campuzano, S. *et al.* (2020) 'Beyond sensitive and selective electrochemical biosensors: Towards continuous, real-time, antibiofouling and calibration-free devices', *Sensors (Switzerland)*, 20(12), pp. 1–22. doi: 10.3390/s20123376.

Carrington, L. B. and Simmons, C. P. (2014) 'Human to mosquito transmission of dengue viruses', *Frontiers in Immunology*, 5, pp. 1–8. doi: 10.3389/fimmu.2014.00290.

Castellanos, J. E. and Coronel-Ruiz, C. (2014) 'Dengue disease diagnosis : A

puzzle to be solved', *Journal of the Faculty of Medicine*, 62(4), pp. 617–629.

Chamie, J. (2020) *World Population: 2020 Overview, YaleGlobal and the MacMillan Center*. Available at: https://yaleglobal.yale.edu/content/world-population-2020-overview (Accessed: 30 April 2021).

Chan, K. R., Ong, E. Z. and Ooi, E. E. (2013) 'Therapeutic antibodies as a treatment option for dengue fever', *Expert Review of Anti-Infective Therapy*, 11(11), pp. 1147–1157. doi: 10.1586/14787210.2013.839941.

Chau, T. N. B. *et al.* (2009) 'Dengue virus infections and maternal antibody decay in a prospective birth cohort study of vietnamese infants', *Journal of Infectious Diseases*, 200(12), pp. 1893–1900. doi: 10.1086/648407.

Cheah, W. K. *et al.* (2014) 'A Review of Dengue Research in Malaysia', *Medical Journal of Malaysia*, 69(Supplement A), pp. 59–67.

Chen, J. *et al.* (2017) 'VEGF amplifies transcription through ETS1 acetylation to enable angiogenesis', *Nature Communications*, 8(383). doi: 10.1038/s41467-017-00405-x.

Cheng, I. F., Han, H. W. and Chang, H. C. (2012) 'Dielectrophoresis and shear-enhanced sensitivity and selectivity of DNA hybridization for the rapid discrimination of Candida species', *Biosensors and Bioelectronics*, 33(1), pp. 36–43. doi: 10.1016/j.bios.2011.12.005.

Ching, K. H. (2015) 'Lateral Flow Immunoassay', in Hnasko, R. (ed.) *ELISA: Methods and Protocols*. New York: Springer Science+Business Media, pp. 127–137. doi: 10.1007/978-1-4939-2742-5.

Claesson-Welsh, L., Dejana, E. and McDonald, D. M. (2021) 'Permeability of the endothelial barrier: identifying and reconciling controversies', *Trends in Molecular Medicine*, 27(4), pp. 314–331. doi: 10.1016/j.molmed.2020.11.006.

Comhair, S. A. A. *et al.* (2012) 'Human primary lung endothelial cells in culture', *American Journal of Respiratory Cell and Molecular Biology*, 46(6), pp. 723–730. doi: 10.1165/rcmb.2011-0416TE.

Curry, F. R. E. and Adamson, R. H. (2010) 'Vascular permeability modulation at the cell, microvessel, or whole organ level: Towards closing gaps in our knowledge', *Cardiovascular Research*, 87(2), pp. 218–229. doi: 10.1093/cvr/cvq115.

Dalrymple, N. A. and MacKow, E. R. (2012) 'Roles for endothelial cells in dengue virus infection', *Advances in Virology*, 2012, pp. 1–8. doi: 10.1155/2012/840654.

Dehghani, S. *et al.* (2018) 'Aptamer-based biosensors and nanosensors for the detection of vascular endothelial growth factor (VEGF): A review', *Biosensors and Bioelectronics*, 110, pp. 23–37. doi: 10.1016/j.bios.2018.03.037.

Dejnirattisai, W. *et al.* (2016) 'Dengue virus sero-cross-reactivity drives antibody-dependent enhancement of infection with zika virus', *Nature Immunology*, 17(9), pp. 1102–1108. doi: 10.1038/ni.3515.

Dominguez-Martinez, D. *et al.* (2021) 'Dengue virus type 2 replication is limited by activation of NOD2 and its interactions with RIP2 and MAVS adaptors in THP-1 macrophage-like cells', *Authorea*, pp. 1–16. doi: 10.22541/au.161883666.69158067/v1.

Du, L. *et al.* (2015) 'Interleukin-1β increases permeability and upregulates the expression of vascular endothelial-cadherin in human renal glomerular endothelial cells', *Molecular Medicine Reports*, 11(5), pp. 3708–3714. doi: 10.3892/mmr.2015.3172.

Dussart, P. *et al.* (2006) 'Evaluation of an enzyme immunoassay for detection of dengue virus NS1 antigen in human serum', *Clinical and Vaccine Immunology*, 13(11), pp. 1185–1189. doi: 10.1128/CVI.00229-06.

Dussart, P. *et al.* (2020) 'Comparison of dengue case classification schemes and evaluation of biological changes in different dengue clinical patterns in a longitudinal follow-up of hospitalized children in cambodia', *PLoS Neglected Tropical Diseases*, 14(9), pp. 1–23. doi: 10.1371/journal.pntd.0008603.

Dwivedi, V. D. *et al.* (2017) 'Genomics, proteomics and evolution of dengue virus', *Briefings in Functional Genomics*, 16(4), pp. 217–227. doi: 10.1093/bfgp/elw040.

Edge, J. *et al.* (2015) 'Ammonium chloride ingestion attenuates exercise-induced mRNA levels in human muscle', *PLoS ONE*, 10(12), pp. 1–14. doi: 10.1371/journal.pone.0141317.

Elsen, K. Van Den and Quek, J. P. (2021) 'Molecular Insights into the Flavivirus Replication Complex', *Viruses*, 13(6), pp. 1–28.

Fahey, E. and Doyle, S. L. (2019) 'IL-1 family cytokine regulation of vascular permeability and angiogenesis', *Frontiers in Immunology*, 10(JUN), pp. 1–15. doi: 10.3389/fimmu.2019.01426.

Farrell, R. E. (2017) 'Quality Control for RNA Preparations', in Farrell, R. E. (ed.) *RNA Methodologies*. 5th Editio. Academic Press, Inc., pp. 167–185. doi: 10.1016/b978-0-12-804678-4.00006-3.

Fitzgerald, K. A. *et al.* (2001) 'TNFa', in *The Cytokine FactsBook and Webfacts*. Second Edi. Academic Press, Inc., pp. 474–480. doi: https://doi.org/10.1016/B978-0-12-155142-1.X5000-3.

Flores-Mendoza, L. K. *et al.* (2017) 'IL-10 and socs3 Are Predictive Biomarkers of Dengue Hemorrhagic Fever', *Mediators of Inflammation*, 2017. doi: 10.1155/2017/5197592.

Fukumura, D. *et al.* (2001) 'Predominant role of endothelial nitric oxide synthase in vascular endothelial growth factor-induced angiogenesis and vascular permeability', *Proceedings of the National Academy of Sciences of the United States of America*, 98(5), pp. 2604–2609. doi: 10.1073/pnas.041359198.

Gaffen, S. L. *et al.* (2014) 'The IL-23-IL-17 immune axis: From mechanisms to therapeutic testing', *Nature Reviews Immunology*, 14(9), pp. 585–600. doi: 10.1038/nri3707.

Garcia, J. *et al.* (2020) 'Bevacizumab (Avastin®) in cancer treatment: A review of 15 years of clinical experience and future outlook', *Cancer Treatment Reviews*, 86, p. 102017. doi: 10.1016/j.ctrv.2020.102017.

Giebe, S. *et al.* (2017) 'Cigarette smoke extract counteracts atheroprotective effects of high laminar flow on endothelial function', *Redox Biology*, 12(April), pp. 776–786. doi: 10.1016/j.redox.2017.04.008.

Goutam, P., Saha, B. and Mukhopadhyay, S. (2019) 'Study of serum VEGF levels in patients with severe dengue infection admitted in a tertiary care hospital in Kolkata', *Journal of Medical Virology*, 91(10), pp. 1873–1873. doi: 10.1002/jmv.25529.

Green, N. M. (1963) 'Avidin. 3. The Nature of the Biotin-binding Site', *Biochemical Journal*, 89(3), pp. 599–609. doi: 10.1042/bj0890599.

Grobusch, M. P. *et al.* (2006) 'Evaluation of the use of RT-PCR for the early diagnosis of dengue fever', *Clinical Microbiology and Infection*, 12(4), pp. 395–397. doi: 10.1111/j.1469-0691.2006.01353.x.

Gubler, D. J. (1998) 'Dengue and Dengue Hemorrhagic fever', *Clinical Microbiology Review*, 11(3), pp. 480–496. doi: 10.1016/S1045-1870(97)80003-9.

Gubler, D. J. (2011) 'Dengue, Urbanization and Globalization: The Unholy Trinity of the 21st Century', *Tropical Medicine and Health*, 39(4 SUPPL.), pp. 3–11. doi: 10.2149/tmh.2011-S05.

Guo, X. *et al.* (2020) 'Aptamer-Based Biosensor for Detection of Mycotoxins', *Frontiers in Chemistry*, 8(April). doi: 10.3389/fchem.2020.00195.

Gurukumar, K. R. *et al.* (2009) 'Development of real time PCR for detection and quantitation of Dengue Viruses', *Virology journal*, 6(10). doi: 10.1186/1743-422X-6-10.

Guzman, M. G. *et al.* (2010) 'Dengue: a continuing global threat', *Nature Reviews Microbiology*, 8(12), pp. S7–S16. doi: 10.1038/nrmicro2460.

Hadinegoro, S. R. S. (2012) 'The revised WHO dengue case classification: Does the system need to be modified?', *Paediatrics and International Child Health*, 32(SUPP1), pp. 33–38. doi: 10.1179/2046904712Z.00000000052.

Han, G. R. and Kim, M. G. (2020) 'Highly sensitive chemiluminescence-based lateral flow immunoassay for cardiac troponin I detection in human serum', *Sensors*, 20(9), pp. 1–11. doi: 10.3390/s20092593.

Harapan, H. *et al.* (2020) 'Dengue : A Minireview', *Viruses*, 12(8), pp. 1–35. doi: 10.3390/v12080829.

Herwig, M. C., Müller, K. M. and Müller, A. M. (2008) 'Endothelial VE-cadherin expression in human lungs', *Pathology Research and Practice*, 204(10), pp. 725–730. doi: 10.1016/j.prp.2008.04.014.

Hoeben, A. *et al.* (2004) 'Vascular endothelial growth factor and angiogenesis.',

Pharmacological reviews, 56(4), pp. 549–580. doi: 10.1124/pr.56.4.3.549.

Hou, W. *et al.* (2015) 'Development of colloidal gold immunochromatographic strips for detection of Riemerella anatipestifer', *PLoS ONE*, 10(3), pp. 2–13. doi: 10.1371/journal.pone.0122952.

Hunsperger, E. A. *et al.* (2009) 'Evaluation of commercially available anti-dengue virus immunoglobulin M tests', *Emerging Infectious Diseases*, 15(3), pp. 436–440. doi: 10.3201/eid1503.080923.

Iswardy, E. *et al.* (2017) 'A bead-based immunofluorescence-assay on a microfluidic dielectrophoresis platform for rapid dengue virus detection', *Biosensors and Bioelectronics*, 95(1), pp. 174–180. doi: 10.1016/j.bios.2017.04.011.

Jiang, H. *et al.* (2016) 'Interleukin-23 may contribute to the pathogenesis of lumbar disc herniation through the IL-23/IL-17 pathway', *Journal of Orthopaedic Surgery and Research*, 11(1), pp. 1–8. doi: 10.1186/s13018-016-0343-8.

St. John, A. L. (2013) 'Influence of Mast Cells on Dengue Protective Immunity and Immune Pathology', *PLoS Pathogens*, 9(12), pp. 1–4. doi: 10.1371/journal.ppat.1003783.

St. John, A. L. and Rathore, A. P. S. (2019) 'Adaptive immune responses to primary and secondary dengue virus infections', *Nature Reviews Immunology*, 19(4), pp. 218–230. doi: 10.1038/s41577-019-0123-x.

John, D. V., Lin, Y. S. and Perng, G. C. (2015) 'Biomarkers of severe dengue disease - A review', *Journal of Biomedical Science*, 22(1), pp. 1–7. doi: 10.1186/s12929-015-0191-6.

Johnson, K. E. and Wilgus, T. A. (2014) 'Vascular Endothelial Growth Factor and Angiogenesis in the Regulation of Cutaneous Wound Repair', *Advances in wound care*, 3(10), pp. 647–661. doi: 10.1089/wound.2013.0517.

Josephs, S. F. *et al.* (2018) 'Unleashing endogenous TNF-alpha as a cancer immunotherapeutic', *Journal of Translational Medicine*, 16(242). doi: 10.1186/s12967-018-1611-7.

Kabir, A., Zilouchian, H. and Younas, M. A. (2021) 'Dengue Detection : Advances in Diagnostic Tools from Conventional Technology to Point of Care', *Biosensors*, 11(7), pp. 1–28. doi: 10.3390/bios11070206.

Katzelnick, L. C. *et al.* (2020) 'Zika virus infection enhances future risk of severe dengue disease', *Science*, 369(6507), pp. 1123–1128. doi: 10.1126/science.abb6143.

Katzelnick, L. C., Coloma, J. and Harris, E. (2017) 'Dengue: knowledge gaps, unmet needs, and research priorities', *The Lancet Infectious Diseases*, 17(3), pp. e88–e100. doi: 10.1016/S1473-3099(16)30473-X.

Khanna, S. *et al.* (2019) 'Current and upcoming anti-VEGF therapies and dosing strategies for the treatment of neovascular AMD: A comparative review', *BMJ*

Open Ophthalmology, 4(1), pp. 1–8. doi: 10.1136/bmjophth-2019-000398.

Khoshmanesh, K. *et al.* (2012) 'On-chip separation of Lactobacillus bacteria from yeasts using dielectrophoresis', *Microfluidics and Nanofluidics*, 12(1–4), pp. 597–606. doi: 10.1007/s10404-011-0900-8.

Kim, K. O. *et al.* (2008) 'Effect of sildenafil citrate on interleukin-1β-induced nitric oxide synthesis and iNOS expression in SW982 cells', *Experimental and Molecular Medicine*, 40(6), p. 728. doi: 10.3858/emm.2008.40.6.728.

Kim Teng, A. and Satwant, S. (2001) 'Epidemiology and new initiatives in the prevention and control of dengue in Malaysia', *Dengue Bulletin*, 25, pp. 7–14.

Kittigul, L. *et al.* (2000) 'Determination of tumor necrosis factor-alpha levels in dengue virus infected patients by sensitive biotin-streptavidin enzyme-linked immunosorbent assay', *Journal of Virological Methods*, 90(1), pp. 51–57. doi: 10.1016/S0166-0934(00)00215-9.

Koczula, K. M. and Gallotta, A. (2016) 'Lateral flow assays', *Essays in Biochemistry*, 60(1), pp. 111–120. doi: 10.1042/EBC20150012.

Kortlever, R. M. *et al.* (2017) 'Myc Cooperates with Ras by Programming Inflammation and Immune Suppression', *Cell*, 171, pp. 1301–1315. doi: 10.1016/j.cell.2017.11.013.

Krump-Konvalinkova, V. *et al.* (2001) 'Generation of human pulmonary microvascular endothelial cell lines', *Laboratory Investigation*, 81(12), pp. 1717–1727. doi: 10.1038/labinvest.3780385.

Kuczera, D. *et al.* (2018) 'Highlights for Dengue Immunopathogenesis: Antibody-Dependent Enhancement, Cytokine Storm, and Beyond', *Journal of Interferon & Cytokine Research*, 38(2), pp. 69–80. doi: 10.1089/jir.2017.0037.

Kulkarni, R. (2020) 'Antibody-Dependent Enhancement of Viral Infections', in Bramhachari, P. V (ed.) *Dynamics of immune activation in viral diseases*. Singapore: Springer, pp. 9–41. doi: 10.1007/978-981-15-1045-8.

Kumar, S. *et al.* (2021) 'Advanced Lyophilised Loop Mediated Isothermal Amplification (L-LAMP) based point of care technique for the detection of dengue virus', *Journal of Virological Methods*, 293. doi: 10.1016/j.jviromet.2021.114168.

Kusumawathie, P. H. D. (2005) 'Larval infestation of Aedes aegypti and Ae. albopictus in six types of institutions in a dengue transmission area in Kandy, Sri Lanka', *Dengue Bulletin*, 29, pp. 165–168.

Liao, J. Y. and Li, H. (2010) 'Lateral flow immunodipstick for visual detection of aflatoxin B1 in food using immuno-nanoparticles composed of a silver core and a gold shell', *Microchimica Acta*, 171(3), pp. 289–295. doi: 10.1007/s00604-010-0431-0.

Liu, F., Zhang, J. Z. H. and Mei, Y. (2016) 'The origin of the cooperativity in the streptavidin-biotin system: A computational investigation through molecular dynamics simulations', *Scientific Reports*, 6(February). doi: 10.1038/srep27190.

Liu, L. *et al.* (2014) 'Development of an immunochromatographic strip test for rapid detection of ciprofloxacin in milk samples', *Sensors*, 14(9), pp. 16785–16798. doi: 10.3390/s140916785.

Loganathan, T. *et al.* (2020) 'Host transcriptome-guided drug repurposing for COVID-19 treatment: a meta-analysis based approach', *PeerJ*, 8:e9357. doi: 10.7717/peerj.9357.

Lou, J. K. *et al.* (1998) 'An improved method for isolation of microvascular endothelial cells from normal and inflamed human lung', *In Vitro Cellular and Developmental Biology - Animal*, 34(7), pp. 529–536. doi: 10.1007/s11626-998-0112-z.

Low, G. K. K. *et al.* (2018) 'The predictive and diagnostic accuracy of vascular endothelial growth factor and pentraxin-3 in severe dengue', *Pathogens and Global Health*, 112(6), pp. 334–341. doi: 10.1080/20477724.2018.1516417.

Low, G. K. K., Gan, S. C. and Ho, S. C. (2015) 'Biomarkers in differentiating clinical dengue cases: A prospective cohort study', *Journal of Coastal Life Medicine*, 3(12), pp. 967–970. doi: 10.12980/jclm.3.2015j5-141.

Lukman, N. *et al.* (2016) 'Comparison of the Hemagglutination Inhibition Test and IgG ELISA in Categorizing Primary and Secondary Dengue Infections Based on the Plaque Reduction Neutralization Test', *BioMed Research International*, 2016. doi: 10.1155/2016/5253842.

Mai, J. *et al.* (2016) 'Interleukin-17A promotes aortic endothelial cell activation via transcriptionally and post-translationally activating p38 mitogen-activated protein kinase (MAPK) pathway', *Journal of Biological Chemistry*, 291(10), pp. 4939–4954. doi: 10.1074/jbc.M115.690081.

Mälarstig, A. *et al.* (2003) 'A quantitative real-time PCR method for tissue factor mRNA', *Thrombosis Research*, 112(3), pp. 175–183. doi: 10.1016/j.thromres.2003.11.001.

Manocha, P., Chandwani, G. and Das, S. (2020) 'Characterization of Dielectrophoresis Based Relay-Assisted Molecular Communication Using Analogue Transmission Line', *IEEE Access*, 8, pp. 33352–33359. doi: 10.1109/ACCESS.2020.2974067.

Martins-Green, M., Petreaca, M. and Yao, M. (2008) 'An assay system for in vitro detection of permeability in human "endothelium"', in *Methods in Enzymology*. Elsevier, Inc., pp. 137–153. doi: 10.1016/S0076-6879(08)02008-9.

Maruo, N. *et al.* (1992) 'IL-6 increases endothelial permeability in vitro', *Endocrinology*, 131(2), pp. 710–714. doi: 10.1210/endo.131.2.1639018.

Maruyama, K. *et al.* (1999) 'Interleukin-1β upregulates cardiac expression of vascular endothelial growth factor and its receptor KDR/flk-1 via activation of protein tyrosine kinases', *Journal of Molecular and Cellular Cardiology*, 31(3), pp. 607–617. doi: 10.1006/jmcc.1998.0895.

Mathew, A. *et al.* (2011) 'B-cell responses during primary and secondary dengue

virus infections in humans', *Journal of Infectious Diseases*, 204(10), pp. 1514–1522. doi: 10.1093/infdis/jir607.

Meadows, K. L. and Hurwitz, H. I. (2012) 'Anti-VEGF therapies in the clinic', *Cold Spring Harbor Perspectives in Biology*, 2(10). doi: 10.1101/cshperspect.a006577.

Mechtcheriakova, D. *et al.* (1999) 'Vascular endothelial cell growth factor–induced tissue factor expression in endothelial cells is mediated by EGR-1', *Blood*, 93(11), pp. 3811–3823. doi: 10.1182/blood.v93.11.3811.

Meena, A. A. *et al.* (2020) 'Increase of Plasma TNF-α Is Associated with Decreased Levels of Blood Platelets in Clinical Dengue Infection', *Viral Immunology*, 33(1), pp. 54–60. doi: 10.1089/vim.2019.0100.

Mia, M. S. *et al.* (2016) 'Assessing the cost burden of dengue infection to households in Seremban, Malaysia', *The Southeast Asian Journal of Tropical Medicine Public Health*, 47(6), pp. 1167–1176.

Ministry of Health Malaysia (2020) *Dengue Statistics*. Available at: https://idengue.mysa.gov.my/pdf/statistik.pdf (Accessed: 6 October 2021).

Moghaddam, S. M. *et al.* (2012) 'Significance of vascular endothelial growth factor in growth and peritoneal dissemination of ovarian cancer.', *Cancer metastasis reviews*, 31(1–2), pp. 143–62. doi: 10.1007/s10555-011-9337-5.

Moi, M. L., Takasaki, T. and Kurane, I. (2016) 'Human antibody response to dengue virus: Implications for dengue vaccine design', *Tropical Medicine and Health*, 44(1), pp. 1–6. doi: 10.1186/s41182-016-0004-y.

Monaghan-Benson, E. and Burridge, K. (2009) 'The regulation of vascular endothelial growth factor-induced microvascular permeability requires Rac and reactive oxygen species', *Journal of Biological Chemistry*, 284(38), pp. 25602–25611. doi: 10.1074/jbc.M109.009894.

Mottram, L. *et al.* (2006) 'The Pennsylvania Green Fluorophore: A Hybrid of Oregon Green and Tokyo Green for the Construction of Hydrophobic and pH-Insensitive Molecular Probes', *Organic Letters*, 8(4), pp. 581–584. doi: 10.1021/nn2045246.Multifunctional.

Muhammad Azami, N. A. *et al.* (2011) 'Dengue epidemic in Malaysia: Not a predominantly urban disease anymore', *BMC Research Notes*, 4. doi: 10.1186/1756-0500-4-216.

Mukherjee, S., Saha, B. and Tripathi, A. (2022) 'Clinical significance of differential serum-signatures for early prediction of severe dengue among Eastern Indian patients', *Clinical and Experimental Immunology*. doi: 10.1093/cei/uxac018.

Muller, D. A., Depelsenaire, A. C. I. and Young, P. R. (2017) 'Clinical and Laboratory Diagnosis of Dengue Virus Infection', *Journal of Infectious Diseases*, 215(Suppl 2), pp. S89–S95. doi: 10.1093/infdis/jiw649.

Mun, M. J. *et al.* (2019) 'One-step multiplex real-time RT-PCR for detection

and typing of dengue virus', *Molecular and Cellular Probes*, 43, pp. 86–91. doi: 10.1016/j.mcp.2018.10.001.

Murugesan, A. and Manoharan, M. (2020) 'Dengue Virus', in Ennaji, M. M. (ed.) *Emerging and Reemerging Viral Pathogens*. 1st Editio. Academic Press, Inc., pp. 281–359. doi: https://doi.org/10.1016/C2018-0-04146-8.

Musso, D., Cao-Lormeau, V. M. and Gubler, D. J. (2015) 'Zika virus: Following the path of dengue and chikungunya?', *The Lancet*, 386(9990), pp. 243–244. doi: 10.1016/S0140-6736(15)61273-9.

Mutiara *et al.* (2019) 'The vascular endothelium in patients with dengue haemorrhagic fever', *Open Access Macedonian Journal of Medical Sciences*, 7(14), pp. 2221–2225. doi: 10.3889/oamjms.2019.621.

Najioullah, F., Viron, F. and Césaire, R. (2014) 'Evaluation of four commercial real-time RT-PCR kits for the detection of dengue viruses in clinical samples', *Virology Journal*, 11. doi: https://doi.org/10.1186/1743-422X-11-164.

Nanaware, N. *et al.* (2021) 'Dengue virus infection: A tale of viral exploitations and host responses', *Viruses*, 13(10). doi: 10.3390/v13101967.

National Institutes of Health (2021) *The Histroy Of The Pregnancy Test*. Available at: https://history.nih.gov/display/history/Pregnancy+Test+-+A+Thin+Blue+Line+The+History+of+the+Pregnancy+Test (Accessed: 17 August 2021).

Nature Immunology (2007) 'Pathogenesis: How far have we come?', p. 1141. doi: 10.1038/ni1107-1141.

Newman, P. J. (1997) 'The biology of PECAM-1', *Journal of Clinical Investigation*, 99(1), pp. 1–5. doi: 10.1172/jci119500.

Nonaka, Y., Abe, K. and Ikebukuro, K. (2012) 'Electrochemical detection of vascular endothelial growth factor with aptamer sandwich', *Electrochemistry*, 80(5), pp. 363–366. doi: 10.5796/electrochemistry.80.363.

O'Farrell, B. (2009) 'Evolution in Lateral Flow–Based Immunoassay Systems', in Wong, R. C. and Tse, H. Y. (eds) *Lateral Flow Immunoassay*. New York: Humana Press, pp. 1–33. doi: 10.1007/978-1-59745-240-3.

Owen-Woods, C. *et al.* (2020) 'Local microvascular leakage promotes trafficking of activated neutrophils to remote organs', *Journal of Clinical Investigation*, 130(5), pp. 2301–2318. doi: 10.1172/JCI133661.

Ozgonenel, L. *et al.* (2010) 'The relation of serum vascular endothelial growth factor level with disease duration and activity in patients with rheumatoid arthritis', *Clinical Rheumatology*, 29(5), pp. 473–477. doi: 10.1007/s10067-009-1343-4.

Pal, S. *et al.* (2015) 'Multicountry prospective clinical evaluation of two enzyme-linked immunosorbent assays and two rapid diagnostic tests for diagnosing dengue fever', *Journal of Clinical Microbiology*, 53(4), pp. 1092–1102. doi: 10.1128/JCM.03042-14.

Pan, P. *et al.* (2019) 'Dengue virus infection activates interleukin-1β to induce tissue injury and vascular leakage', *Frontiers in Microbiology*, 10, pp. 1–14. doi: 10.3389/fmicb.2019.02637.

Pang, E. L. and Loh, H. S. (2016) 'Current perspectives on dengue episode in Malaysia', *Asian Pacific Journal of Tropical Medicine*, 9(4), pp. 395–401. doi: 10.1016/j.apjtm.2016.03.004.

Parolo, C., de la Escosura-Muñiz, A. and Merkoçi, A. (2013) 'Enhanced lateral flow immunoassay using gold nanoparticles loaded with enzymes', *Biosensors and Bioelectronics*, 40(1), pp. 412–416. doi: 10.1016/j.bios.2012.06.049.

Paz-Bailey, G. *et al.* (2021) *Dengue Vaccine : Recommendations of the Advisory Committee on Immunization Practices , United States , 2021*. Georgia. doi: http://dx.doi.org/10.15585/mmwr.rr7006a1.

Peeling, R. W. *et al.* (2006) 'Rapid tests for sexually transmitted infections (STIs): The way forward', *Sexually Transmitted Infections*, 82(SUPPL. 5), pp. v1–v6. doi: 10.1136/sti.2006.024265.

Peeling, R. W. *et al.* (2010) 'Evaluation of diagnostic tests: dengue', *Nat. Rev. Microbiol.*, 8(12), pp. 530–538. doi: 10.1038/nrmicro2459.

Peters, S. *et al.* (2007) 'Antipermeability and antiproliferative effects of standard and frozen bevacizumab on choroidal endothelial cells', *British Journal of Ophthalmology*, 91(6), pp. 827–831. doi: 10.1136/bjo.2006.109702.

Poovaneswari, S. (1993) 'Dengue situation in Malaysia.', *The Malaysian journal of pathology*, 15(1), pp. 3–7.

Posthuma-Trumpie, G. A., Korf, J. and Van Amerongen, A. (2009) 'Lateral flow (immuno)assay: Its strengths, weaknesses, opportunities and threats. A literature survey', *Analytical and Bioanalytical Chemistry*, 393(2), pp. 569–582. doi: 10.1007/s00216-008-2287-2.

Puc, I. *et al.* (2021) 'Cytokine Signature of Dengue Patients at Different Severity of the Disease', *International Journal of Molecular Sciences*, 22, pp. 1–15. doi: 10.3390/ijms22062879.

Puhlmann, M. *et al.* (2005) 'Interleukin-1β induced vascular permeability is dependent on induction of endothelial tissue factor (TF) activity', *Journal of Translational Medicine*, 3(37). doi: 10.1186/1479-5876-3-37.

Qian, C. *et al.* (2014) 'Dielectrophoresis for bioparticle manipulation', *International Journal of Molecular Sciences*, 15(10), pp. 18281–18309. doi: 10.3390/ijms151018281.

Rahman, N. A., Ibrahim, F. and Yafouz, B. (2017) 'Dielectrophoresis for Biomedical Sciences Applications : A Review', *Sensors*, 17(449), pp. 1–27. doi: 10.3390/s17030449.

Ramirez-Murillo, C. J., de los Santos-Ramirez, J. M. and Perez-Gonzalez, V. H. (2021) 'Toward low-voltage dielectrophoresis-based microfluidic systems: A review', *Electrophoresis*, 42(5), pp. 565–587. doi: 10.1002/elps.202000213.

Ravindran, S. (2021) '40% drop in dengue cases', *The Star*, 11 January. Available at: https://www.thestar.com.my/metro/metro-news/2021/01/11/40-drop-in-dengue-cases.

Rosales Ramirez, R. and Ludert, J. E. (2019) 'The Dengue Virus Nonstructural Protein 1 (NS1) Is Secreted from Mosquito Cells in Association with the Intracellular Cholesterol Transporter Chaperone Caveolin Complex', *Journal of Virology*, 93(4). doi: 10.1128/jvi.01985-18.

Rothman, A. L. (2011) 'Immunity to dengue virus: A tale of original antigenic sin and tropical cytokine storms', *Nature Reviews Immunology*, 11(8), pp. 532–543. doi: 10.1038/nri3014.

Roy, S. K. and Bhattacharjee, S. (2021) 'Dengue virus: Epidemiology, biology, and disease aetiology', *Canadian Journal of Microbiology*, 67(10), pp. 687–702. doi: 10.1139/cjm-2020-0572.

Sanghavi, B. J. *et al.* (2014) 'Electrokinetic preconcentration and detection of neuropeptides at patterned graphene-modified electrodes in a nanochannel', *Analytical Chemistry*, 86(9), pp. 4120–4125. doi: 10.1021/ac500155g.

Santoro, M. M. *et al.* (2007) 'Birc2 (cIap1) regulates endothelial cell integrity and blood vessel homeostasis', *Nature Genetics*, 39(11), pp. 1397–1402. doi: 10.1038/ng.2007.8.

Scaturro, P. *et al.* (2015) 'Dengue Virus Non-structural Protein 1 Modulates Infectious Particle Production via Interaction with the Structural Proteins', *PLoS Pathogens*, 11(11), pp. 1–32. doi: 10.1371/journal.ppat.1005277.

Schaub, B. *et al.* (2004) 'TLR2 and TLR4 stimulation differentially induce cytokine secretion in human neonatal, adult, and murine mononuclear cells', *Journal of Interferon & Cytokine Research*, 24(9), pp. 543–552. doi: 10.1089/jir.2004.24.543.

Seet, R. C. S. *et al.* (2009) 'Relationship between circulating vascular endothelial growth factor and its soluble receptors in adults with dengue virus infection: a case-control study', *International Journal of Infectious Diseases*, 13(5), pp. 248–253. doi: 10.1016/j.ijid.2008.11.028.

Senger, D. R. *et al.* (1983) 'Tumor cells secrete a vascular permeability factor that promotes accumulation of ascites fluid.', *Science*, 219(4587), pp. 983–985. doi: 6823562.

Shepard, D. S. *et al.* (2012) 'Use of Multiple Data Sources to Estimate the Economic Cost of Dengue Illness in Malaysia', *American Journal of Tropical Medicine and Hygiene*, 87(5), pp. 796–805. doi: 10.4269/ajtmh.2012.12-0019.

Shin, Y.-H., Teresa Gutierrez-Wing, M. and Choi, J.-W. (2021) 'Review—Recent Progress in Portable Fluorescence Sensors', *Journal of The Electrochemical Society*, 168(1). doi: 10.1149/1945-7111/abd494.

Sim, S. and Hibberd, M. L. (2016) 'Genomic approaches for understanding dengue: Insights from the virus, vector, and host', *Genome Biology*, 17(38), pp. 1–15. doi: 10.1186/s13059-016-0907-2.

Sjölinder, M. *et al.* (2012) 'The meningococcal adhesin NhhA provokes proinflammatory responses in macrophages via toll-like receptor 4-dependent and -independent pathways', *Infection and Immunity*, pp. 4027–4033. doi: 10.1128/IAI.00456-12.

Song, H. *et al.* (2015) 'Continuous-flow sorting of stem cells and differentiation products based on dielectrophoresis', *Lab on a Chip*, 15(5), pp. 1320–1328. doi: 10.1039/c4lc01253d.

Spiropoulou, C. F. and Srikiatkhachorn, A. (2013) 'The role of endothelial activation in dengue hemorrhagic fever and hantavirus pulmonary syndrome', *Virulence*, 4(6), pp. 525–536. doi: 10.4161/viru.25569.

Srikiatkhachorn, A. *et al.* (2006) 'Virus-induced decline in soluble vascular endothelial growth receptor 2 is associated with plasma leakage in dengue hemorrhagic fever', *Journal of Virology*, 81(4), pp. 1592–1600. doi: 10.1128/JVI.01642-06.

Srikiatkhachorn, A., Mathew, A. and Rothman, A. L. (2017) 'Immune-mediated cytokine storm and its role in severe dengue', *Seminars in Immunopathology*, 39(5), pp. 563–574. doi: 10.1007/s00281-017-0625-1.

Stanaway, J. D. *et al.* (2016) 'The global burden of dengue: an analysis from the Global Burden of Disease Study 2013', *The Lancet Infectious Diseases*, 3099(16), pp. 1–12. doi: 10.1016/S1473-3099(16)00026-8.

Strimbu, K. and Tavel, J. A. (2010) 'What are Biomarkers?', *Current Opinion in HIV and AIDS*, 5(6), pp. 463–466. doi: 10.1097/COH.0b013e32833ed177.What.

Strober, W. and Watanabe, T. (2011) 'NOD2, an intracellular innate immune sensor involved in host defense and Crohn's disease', *Mucosal Immunology*, 4(5), pp. 484–495. doi: 10.1038/mi.2011.29.

Su, W. *et al.* (2015) 'Microfluidic platform towards point-of-care diagnostics in infectious diseases', *Journal of Chromatography A*, 1377, pp. 13–26. doi: 10.1016/j.chroma.2014.12.041.

Thakur, P. *et al.* (2016) 'Elevated levels of vascular endothelial growth factor in adults with severe dengue infection', *Virus Disease*, 27(1), pp. 48–54. doi: 10.1007/s13337-015-0296-2.

The Gene Ontology Consortium *et al.* (2000) 'Gene Ontology: tool for the unification of biology', *Nature Genetics*, 25(1), pp. 25–29. doi: 10.1038/75556.Gene.

Thomas, S. J. and Yoon, I. K. (2019) 'A review of Dengvaxia®: development to deployment', *Human Vaccines and Immunotherapeutics*, 15(10), pp. 2295–2314. doi: 10.1080/21645515.2019.1658503.

Tran, T. V. *et al.* (2019) 'Development of a highly sensitive magneto-enzyme lateral flow immunoassay for dengue NS1 detection', *PeerJ*, 2019(9), pp. 1–18. doi: 10.7717/peerj.7779.

Tseng, C.-S. *et al.* (2005) 'Elevated levels of plasma VEGF in patients with dengue hemorrhagic fever', *FEMS immunology and medical microbiology*, 43, pp. 99–102. doi: 10.1016/j.femsim.2004.10.004.

Tuohimaa, P. *et al.* (2013) 'Gene Expression Profiles in Human and Mouse Primary Cells Provide New Insights into the Differential Actions of Vitamin D3 Metabolites', *PLoS ONE*, 8(10). doi: 10.1371/journal.pone.0075338.

Tuyen, T. T. *et al.* (2020) 'Proinflammatory Cytokines Are Modulated in Vietnamese Patients with Dengue Fever', *Viral Immunology*, 33(7), pp. 514–520. doi: 10.1089/vim.2020.0023.

Ubol, S. *et al.* (2010) 'Mechanisms of immune evasion induced by a complex of dengue virus and preexisting enhancing antibodies', *Journal of Infectious Diseases*, 201(6), pp. 923–935. doi: 10.1086/651018.

Uno, N. and Ross, T. M. (2018) 'Dengue virus and the host innate immune response', *Emerging Microbes and Infections*, 7(1), pp. 1–11. doi: 10.1038/s41426-018-0168-0.

Urmann, K. *et al.* (2017) 'Aptamer-modified nanomaterials: Principles and applications', *BioNanoMaterials*, 18(1–2), pp. 1–17. doi: 10.1515/bnm-2016-0012.

Viefhues, M. and Eichhorn, R. (2017a) 'DNA dielectrophoresis : Theory and Applications A Reveiw', *Electrophoresis*, 38, pp. 1483–1506. doi: 10.1002/elps.201600482.

Viefhues, M. and Eichhorn, R. (2017b) 'DNA dielectrophoresis: Theory and applications a review', *Electrophoresis*, pp. 1483–1506. doi: 10.1002/elps.201600482.

Waggoner, J. J. *et al.* (2016) 'Homotypic Dengue Virus Reinfections in Nicaraguan Children', *Journal of Infectious Diseases*, 214(7), pp. 986–993. doi: 10.1093/infdis/jiw099.

Wang, L. *et al.* (2016) 'Predictive Significance of Serum Level of Vascular Endothelial Growth Factor in Gastric Cancer Patients', *BioMed Research International*, 2016. doi: 10.1155/2016/8103019.

Wang, W. H. *et al.* (2020) 'Dengue hemorrhagic fever – A systemic literature review of current perspectives on pathogenesis, prevention and control', *Journal of Microbiology, Immunology and Infection*, 53(6), pp. 963–978. doi: 10.1016/j.jmii.2020.03.007.

Wedmore, C. V. and Williams, T. J. (1981) 'Control of vascular permeability by polymorphonuclear leukocytes in inflammation', *Nature*, 289, pp. 646–650.

WHO International Programme on Chemical Safety (1993) *Biomarkers and Risk Assessment: Concepts and Principles*. Available at: http://www.inchem.org/documents/ehc/ehc/ehc155.htm (Accessed: 16 August 2021).

Wilfinger, W. W., Mackey, K. and Chomczynski, P. (1997) 'Effect of pH and

ionic strength on the spectrophotometric assessment of nucleic acid purity', *BioTechniques*, 22(3), pp. 474–481. doi: 10.2144/97223st01.

Wong, P. F., Wong, L. P. and AbuBakar, S. (2020) 'Diagnosis of severe dengue: Challenges, needs and opportunities', *Journal of Infection and Public Health*, 13(2), pp. 193–198. doi: 10.1016/j.jiph.2019.07.012.

Woon, Y. L. *et al.* (2019) 'Zika virus infection in Malaysia: An epidemiological, clinical and virological analysis', *BMC Infectious Diseases*, 19(1), pp. 1–9. doi: 10.1186/s12879-019-3786-9.

World Health Organization (1997) *Dengue Hemorrhagic Fever: Diagnosis, Treatment and Control, World Health Organization*. doi: 10.4269/ajtmh.1987.36.670.

World Health Organization (2009) *Dengue: guidelines for diagnosis, treatment, prevention and control, World Health Organization*. doi: WHO/HTM/NTD/DEN/2009.1.

World Health Organization (2011) *Comprehensive guidelines for prevention and control of dengue and dengue haemorrhagic fever, WHO Regional Publication SEARO*. Available at: https://apps.who.int/iris/handle/10665/204894.

World Health Organization (2012a) *Global Strategy for Dengue Prevention and Control 2012-2020*.

World Health Organization (2012b) *Handbook for clinical management of dengue, World Health Organization*. Available at: https://apps.who.int/iris/handle/10665/76887.

World Health Organization (2020) *Dengue and Severe Dengue, World Health Organization*. Available at: https://www.who.int/news-room/fact-sheets/detail/dengue-and-severe-dengue.

World Health Organization (2021) *Dengue and Severe Dengue, World Health Organization*. Available at: https://www.who.int/news-room/fact-sheets/detail/dengue-and-severe-dengue (Accessed: 6 July 2021).

Yang, B. *et al.* (2015) 'Nitric oxide increases arterial endotheial permeability through mediating VE-cadherin expression during arteriogenesis', *PLoS ONE*, 10(7), pp. 1–15. doi: 10.1371/journal.pone.0127931.

Yow, K. S. *et al.* (2021) 'Rapid diagnostic tests for the detection of recent dengue infections: An evaluation of six kits on clinical specimens', *PLoS ONE*, 16(4 April), pp. 1–11. doi: 10.1371/journal.pone.0249602.

Zamora, R., Vodovotz, Y. and Billiar, T. R. (2000) 'Inducible nitric oxide synthase and inflammatory diseases', *Molecular medicine*, 6(5), pp. 347–373. doi: 10.1007/bf03401781.

Zhang, H., Chang, H. and Neuzil, P. (2019) 'DEP-on-a-chip: Dielectrophoresis applied to microfluidic platforms', *Micromachines*, 10(6), pp. 1–22. doi: 10.3390/mi10060423.

Zhang, Y. *et al.* (2017) ‘DT-13 ameliorates TNF-α-induced vascular endothelial hyperpermeability via non-muscle myosin IIA and the Src/PI3K/Akt signaling pathway’, *Frontiers in Immunology*. doi: 10.3389/fimmu.2017.00925.

Zhao, Z. *et al.* (2015) ‘On-chip porous microgel generation for microfluidic enhanced VEGF detection’, *Biosensors and Bioelectronics*, 74, pp. 305–312. doi: 10.1016/j.bios.2015.06.047.

Zhu, H. *et al.* (2015) ‘Screen-printed microfluidic dielectrophoresis chip for cell separation’, *Biosensors and Bioelectronics*, 63, pp. 371–378. doi: 10.1016/j.bios.2014.07.072.

Zirlik, K. and Duyster, J. (2018) ‘Anti-angiogenics: current situation and future perspectives’, *Oncology Research and Treatment*, 41(4), pp. 166–171. doi: 10.1159/000488087.

Zompi, S. and Harris, E. (2012) ‘Animal models of dengue virus infection’, *Viruses*, 4(1), pp. 62–82. doi: 10.3390/v4010062.

APPENDICES

APPENDIX A

VEGF-treated Endothelial Cells (Upregulated Genes)

Probe Name	Gene Symbol	Fold Change	Regulation	Description
A_33_P3226832	F3	330.17462	up	Homo sapiens coagulation factor III (thromboplastin, tissue factor) (F3), transcript variant 1, mRNA [NM_001993]
A_23_P133408	CSF2	299.6112	up	Homo sapiens colony stimulating factor 2 (granulocyte-macrophage) (CSF2), mRNA [NM_000758]
A_24_P122137	LIF	191.54172	up	Homo sapiens leukemia inhibitory factor (LIF), transcript variant 1, mRNA [NM_002309]
A_23_P376488	TNF	180.81662	up	Homo sapiens tumor necrosis factor (TNF), mRNA [NM_000594]
A_24_P183150	CXCL3	175.95335	up	Homo sapiens chemokine (C-X-C motif) ligand 3 (CXCL3), mRNA [NM_002090]
A_23_P501754	CSF3	92.72717	up	Homo sapiens colony stimulating factor 3 (granulocyte) (CSF3), transcript variant 1, mRNA [NM_000759]
A_33_P3356462	C2CD4A	85.61715	up	Homo sapiens C2 calcium-dependent domain containing 4A (C2CD4A), mRNA [NM_207322]
A_23_P76078	IL23A	68.99076	up	Homo sapiens interleukin 23, alpha subunit p19 (IL23A), mRNA [NM_016584]
A_23_P79518	IL1B	66.465576	up	Homo sapiens interleukin 1, beta (IL1B), mRNA [NM_000576]
A_24_P257416	CXCL2	57.754406	up	Homo sapiens chemokine (C-X-C motif) ligand 2 (CXCL2), mRNA [NM_002089]
A_33_P3421053	SELE	44.248363	up	Homo sapiens selectin E (SELE), mRNA [NM_000450]
A_33_P3222424	CSF3	42.32525	up	Homo sapiens colony stimulating factor 3 (granulocyte) (CSF3), transcript variant 1, mRNA [NM_000759]
A_23_P71037	IL6	34.07459	up	Homo sapiens interleukin 6 (IL6), mRNA [NM_000600]
A_23_P420863	NOD2	33.842346	up	Homo sapiens nucleotide-binding oligomerization domain containing 2 (NOD2), transcript variant 1, mRNA [NM_022162]
A_23_P320578	RGS16	29.848503	up	Homo sapiens regulator of G-protein signaling 16 (RGS16), mRNA [NM_002928]

APPENDIX A (CONTINUED)

A_23_P23947	MAP3K8	27.343248	up	Homo sapiens mitogen-activated protein kinase kinase kinase 8 (MAP3K8), transcript variant 1, mRNA [NM_005204]
A_23_P315364	CXCL2	27.191536	up	Homo sapiens chemokine (C-X-C motif) ligand 2 (CXCL2), mRNA [NM_002089]
A_23_P420196	SOCS1	20.916885	up	Homo sapiens suppressor of cytokine signaling 1 (SOCS1), mRNA [NM_003745]
A_23_P98350	BIRC3	20.455994	up	Homo sapiens baculoviral IAP repeat containing 3 (BIRC3), transcript variant 1, mRNA [NM_001165]
A_23_P155755	CXCL6	20.105919	up	Homo sapiens chemokine (C-X-C motif) ligand 6 (CXCL6), mRNA [NM_002993]
A_23_P97112	SELE	19.432842	up	Homo sapiens selectin E (SELE), mRNA [NM_000450]
A_23_P53370	RND1	18.93252	up	Homo sapiens Rho family GTPase 1 (RND1), mRNA [NM_014470]
A_23_P131676	ACKR3	17.838457	up	Homo sapiens atypical chemokine receptor 3 (ACKR3), mRNA [NM_020311]
A_24_P157926	TNFAIP3	15.883922	up	Homo sapiens tumor necrosis factor, alpha-induced protein 3 (TNFAIP3), transcript variant 3, mRNA [NM_006290]
A_23_P128744	BDKRB1	15.623361	up	Homo sapiens bradykinin receptor B1 (BDKRB1), mRNA [NM_000710]
A_24_P390495	CX3CL1	15.307315	up	chemokine (C-X3-C motif) ligand 1 [Source:HGNC Symbol;Acc:HGNC:10647] [ENST00000006053]
A_23_P393034	HAS3	14.883393	up	Homo sapiens hyaluronan synthase 3 (HAS3), transcript variant 1, mRNA [NM_005329]
A_23_P328740	NEURL3	13.242845	up	Homo sapiens neuralized E3 ubiquitin protein ligase 3 (NEURL3), transcript variant 2, mRNA [NM_001285486]
A_24_P250922	PTGS2	12.991401	up	Homo sapiens prostaglandin-endoperoxide synthase 2 (prostaglandin G/H synthase and cyclooxygenase) (PTGS2), mRNA [NM_000963]
A_23_P421423	TNFAIP2	12.9567175	up	Homo sapiens tumor necrosis factor, alpha-induced protein 2 (TNFAIP2), mRNA [NM_006291]
A_23_P39237	ZFP36	12.595078	up	Homo sapiens ZFP36 ring finger protein (ZFP36), mRNA [NM_003407]
A_33_P3330264	CXCL1	12.20536	up	Homo sapiens chemokine (C-X-C motif) ligand 1 (melanoma growth stimulating activity, alpha) (CXCL1), transcript variant 1, mRNA [NM_001511]
A_23_P87879	CD69	10.859992	up	Homo sapiens CD69 molecule (CD69), mRNA [NM_001781]

APPENDIX A (CONTINUED)

A_33_P3237150	BMP2	10.534904	up	Homo sapiens bone morphogenetic protein 2 (BMP2), mRNA [NM_001200]
A_33_P3370575	CD200	10.107875	up	Homo sapiens CD200 molecule (CD200), transcript variant 2, mRNA [NM_001004196]
A_32_P83845	HEY1	9.841812	up	Homo sapiens hes-related family bHLH transcription factor with YRPW motif 1 (HEY1), transcript variant 2, mRNA [NM_001040708]
A_21_P0000174	C5orf56	9.199766	up	Homo sapiens cDNA, FLJ99232. [AK309191]
A_33_P3214720	ZC3H12A	9.014324	up	Homo sapiens zinc finger CCCH-type containing 12A (ZC3H12A), mRNA [NM_025079]
A_23_P70670	CD83	8.77285	up	Homo sapiens CD83 molecule (CD83), transcript variant 1, mRNA [NM_004233]
A_23_P121480	CD200	8.579126	up	Homo sapiens CD200 molecule (CD200), transcript variant 2, mRNA [NM_001004196]
A_23_P144337	CCRN4L	8.525857	up	Homo sapiens CCR4 carbon catabolite repression 4-like (S. cerevisiae) (CCRN4L), mRNA [NM_012118]
A_24_P788878	C2CD4B	8.509412	up	Homo sapiens C2 calcium-dependent domain containing 4B (C2CD4B), mRNA [NM_001007595]
A_23_P212089	NFKBIZ	8.321529	up	Homo sapiens nuclear factor of kappa light polypeptide gene enhancer in B-cells inhibitor, zeta (NFKBIZ), transcript variant 1, mRNA [NM_031419]
A_23_P118392	RASD1	7.7283387	up	Homo sapiens RAS, dexamethasone-induced 1 (RASD1), transcript variant 1, mRNA [NM_016084]
A_23_P109034	SDC4	7.5433693	up	Homo sapiens syndecan 4 (SDC4), mRNA [NM_002999]
A_23_P119478	EBI3	7.361379	up	Homo sapiens Epstein-Barr virus induced 3 (EBI3), mRNA [NM_005755]
A_33_P3311439	GCH1	6.77119	up	Homo sapiens GTP cyclohydrolase 1 (GCH1), transcript variant 4, mRNA [NM_001024071]
A_24_P167642	GCH1	6.716286	up	Homo sapiens GTP cyclohydrolase 1 (GCH1), transcript variant 1, mRNA [NM_000161]
A_23_P41765	IRF1	5.8745155	up	Homo sapiens interferon regulatory factor 1 (IRF1), mRNA [NM_002198]
A_23_P201808	PPAP2B	5.686889	up	Homo sapiens phosphatidic acid phosphatase type 2B (PPAP2B), mRNA [NM_003713]
A_33_P3220390	WTAP	5.5991445	up	Homo sapiens Wilms tumor 1 associated protein, mRNA (cDNA clone IMAGE:5399821), partial cds. [BC028180]
A_23_P34915	ATF3	5.3914394	up	Homo sapiens activating transcription factor 3 (ATF3), transcript variant 4, mRNA [NM_001040619]

APPENDIX A (CONTINUED)

A_23_P69573	GUCY1A3	5.36671	up	Homo sapiens guanylate cyclase 1, soluble, alpha 3 (GUCY1A3), transcript variant 1, mRNA [NM_000856]
A_33_P3368646	CNKSR3	4.9159584	up	Homo sapiens CNKSR family member 3 (CNKSR3), mRNA [NM_173515]
A_23_P134176	SOD2	4.8219233	up	Homo sapiens superoxide dismutase 2, mitochondrial (SOD2), transcript variant 2, mRNA [NM_001024465]
A_33_P3211666	IL18R1	4.756661	up	Homo sapiens interleukin 18 receptor 1 (IL18R1), transcript variant 1, mRNA [NM_003855]
A_23_P388993	ZC3H12C	4.7022414	up	Homo sapiens zinc finger CCCH-type containing 12C (ZC3H12C), mRNA [NM_033390]
A_23_P81898	UBD	4.5020127	up	Homo sapiens ubiquitin D (UBD), mRNA [NM_006398]
A_23_P153320	ICAM1	4.4947906	up	Homo sapiens intercellular adhesion molecule 1 (ICAM1), mRNA [NM_000201]
A_33_P3253804	CEBPD	4.3150225	up	Homo sapiens CCAAT/enhancer binding protein (C/EBP), delta (CEBPD), mRNA [NM_005195]
A_23_P360291	TAPBP	4.2945623	up	TAP binding protein (tapasin) [Source:HGNC Symbol;Acc:HGNC:11566] [ENST00000480730]
A_23_P106002	NFKBIA	4.206646	up	Homo sapiens nuclear factor of kappa light polypeptide gene enhancer in B-cells inhibitor, alpha (NFKBIA), mRNA [NM_020529]
A_23_P24884	ST5	4.120563	up	Homo sapiens suppression of tumorigenicity 5 (ST5), transcript variant 1, mRNA [NM_005418]
A_24_P241815	JUNB	4.0271993	up	Homo sapiens jun B proto-oncogene (JUNB), mRNA [NM_002229]
A_33_P3267814	MICAL3	3.977695	up	Homo sapiens microtubule associated monooxygenase, calponin and LIM domain containing 3 (MICAL3), transcript variant 2, mRNA [NM_001136004]
A_33_P3382276	ST6GAL1	3.974046	up	ST6 beta-galactosamide alpha-2,6-sialyltranferase 1 [Source:HGNC Symbol;Acc:HGNC:10860] [ENST00000468614]
A_23_P152995	SLC6A4	3.8124597	up	Homo sapiens solute carrier family 6 (neurotransmitter transporter), member 4 (SLC6A4), mRNA [NM_001045]
A_23_P92499	TLR2	3.5773644	up	Homo sapiens toll-like receptor 2 (TLR2), mRNA [NM_003264]
A_33_P3321130	DENND3	3.5360558	up	DENN/MADD domain containing 3 [Source:HGNC Symbol;Acc:HGNC:29134] [ENST00000520482]

APPENDIX A (CONTINUED)

A_24_P751074	ETS1	3.5269992	up	Homo sapiens v-ets avian erythroblastosis virus E26 oncogene homolog 1 (ETS1), transcript variant 2, mRNA [NM_005238]
A_33_P3222341	PITPNC1	3.489173	up	Homo sapiens phosphatidylinositol transfer protein, cytoplasmic 1 (PITPNC1), transcript variant 1, mRNA [NM_012417]
A_24_P122732	SLC41A1	3.4554486	up	Homo sapiens solute carrier family 41 (magnesium transporter), member 1 (SLC41A1), mRNA [NM_173854]
A_23_P360754	ADAMTS4	3.4494886	up	Homo sapiens ADAM metallopeptidase with thrombospondin type 1 motif, 4 (ADAMTS4), mRNA [NM_005099]
A_24_P277367	CXCL5	3.4438717	up	Homo sapiens chemokine (C-X-C motif) ligand 5 (CXCL5), mRNA [NM_002994]
A_23_P50946	RAMP1	3.371158	up	Homo sapiens receptor (G protein-coupled) activity modifying protein 1 (RAMP1), mRNA [NM_005855]
A_23_P40217	DOK5	3.3078184	up	Homo sapiens docking protein 5 (DOK5), transcript variant 1, mRNA [NM_018431]
A_23_P32404	ISG20	3.2873363	up	Homo sapiens interferon stimulated exonuclease gene 20kDa (ISG20), transcript variant 1, mRNA [NM_002201]
A_23_P59950	SLC39A14	3.198687	up	Homo sapiens solute carrier family 39 (zinc transporter), member 14 (SLC39A14), transcript variant 2, mRNA [NM_015359]
A_33_P3354940	CSF1	3.1914124	up	Homo sapiens colony stimulating factor 1 (macrophage) (CSF1), transcript variant 1, mRNA [NM_000757]
A_23_P210253	DGKD	3.0567844	up	Homo sapiens diacylglycerol kinase, delta 130kDa (DGKD), transcript variant 2, mRNA [NM_152879]
A_23_P76914	SIX1	2.930658	up	Homo sapiens SIX homeobox 1 (SIX1), mRNA [NM_005982]
A_24_P269062	SPRY4	2.9079483	up	Homo sapiens sprouty homolog 4 (Drosophila) (SPRY4), transcript variant 1, mRNA [NM_030964]
A_23_P20122	ZC3HAV1	2.8883562	up	Homo sapiens zinc finger CCCH-type, antiviral 1 (ZC3HAV1), transcript variant 2, mRNA [NM_024625]
A_23_P114947	RGS2	2.880377	up	Homo sapiens regulator of G-protein signaling 2 (RGS2), mRNA [NM_002923]
A_23_P89431	CCL2	2.8228168	up	Homo sapiens chemokine (C-C motif) ligand 2 (CCL2), mRNA [NM_002982]
A_24_P942630	KDM6B	2.7633564	up	Homo sapiens lysine (K)-specific demethylase 6B (KDM6B), mRNA [NM_001080424]

APPENDIX A (CONTINUED)

A_23_P110430	MSX1	2.7195458	up	Homo sapiens msh homeobox 1 (MSX1), mRNA [NM_002448]
A_32_P196263	ADAMTS9	2.6610515	up	Homo sapiens ADAM metallopeptidase with thrombospondin type 1 motif, 9 (ADAMTS9), mRNA [NM_182920]
A_33_P3343485	HIP1	2.6098313	up	huntingtin interacting protein 1 [Source:HGNC Symbol;Acc:HGNC:4913] [ENST00000479835]
A_23_P46470	ERRFI1	2.5339973	up	Homo sapiens ERBB receptor feedback inhibitor 1 (ERRFI1), mRNA [NM_018948]
A_33_P3304688	TNAP	2.5286076	up	Homo sapiens NIK-associated protein mRNA, complete cds. [AF463496]
A_23_P204286	MGP	2.4901438	up	Homo sapiens matrix Gla protein (MGP), transcript variant 2, mRNA [NM_000900]
A_24_P12435	NCOA7	2.4204347	up	Homo sapiens nuclear receptor coactivator 7 (NCOA7), transcript variant 1, mRNA [NM_181782]
A_23_P71530	TNFRSF11B	2.3821678	up	Homo sapiens tumor necrosis factor receptor superfamily, member 11b (TNFRSF11B), mRNA [NM_002546]
A_23_P48936	SMAD3	2.3598776	up	Homo sapiens SMAD family member 3 (SMAD3), transcript variant 1, mRNA [NM_005902]
A_23_P137016	SAT1	2.3528972	up	Homo sapiens spermidine/spermine N1-acetyltransferase 1 (SAT1), transcript variant 1, mRNA [NM_002970]
A_33_P3321136	DENND3	2.293544	up	Homo sapiens DENN/MADD domain containing 3 (DENND3), mRNA [NM_014957]
A_23_P26024	C15orf48	2.2672188	up	Homo sapiens chromosome 15 open reading frame 48 (C15orf48), transcript variant 2, mRNA [NM_032413]
A_33_P3389728	NR5A2	2.1964734	up	Homo sapiens nuclear receptor subfamily 5, group A, member 2 (NR5A2), transcript variant 1, mRNA [NM_205860]
A_23_P74278	PDE4B	2.1614707	up	Homo sapiens phosphodiesterase 4B, cAMP-specific (PDE4B), transcript variant d, mRNA [NM_001037341]
A_24_P140608	HBEGF	2.1421702	up	Homo sapiens heparin-binding EGF-like growth factor (HBEGF), mRNA [NM_001945]
A_23_P12053	SPEN	2.1273556	up	Homo sapiens spen family transcriptional repressor (SPEN), mRNA [NM_015001]
A_33_P3363355	ICAM4	2.0286949	up	Homo sapiens intercellular adhesion molecule 4 (Landsteiner-Wiener blood group) (ICAM4), transcript variant 2, mRNA [NM_022377]

APPENDIX B

VEGF-treated Endothelial Cells (Downregulated Genes)

Probe Name	Gene Symbol	Fold Change	Regulation	Description
A_33_P3361991	OR9A2	-2.9017968	down	Homo sapiens olfactory receptor, family 9, subfamily A, member 2 (OR9A2), mRNA [NM_001001658]
A_24_P183664	TRIL	-2.8269997	down	Homo sapiens TLR4 interactor with leucine-rich repeats (TRIL), mRNA [NM_014817]
A_23_P211345	TBX1	-2.613333	down	Homo sapiens T-box 1 (TBX1), transcript variant C, mRNA [NM_080647]
A_33_P3314594	RAB37	-2.2359555	down	Homo sapiens RAB37, member RAS oncogene family (RAB37), transcript variant 3, mRNA [NM_175738]
A_33_P3331125	SLC2A12	-2.166084	down	Homo sapiens solute carrier family 2 (facilitated glucose transporter), member 12 (SLC2A12), mRNA [NM_145176]
A_23_P212844	TACC3	-2.156313	down	Homo sapiens transforming, acidic coiled-coil containing protein 3 (TACC3), mRNA [NM_006342]
A_33_P3240679	BRD3	-2.0757196	down	bromodomain containing 3 [Source:HGNC Symbol;Acc:HGNC:1104] [ENST00000371842]
A_33_P3234048	NRDE2	-2.002222	down	NRDE-2, necessary for RNA interference, domain containing [Source:HGNC Symbol;Acc:HGNC:20186] [ENST00000354366]

APPENDIX C

VEGF/anti-VEGF treated Endothelial Cells (Upregulated Genes)

Probe Name	Gene Symbol	Fold Change	Regulation	Description
A_23_P133408	CSF2	425.05856	up	Homo sapiens colony stimulating factor 2 (granulocyte-macrophage) (CSF2), mRNA [NM_000758]
A_33_P3226832	F3	256.09732	up	Homo sapiens coagulation factor III (thromboplastin, tissue factor) (F3), transcript variant 1, mRNA [NM_001993]
A_23_P376488	TNF	252.28873	up	Homo sapiens tumor necrosis factor (TNF), mRNA [NM_000594]
A_24_P122137	LIF	242.85248	up	Homo sapiens leukemia inhibitory factor (LIF), transcript variant 1, mRNA [NM_002309]
A_24_P183150	CXCL3	201.89256	up	Homo sapiens chemokine (C-X-C motif) ligand 3 (CXCL3), mRNA [NM_002090]
A_23_P501754	CSF3	140.06789	up	Homo sapiens colony stimulating factor 3 (granulocyte) (CSF3), transcript variant 1, mRNA [NM_000759]
A_23_P76078	IL23A	95.34212	up	Homo sapiens interleukin 23, alpha subunit p19 (IL23A), mRNA [NM_016584]
A_33_P3356462	C2CD4A	89.698975	up	Homo sapiens C2 calcium-dependent domain containing 4A (C2CD4A), mRNA [NM_207322]
A_24_P257416	CXCL2	86.34343	up	Homo sapiens chemokine (C-X-C motif) ligand 2 (CXCL2), mRNA [NM_002089]
A_33_P3421053	SELE	66.95831	up	Homo sapiens selectin E (SELE), mRNA [NM_000450]
A_23_P79518	IL1B	56.557697	up	Homo sapiens interleukin 1, beta (IL1B), mRNA [NM_000576]
A_33_P3222424	CSF3	42.395	up	Homo sapiens colony stimulating factor 3 (granulocyte) (CSF3), transcript variant 1, mRNA [NM_000759]
A_23_P23947	MAP3K8	35.903305	up	Homo sapiens mitogen-activated protein kinase kinase kinase 8 (MAP3K8), transcript variant 1, mRNA [NM_005204]
A_23_P420863	NOD2	35.064457	up	Homo sapiens nucleotide-binding oligomerization domain containing 2 (NOD2), transcript variant 1, mRNA [NM_022162]

APPENDIX C (CONTINUED)

A_23_P71037	IL6	34.94591	up	Homo sapiens interleukin 6 (IL6), mRNA [NM_000600]
A_23_P320578	RGS16	26.945967	up	Homo sapiens regulator of G-protein signaling 16 (RGS16), mRNA [NM_002928]
A_23_P315364	CXCL2	25.536283	up	Homo sapiens chemokine (C-X-C motif) ligand 2 (CXCL2), mRNA [NM_002089]
A_23_P155755	CXCL6	23.427729	up	Homo sapiens chemokine (C-X-C motif) ligand 6 (CXCL6), mRNA [NM_002993]
A_23_P98350	BIRC3	23.188213	up	Homo sapiens baculoviral IAP repeat containing 3 (BIRC3), transcript variant 1, mRNA [NM_001165]
A_24_P390495	CX3CL1	23.02112	up	chemokine (C-X3-C motif) ligand 1 [Source:HGNC Symbol;Acc:HGNC:10647] [ENST00000006053]
A_23_P420196	SOCS1	20.426603	up	Homo sapiens suppressor of cytokine signaling 1 (SOCS1), mRNA [NM_003745]
A_23_P128744	BDKRB1	20.300615	up	Homo sapiens bradykinin receptor B1 (BDKRB1), mRNA [NM_000710]
A_23_P97112	SELE	19.53439	up	Homo sapiens selectin E (SELE), mRNA [NM_000450]
A_24_P157926	TNFAIP3	18.72247	up	Homo sapiens tumor necrosis factor, alpha-induced protein 3 (TNFAIP3), transcript variant 3, mRNA [NM_006290]
A_23_P131676	ACKR3	18.040522	up	Homo sapiens atypical chemokine receptor 3 (ACKR3), mRNA [NM_020311]
A_23_P53370	RND1	17.583889	up	Homo sapiens Rho family GTPase 1 (RND1), mRNA [NM_014470]
A_33_P3330264	CXCL1	17.16899	up	Homo sapiens chemokine (C-X-C motif) ligand 1 (melanoma growth stimulating activity, alpha) (CXCL1), transcript variant 1, mRNA [NM_001511]
A_23_P328740	NEURL3	17.084877	up	Homo sapiens neuralized E3 ubiquitin protein ligase 3 (NEURL3), transcript variant 2, mRNA [NM_001285486]
A_23_P393034	HAS3	16.420221	up	Homo sapiens hyaluronan synthase 3 (HAS3), transcript variant 1, mRNA [NM_005329]
A_23_P87879	CD69	15.20997	up	Homo sapiens CD69 molecule (CD69), mRNA [NM_001781]
A_33_P3214720	ZC3H12A	14.174281	up	Homo sapiens zinc finger CCCH-type containing 12A (ZC3H12A), mRNA [NM_025079]

APPENDIX C (CONTINUED)

A_23_P421423	TNFAIP2	13.834753	up	Homo sapiens tumor necrosis factor, alpha-induced protein 2 (TNFAIP2), mRNA [NM_006291]
A_24_P250922	PTGS2	13.60944	up	Homo sapiens prostaglandin-endoperoxide synthase 2 (prostaglandin G/H synthase and cyclooxygenase) (PTGS2), mRNA [NM_000963]
A_33_P3237150	BMP2	11.323765	up	Homo sapiens bone morphogenetic protein 2 (BMP2), mRNA [NM_001200]
A_21_P0000174	C5orf56	11.290861	up	Homo sapiens cDNA, FLJ99232. [AK309191]
A_23_P39237	ZFP36	11.177651	up	Homo sapiens ZFP36 ring finger protein (ZFP36), mRNA [NM_003407]
A_23_P144337	CCRN4L	10.649158	up	Homo sapiens CCR4 carbon catabolite repression 4-like (S. cerevisiae) (CCRN4L), mRNA [NM_012118]
A_23_P119478	EBI3	10.631446	up	Homo sapiens Epstein-Barr virus induced 3 (EBI3), mRNA [NM_005755]
A_23_P109034	SDC4	10.369788	up	Homo sapiens syndecan 4 (SDC4), mRNA [NM_002999]
A_24_P788878	C2CD4B	10.014265	up	Homo sapiens C2 calcium-dependent domain containing 4B (C2CD4B), mRNA [NM_001007595]
A_33_P3370575	CD200	9.658725	up	Homo sapiens CD200 molecule (CD200), transcript variant 2, mRNA [NM_001004196]
A_23_P121480	CD200	9.119013	up	Homo sapiens CD200 molecule (CD200), transcript variant 2, mRNA [NM_001004196]
A_32_P83845	HEY1	9.072948	up	Homo sapiens hes-related family bHLH transcription factor with YRPW motif 1 (HEY1), transcript variant 2, mRNA [NM_001040708]
A_23_P212089	NFKBIZ	8.613695	up	Homo sapiens nuclear factor of kappa light polypeptide gene enhancer in B-cells inhibitor, zeta (NFKBIZ), transcript variant 1, mRNA [NM_031419]
A_23_P41765	IRF1	8.604613	up	Homo sapiens interferon regulatory factor 1 (IRF1), mRNA [NM_002198]
A_23_P70670	CD83	8.228603	up	Homo sapiens CD83 molecule (CD83), transcript variant 1, mRNA [NM_004233]
A_33_P3311439	GCH1	8.10659	up	Homo sapiens GTP cyclohydrolase 1 (GCH1), transcript variant 4, mRNA [NM_001024071]

APPENDIX C (CONTINUED)

A_23_P360291	TAPBP	7.963206	up	TAP binding protein (tapasin) [Source:HGNC Symbol;Acc:HGNC:11566] [ENST00000480730]
A_23_P34915	ATF3	7.5505395	up	Homo sapiens activating transcription factor 3 (ATF3), transcript variant 4, mRNA [NM_001040619]
A_23_P118392	RASD1	6.4175315	up	Homo sapiens RAS, dexamethasone-induced 1 (RASD1), transcript variant 1, mRNA [NM_016084]
A_24_P167642	GCH1	6.2390018	up	Homo sapiens GTP cyclohydrolase 1 (GCH1), transcript variant 1, mRNA [NM_000161]
A_23_P153320	ICAM1	5.8788643	up	Homo sapiens intercellular adhesion molecule 1 (ICAM1), mRNA [NM_000201]
A_23_P69573	GUCY1A3	5.7578545	up	Homo sapiens guanylate cyclase 1, soluble, alpha 3 (GUCY1A3), transcript variant 1, mRNA [NM_000856]
A_33_P3211666	IL18R1	5.742287	up	Homo sapiens interleukin 18 receptor 1 (IL18R1), transcript variant 1, mRNA [NM_003855]
A_23_P83838	CA8	5.4373765	up	Homo sapiens carbonic anhydrase VIII (CA8), mRNA [NM_004056]
A_33_P3368646	CNKSR3	5.308913	up	Homo sapiens CNKSR family member 3 (CNKSR3), mRNA [NM_173515]
A_24_P241815	JUNB	4.9713707	up	Homo sapiens jun B proto-oncogene (JUNB), mRNA [NM_002229]
A_23_P134176	SOD2	4.958952	up	Homo sapiens superoxide dismutase 2, mitochondrial (SOD2), transcript variant 2, mRNA [NM_001024465]
A_33_P3354940	CSF1	4.856009	up	Homo sapiens colony stimulating factor 1 (macrophage) (CSF1), transcript variant 1, mRNA [NM_000757]
A_23_P81898	UBD	4.8113494	up	Homo sapiens ubiquitin D (UBD), mRNA [NM_006398]
A_23_P24884	ST5	4.7610745	up	Homo sapiens suppression of tumorigenicity 5 (ST5), transcript variant 1, mRNA [NM_005418]
A_33_P3253804	CEBPD	4.6508417	up	Homo sapiens CCAAT/enhancer binding protein (C/EBP), delta (CEBPD), mRNA [NM_005195]
A_23_P106002	NFKBIA	4.530811	up	Homo sapiens nuclear factor of kappa light polypeptide gene enhancer in B-cells inhibitor, alpha (NFKBIA), mRNA [NM_020529]

APPENDIX C (CONTINUED)

A_24_P122732	SLC41A1	4.40035	up	Homo sapiens solute carrier family 41 (magnesium transporter), member 1 (SLC41A1), mRNA [NM_173854]
A_24_P277367	CXCL5	4.1818204	up	Homo sapiens chemokine (C-X-C motif) ligand 5 (CXCL5), mRNA [NM_002994]
A_33_P3363355	ICAM4	4.147376	up	Homo sapiens intercellular adhesion molecule 4 (Landsteiner-Wiener blood group) (ICAM4), transcript variant 2, mRNA [NM_022377]
A_23_P152995	SLC6A4	4.0747046	up	Homo sapiens solute carrier family 6 (neurotransmitter transporter), member 4 (SLC6A4), mRNA [NM_001045]
A_33_P3220390	WTAP	4.0711346	up	Homo sapiens Wilms tumor 1 associated protein, mRNA (cDNA clone IMAGE:5399821), partial cds. [BC028180]
A_24_P942630	KDM6B	4.034418	up	Homo sapiens lysine (K)-specific demethylase 6B (KDM6B), mRNA [NM_001080424]
A_23_P32404	ISG20	3.683652	up	Homo sapiens interferon stimulated exonuclease gene 20kDa (ISG20), transcript variant 1, mRNA [NM_002201]
A_33_P3304688	TNAP	3.6189506	up	Homo sapiens NIK-associated protein mRNA, complete cds. [AF463496]
A_33_P3382276	ST6GAL1	3.5663428	up	ST6 beta-galactosamide alpha-2,6-sialyltranferase 1 [Source:HGNC Symbol;Acc:HGNC:10860] [ENST00000468614]
A_23_P388993	ZC3H12C	3.490631	up	Homo sapiens zinc finger CCCH-type containing 12C (ZC3H12C), mRNA [NM_033390]
A_23_P201808	PPAP2B	3.4547002	up	Homo sapiens phosphatidic acid phosphatase type 2B (PPAP2B), mRNA [NM_003713]
A_23_P26024	C15orf48	3.4385545	up	Homo sapiens chromosome 15 open reading frame 48 (C15orf48), transcript variant 2, mRNA [NM_032413]
A_23_P360754	ADAMTS4	3.397446	up	Homo sapiens ADAM metallopeptidase with thrombospondin type 1 motif, 4 (ADAMTS4), mRNA [NM_005099]
A_23_P92499	TLR2	3.387775	up	Homo sapiens toll-like receptor 2 (TLR2), mRNA [NM_003264]
A_23_P59950	SLC39A14	3.3834279	up	Homo sapiens solute carrier family 39 (zinc transporter), member 14 (SLC39A14), transcript variant 2, mRNA [NM_015359]

APPENDIX C (CONTINUED)

A_33_P3222341	PITPNC1	3.3600008	up	Homo sapiens phosphatidylinositol transfer protein, cytoplasmic 1 (PITPNC1), transcript variant 1, mRNA [NM_012417]
A_23_P110430	MSX1	3.284974	up	Homo sapiens msh homeobox 1 (MSX1), mRNA [NM_002448]
A_23_P383422	NFKBID	3.2749078	up	Homo sapiens nuclear factor of kappa light polypeptide gene enhancer in B-cells inhibitor, delta (NFKBID), mRNA [NM_139239]
A_24_P751074	ETS1	3.2576258	up	Homo sapiens v-ets avian erythroblastosis virus E26 oncogene homolog 1 (ETS1), transcript variant 2, mRNA [NM_005238]
A_23_P89431	CCL2	2.9644387	up	Homo sapiens chemokine (C-C motif) ligand 2 (CCL2), mRNA [NM_002982]
A_23_P71530	TNFRSF11B	2.8183374	up	Homo sapiens tumor necrosis factor receptor superfamily, member 11b (TNFRSF11B), mRNA [NM_002546]
A_33_P3321130	DENND3	2.7933233	up	DENN/MADD domain containing 3 [Source:HGNC Symbol;Acc:HGNC:29134] [ENST00000520482]
A_24_P12435	NCOA7	2.7803702	up	Homo sapiens nuclear receptor coactivator 7 (NCOA7), transcript variant 1, mRNA [NM_181782]
A_32_P196263	ADAMTS9	2.739076	up	Homo sapiens ADAM metallopeptidase with thrombospondin type 1 motif, 9 (ADAMTS9), mRNA [NM_182920]
A_23_P355536	USP54	2.661847	up	Homo sapiens ubiquitin specific peptidase 54 (USP54), mRNA [NM_152586]
A_23_P46470	ERRFI1	2.6534	up	Homo sapiens ERBB receptor feedback inhibitor 1 (ERRFI1), mRNA [NM_018948]
A_23_P210330	LGALSL	2.6393266	up	Homo sapiens lectin, galactoside-binding-like (LGALSL), mRNA [NM_014181]
A_23_P166	MOB3C	2.5792663	up	Homo sapiens MOB kinase activator 3C (MOB3C), transcript variant 1, mRNA [NM_145279]
A_24_P140608	HBEGF	2.5710876	up	Homo sapiens heparin-binding EGF-like growth factor (HBEGF), mRNA [NM_001945]
A_33_P3321136	DENND3	2.483913	up	Homo sapiens DENN/MADD domain containing 3 (DENND3), mRNA [NM_014957]
A_23_P257743	SHB	2.4807193	up	Homo sapiens Src homology 2 domain containing adaptor protein B (SHB), mRNA [NM_003028]

APPENDIX C (CONTINUED)

A_23_P219197	RGS3	2.425084	up	Homo sapiens regulator of G-protein signaling 3 (RGS3), transcript variant 4, mRNA [NM_134427]
A_23_P137016	SAT1	2.335225	up	Homo sapiens spermidine/spermine N1-acetyltransferase 1 (SAT1), transcript variant 1, mRNA [NM_002970]
A_23_P12053	SPEN	2.299307	up	Homo sapiens spen family transcriptional repressor (SPEN), mRNA [NM_015001]
A_23_P160438	MYOG	2.2400267	up	Homo sapiens myogenin (myogenic factor 4) (MYOG), mRNA [NM_002479]
A_23_P48936	SMAD3	2.225895	up	Homo sapiens SMAD family member 3 (SMAD3), transcript variant 1, mRNA [NM_005902]
A_21_P0001952	CFLAR	2.1662629	up	Homo sapiens CASP8 and FADD-like apoptosis regulator (CFLAR), transcript variant 8, mRNA [NM_001202519]
A_33_P3396872	CPED1	2.1546605	up	Homo sapiens cadherin-like and PC-esterase domain containing 1 (CPED1), transcript variant 2, mRNA [NM_001105533]
A_33_P3343485	HIP1	2.1365683	up	huntingtin interacting protein 1 [Source:HGNC Symbol;Acc:HGNC:4913] [ENST00000479835]
A_33_P3267814	MICAL3	2.1138618	up	Homo sapiens microtubule associated monooxygenase, calponin and LIM domain containing 3 (MICAL3), transcript variant 2, mRNA [NM_001136004]
A_23_P19619	HIVEP1	2.0943103	up	Homo sapiens human immunodeficiency virus type I enhancer binding protein 1 (HIVEP1), mRNA [NM_002114]
A_24_P120115	CFLAR	2.0485663	up	Homo sapiens CASP8 and FADD-like apoptosis regulator (CFLAR), transcript variant 1, mRNA [NM_003879]
A_24_P365807	EFNB1	2.00224	up	Homo sapiens ephrin-B1 (EFNB1), mRNA [NM_004429]

APPENDIX D

VEGF/anti-VEGF treated Endothelial Cells (Downregulated Genes)

Probe Name	Gene Symbol	Fold Change	Regulation	Description
A_23_P86470	CH25H	-4.4450297	down	Homo sapiens cholesterol 25-hydroxylase (CH25H), mRNA [NM_003956]
A_33_P3322909	CUL4A	-3.4879894	down	Homo sapiens cullin 4A (CUL4A), transcript variant 3, mRNA [NM_001278513]
A_24_P243749	PDK4	-3.430277	down	Homo sapiens pyruvate dehydrogenase kinase, isozyme 4 (PDK4), mRNA [NM_002612]
A_24_P183664	TRIL	-3.3465662	down	Homo sapiens TLR4 interactor with leucine-rich repeats (TRIL), mRNA [NM_014817]
A_33_P3361991	OR9A2	-3.0988214	down	Homo sapiens olfactory receptor, family 9, subfamily A, member 2 (OR9A2), mRNA [NM_001001658]
A_23_P211345	TBX1	-2.802421	down	Homo sapiens T-box 1 (TBX1), transcript variant C, mRNA [NM_080647]
A_23_P44648	ADAMTS12	-2.4099848	down	Homo sapiens ADAM metallopeptidase with thrombospondin type 1 motif, 12 (ADAMTS12), mRNA [NM_030955]
A_33_P3372099	DDIT4L	-2.3853557	down	Homo sapiens DNA-damage-inducible transcript 4-like (DDIT4L), mRNA [NM_145244]
A_33_P3314594	RAB37	-2.2795978	down	Homo sapiens RAB37, member RAS oncogene family (RAB37), transcript variant 3, mRNA [NM_175738]
A_33_P3240679	BRD3	-2.2253559	down	bromodomain containing 3 [Source:HGNC Symbol;Acc:HGNC:1104] [ENST00000371842]
A_33_P3331125	SLC2A12	-2.1595178	down	Homo sapiens solute carrier family 2 (facilitated glucose transporter), member 12 (SLC2A12), mRNA [NM_145176]
A_33_P3234048	NRDE2	-2.0419924	down	NRDE-2, necessary for RNA interference, domain containing [Source:HGNC Symbol;Acc:HGNC:20186] [ENST00000354366]

APPENDIX E

Quality Control for Samples Used in Microarray Analysis – 3D PCA Plot

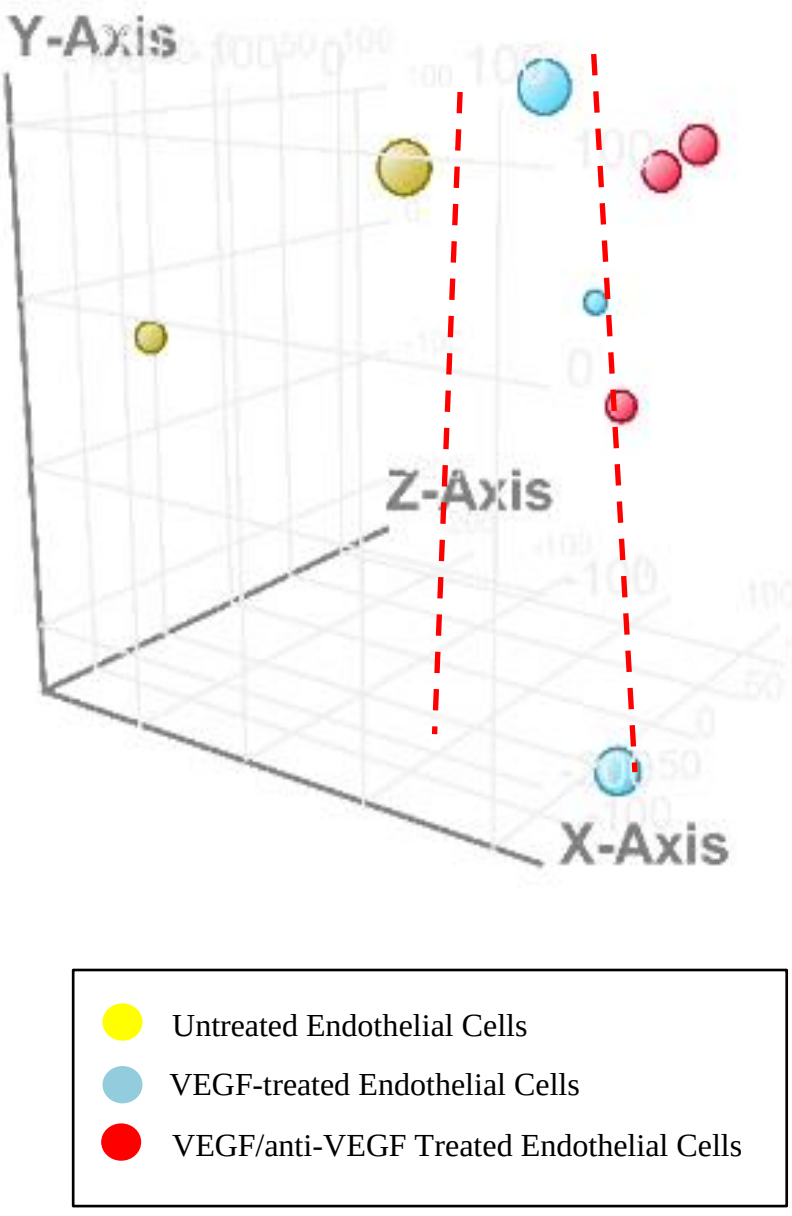

APPENDIX E

Primer-Blast Results for Primers, TRIL and GAPDH

TRIL

Primer pair 1

	Sequence (5'->3')	Length	Tm	GC%
Forward primer	CCTCGGCGGCAACTTCATAA	20	60.74	55.00
Reverse primer	AGAGCGGATCTGGTTGTACTG	21	59.52	52.38

Products on target templates

>NM_014817.4 Homo sapiens TLR4 interactor with leucine rich repeats (TRIL), mRNA

```
product length = 97
Forward primer  1    CCTCGGCGGCAACTTCATAA  20
Template        479  ....................  498

Reverse primer  1    AGAGCGGATCTGGTTGTACTG  21
Template        575  ....................  555
```

GAPDH

Primer pair 1

	Sequence (5'->3')	Length	Tm	GC%
Forward primer	GAAATCCCATCACCATCTTCCAGG	24	61.23	50.00
Reverse primer	GAGCCCCAGCCTTCTCCATG	20	62.62	65.00

Products on target templates

>NM_001357943.2 Homo sapiens glyceraldehyde-3-phosphate dehydrogenase (GAPDH), transcript variant 7, mRNA

```
product length = 120
Forward primer  1    GAAATCCCATCACCATCTTCCAGG  24
Template        234  ........................  257

Reverse primer  1    GAGCCCCAGCCTTCTCCATG  20
Template        353  ....................  334
```

>NM_001256799.3 Homo sapiens glyceraldehyde-3-phosphate dehydrogenase (GAPDH), transcript variant 2, mRNA

```
product length = 120
Forward primer  1    GAAATCCCATCACCATCTTCCAGG  24
Template        389  ........................  412

Reverse primer  1    GAGCCCCAGCCTTCTCCATG  20
Template        508  ....................  489
```